FINAL TECHNICAL REPORT

PROJECT NO. A–2343

INTRAPULSE POLARIZATION AGILE RADAR

By

B. C. Appling, E. S. Sjoberg, E. E. Martin

Prepared for

NAVAL SEA SYSTEMS COMMAND (Code 62R13)
WASHINGTON, D.C. 20362

SCEEE MANAGEMENT OFFICE
ST. CLOUD, FLORIDA 32769

Under

Prime Contract No. N00024–78–C–5338
SCEEE Subcontract No. SCEEE–NAVSEA/79–2

July 1981

GEORGIA INSTITUTE OF TECHNOLOGY

A Unit of the University System of Georgia
Engineering Experiment Station
Atlanta, Georgia 30332

1981

FINAL TECHNICAL REPORT

PROJECT NO. A-2343

PRIME CONTRACT NO. N00024-78-C-5338

SCEEE SUBCONTRACT NO. SCEEE-NAVSEA/79-2

INTRAPULSE POLARIZATION AGILE RADAR (IPAR)

By

B. C. Appling, E. S. Sjoberg, E. E. Martin

of

Georgia Institute of Technology

Engineering Experiment Station

(GIT/EES)

July 1981

Final Technical Report for Period Ending 31 December 1980

Prepared for

Naval Sea Systems Command (Code 62R13)

Washington, D. C. 20362

SCEEE Management Office

1101 Massachusetts Avenue

St. Cloud, Florida 32769

TABLE OF CONTENTS

SECTION	TITLE	PAGE

LIST OF TABLES

LIST OF ILLUSTRATIONS

PREFACE

The effort documented by this report is expected to be the first in a multi-phase program. While this phase consisted of the fabrication, demonstration of the equipment and a limited analysis, succeeding phases are expected to include measurements, data analysis, and operational configuration studies and demonstrations.

Aside from conventional radar components, a mobile van, test equipment, etc., the primary development was the IPAR processor. The most essential components for the IPAR processor were high speed digital correlators, developed by TRW under another U. S. Navy program, which perform well at clock rates of 100 MHz.

Each individual involved in the project performed their tasks well. However, special recognition must be given to Mr. E. S. Sjoberg, Senior Research Engineer, who designed and constructed the IPAR processor and assisted with the analysis. It is an understatement to declare that his efforts were beyond the call of duty.

Georgia Tech would like to thank Mr. Alan Templin, Mr. Corey Eng and Mr. Diogenes Cordero of TRW, Inc., for their 32-DOC correlator circuits.

SECTION 1
INTRODUCTION AND SUMMARY

The Intrapulse Polarization Agile Radar (IPAR) technique has been reduced to practice under the U.S. Navy contract for which this document is the final technical report. This report documents the IPAR hardware configuration, provides discussions related to the characteristics and potential advantages of the technique, and contains a theoretical analysis of the signal-to-interference improvement expected of the technique. Much of the mathematical detail and physical justifications for the analytical expressions used in assessing the relative performance of various techniques are contained in the Appendix, in order to permit the main body of the report to be read with greater ease.

IPAR offers potential advantages in the following areas:

(a) Low Probability of Intercept (LPI), Stealth

(b) Clutter Discrimination

(c) ECCM

(d) Discrimination and Recognition

(e) Anti-Multipath

(f) Detection Range Improvement.

Pseudo-Coherent-Detection (PCD) is one of several sub-techniques of the IPAR technique. The potential advantages offered by IPAR in clutter discrimination derive from signal characteristics that are closely related to those of the PCD technique. Consequently, any analysis or measurement for one technique has some applicability to the other in terms of clutter discrimination characteristics.

1.1 BACKGROUND

Under contract to the Air Force five to six years ago, GIT/EES was tasked to investigate Stationary Target Indication (STI) techniques. During this project (A-1686), the relative usefulness of employing frequency agility and polarization agility, independently and together, to simulate clutter decorrelation were tested. Two processors were constructed to discriminate between

clutter and hard targets: Dynamic Threshold Gating (DTG) and Correlation Coefficient Discrimination (CCD) processors. Some success was achieved, but it was difficult to state the degree of improvement in quantitative terms. Of greater significance were two observations made by project personnel during the final phase of that program. The processors were designed to work primarily with amplitude discriminants, but discriminants (i.e., difference between clutter and targets) were also observed in the relative phase characteristics of two orthogonal polarizations as well as the amplitude characteristics.

Subsequent to project A-1686, several field experiments, at least some of which were internally funded, and demonstrations were conducted. One of the more notable demonstrations, in terms of technique exposure, was conducted at Missile Command (MICOM), Huntsville, Alabama. GIT/EES personnel were positioned on a hill with Radar Van GT-2. The radar (AN/APQ-126) which had been used in project A-1686 was used. Normal amplitude, phase detected, and threshold gated integrated digital video were simultaneously displayed. Targets included corner reflectors and tanks. MICOM personnel were given briefings and they observed the simultaneous A-scope presentation of amplitude, phase and integrated digital video. The tank was moved around during the demonstration so that the observers could be certain of what they were viewing. Polarization, frequency agility, threshold setting and integration time were all variable and were varied during the demonstration. Photographs (i.e., both Army and GIT/EES) were made during the demonstration. Attenuators were used to attenuate the clutter signal until its amplitude matched the unattenuated target amplitude. The relative clutter-to-target amplitude was thusly found to be approximately 20 dB. Yet, the target could still be detected and displayed without clutter false alarms. Project personnel who had been involved in project A-1686 had made similar observations that performance varied between inter-cell and intra-cell conditions.

In 1978, an analysis of Pseudo-Coherent Detection (PCD) techniques was conducted. This analysis is documented by report DELCS-TR-76-0961-F, entitled "Stationary Target Detection and Classification Studies," dated April, 1979. The analysis did not predict the performance which had already been demonstrated. Subsequently, it was learned that the analysis did not include the

considerations which would have been representative of the conditions under which the demonstration was conducted. For the demonstration, the average clutter in the vicinity of the target was tens of dB larger than the target, whereas the clutter in the exact resolution cell containing the target was nil. For that particular technique, lower in-cell clutter, which reduces target plus in-cell clutter combined amplitude relative to the average regional clutter, increases the detection probability. The equations and graphs contained in the Appendix illustrate why this phenomena occurs. Subsequently, similar situations have been simulated by scaling real data and similar results have been obtained.

While IPAR was initially perceived as a stealth technique, other potential advantages have since been indentified. Among these are anti-clutter advantages deriving from signal characteristic similarities to the PCD technique. The various PCD techniques are important to understanding IPAR, as will be appreciated as one progresses through this report.

1.2 SUMMARY

The remainder of this report consists of Section 2, a description of the system as fabricated; Section 3, a description of the demonstration of the system; Section 4, the signal-to-interference performance analysis; and the Appendix. Various topics are covered in the Appendix in addition to the analytical support for the equations used in Section 4.

1.2.1 SYSTEM HARDWARE CONFIGURATION SUMMARY

The IPAR hardware was constructed as proposed and functions as anticipated.

1.2.2 SYSTEM DEMONSTRATION SUMMARY

The IPAR hardware was successfully demonstrated to function as proposed and was shown to possess the general characteristics and capabilities suggested by the analysis contained herein.

1.2.3 SYSTEM ANALYSIS SUMMARY

The analysis compares the signal-to-interference (S/I) improvement of the

IPAR technique to various other radar signal processing techniques. IPAR is shown to provide an improvement in S/I relative to all the other techniques. Although an accurate methodology of comparing system approaches in terms of relative S/I improvement was demonstrated (see Appendix), an approximate method was identified from which an estimate of improvement could be determined. IPAR was shown to provide the potential for considerable performance improvement over all other techniques with which it was compared in S/I ratio improvement. In addition to the basic improvement for an advantageous clutter model, IPAR also provides improvement in non-ideal clutter, which is distributed. Additional analyses conducted in the Appendix shows additional characteristics of the various techniques such as their behavior under various "in cell" to "out of cell" clutter or interference. In general, the performance of an IPAR technique in S/I improvement may be derived from the "dot product" or "phase only" PCD techniques and accounting for the additional improvement deriving from the correlation and compression. Whatever basic polarimetric phase processing technique is incorporated prior to correlation and compression processing, the IPAR S/I improvement performance is roughly twice the square root of the compression ratio or greater for non-target-like clutter or interference. For target-like interference (clutter) which is distributed, IPAR retains its improvement, whereas the other polarimetric phase processing techniques lose their advantage over conventional amplitude techniques.

1.2.4 SUMMARY OF RECOMMENDATIONS

The following recommendations are made in regard the system.

1. Continue the analysis of the advantages of IPAR under multipath conditions for surveillance and track radars.
2. Perform a measurements program to gather data from which a quantitative determination of S/I and multipath advantages can be made.
3. Plan for follow-on improvements, modifications, and growth in the present system to take advantage of current observations and planned automation.

   (a) Automated pulse-to-pulse code control by a processor for time side

lobe cancellations, etc.

(b) Increased correlation length.

(c) Multiple pulse correlations integrator.

(d) Analyze the LPI, ECCM, and target recognition (identification) potential of IPAR.

SECTION 2
IPAR HARDWARE CONFIGURATION

2.1 SYSTEM DESIGN

The system was designed as a minimum demonstration and data collection system. The goal was first to establish that the technique would work, once reduced to practice, and to collect data in the future which could be used to quantify the relative advantages.

Some of the overall design goals in addition to implementing the basic technique were as follows:

(a) To achieve a 100 MHz correlation and compression rate.

(b) To be able to correlate and compress using noncoherent techniques and a wide bandwith noise rf carrier.

(c) To permit growth for future processor or computer control and data analysis.

(d) To have the ability to range gate and replay correlation data for quick on-site observation and analysis.

Figure 1 shows the resulting system. Functionally, the system may be viewed as two subsystems: the RF subsystem and the IPAR processor subsystem. Sections 2.2 and 2.3 describe these two subsystems. The basic system operation is described in the following paragraphs.

The basic system includes a master oscillator power amplifier (MOPA) radar transmitter. There appeared to be ways to implement the technique with a single channel high powered oscillator, but it was considered to be too risky and less flexible than a two channel MOPA approach.

The two channels are connected to the vertical and horizontal inputs of a dual polarized antenna feed. Whenever a 90° phase relationship exists between the two channels, the resultant transmission is circularly polarized. By switching the phase relationship to a negative 90°, the opposite sense circular polarization is transmitted. By switching in accordance with an advantageous coding sequence, a pulse is transmitted which is coded right and left circular. Of course, various elliptical polarizations could also be generated. The returned signal would have the code preserved or reversed with great fidelity if it were backscattered from certain simple structures.

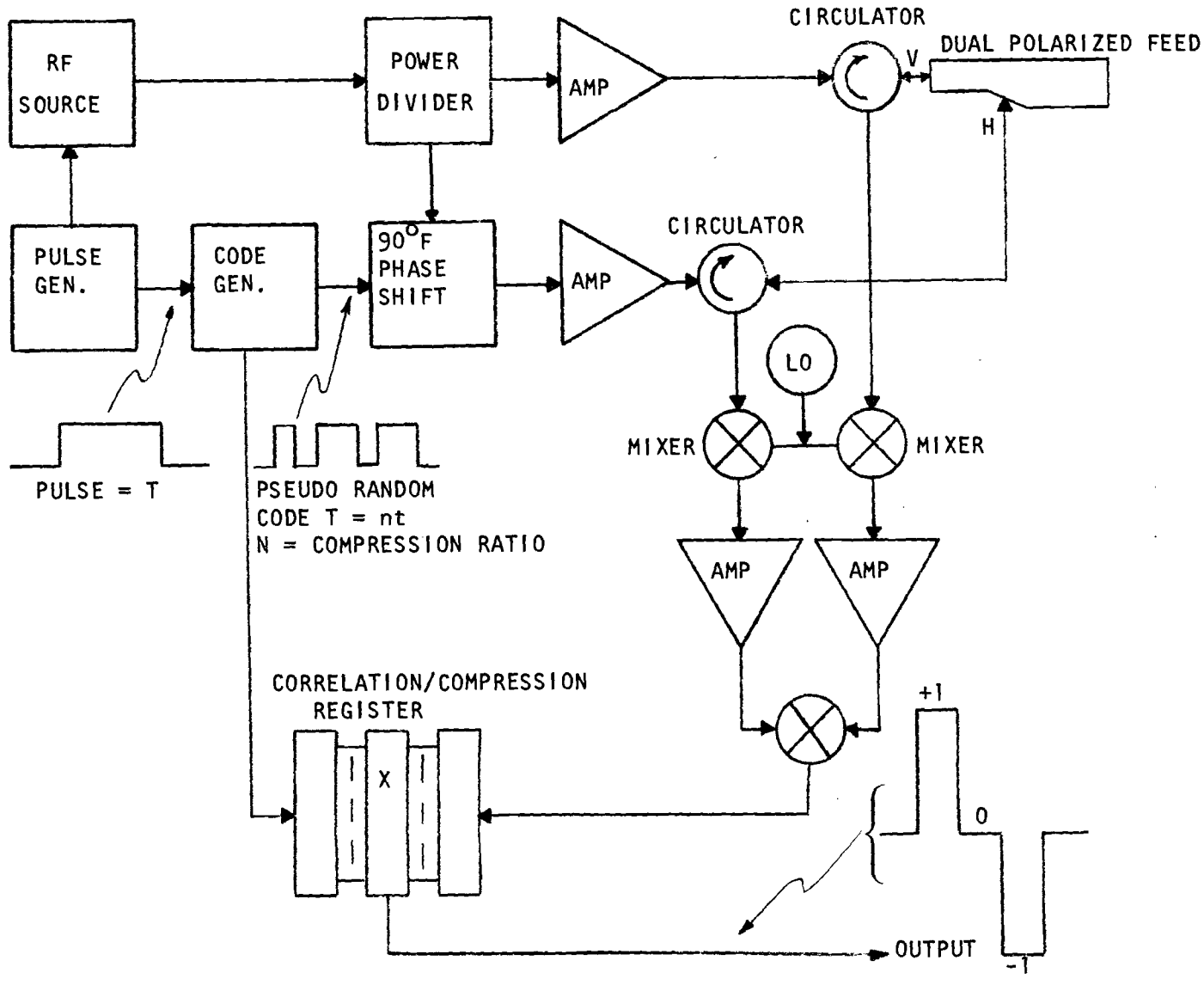

FIGURE 1. IPAR block diagram.

Noise, unlike the return from simple scatterers, would result in a random code for the return signal. Hence, a signal to noise advantage is gained relative to a simple narrow pulse radar with the same resolution. The signal to noise gain results from the compression, as in any bi-phase modulated pulse compression radar. The difference lies in the fact that IPAR does not require a coherent phase shift reference, directly or indirectly, as do other such compression techniques. In fact, IPAR correlates and compresses returned signals even if the RF carrier is true wide bandwidth random noise. This may be the first radar to accomplish this feat.

The phase shift for one channel as referenced to the other is achieved at low power level due to the speed limitations of high powered phase shifters. This is the reason the experimental system was built with two high power amplifier channels. The phase shift of one channel is accomplished at low power using a mixer. The phase shifts could conceivably be accomplished at rates in excess of 2 GHz for the devices used. The mixer (i.e., phase shifter or phase modulator) has the characteristic that a high level signal (i.e., +1) at the IF port causes one phase transfer from the input to output, whereas a low level signal (i.e., -1) causes a relative phase shift of 180°. With a permanent 90° phase shift added to the 0°, 180° phase shift combinations, the result is -90°, 90°. Hence, the required phase relationships are generated for the coded right and left circular or complimentary elliptical polarization transmissions, and the coded transmissions may be at a high data rate with a non-coherent carrier, even noise.

Obviously, the input for the phase modulator is compatible with digital techniques. The digital code which is applied to the modulator is generated by recirculating the code from the output to the input of a shift register during the transmit time interval. The shift register is one of the two contained within the high speed digital correlators. After each transmission, the code is retained in the correlator for correlation and compression of the returned signal.

As in transmission, two receive channels are employed. As the signals in the two receive channels are translated down in frequency, the relative phase between the two signals is retained. Finally, the two signals are applied to a phase detector. The polarity and amplitude of the resultant bi-polar video

contains the phase coding impressed on the transmission and stored in the correlator; that is, if the return is of high fidelity and not noise-like. The high speed correlator clocks the returning code in real time at a maximum rate of 100 MHz, at present. Future VHSIC advances could update this rate considerably. Once the code has been extracted and input to the correlator, the remainder of the operation is like conventional bi-phase modulated pulse compression techniques. Prior to the phase detection, if a limiting amplifier has been used, the amplitude information will have been essentially destroyed and the processing is referred to as Phase Only Pseudo Coherent Detection (PO PCD). Mathematically, the results of this technique may be approximated by a nonlimited PCD model which includes Instantaneous Automatic Gain Control (IAGC). Each of the techniques, PCD without amplitude limiting and PCD with IAGC, are analyzed in Section 4. IPAR, of course, has the additional features of correlation and compression of the coded waveform.

2.2 DIGITAL HARDWARE

The IPAR digital processor is designed to provide a flexible, complete and self contained radar signal correlation processor. It may be operated in a stand-alone mode, under front panel control, or connected to and controlled by a minicomputer or microcomputer. The processor is capable of correlating received signals in real time with the stored reference code at selected rates up to 100 MHz. The operator has freedom to independently determine the transmitted code, subpulse width, PRF, and range gate setting to achieve his objectives. The design philosophy followed for this processor was to provide a logical, complete, and easily used system.

Figure 2 presents a simplified block diagram of the digital processor and its interfaces to the external world. The slower TTL processor (to 6 MHz) may be considered the host or control portion of the unit which interfaces with the front panel controls and the control computer (when provided), and determines the operational mode of the processor. The high speed (to 100 MHz) ECL processor interfaces with the radar, generating the transmit and coding signals, receiving the video from the radar, range gating, and performing correlation processing in real-time.

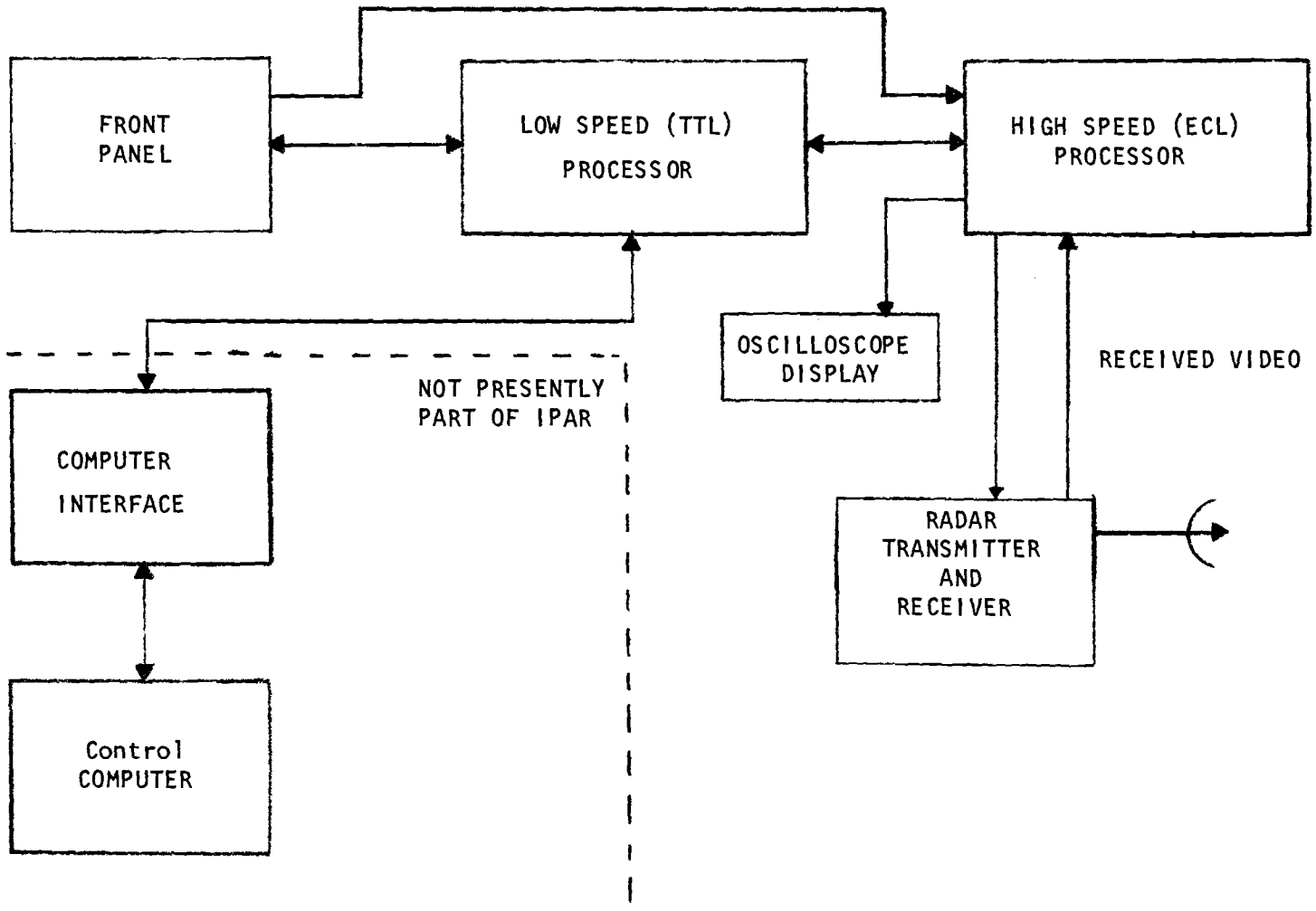

FIGURE 2. IPAR digital processor block diagram.

The heart of the system is a pair of correlator chips, designated the "32-DOC," which were designed and built by TRW under contract to the Naval Research Laboratory. The high speed requirements of the devices necessitated the use of emitter coupled logic (ECL) internal to the chip; this in turn required ECL to be used externally to those devices in the IPAR processor. The reader is referred to Reference [1] for a complete description of the correlator chips.

Table 1 presents a list of the capabilities of the digital processor. Most of these features are self explanatory and the others will be explained more fully in the following sections. Table 2 lists the inputs to and outputs from the digital processor and provides a brief desciption of each of their functions.

2.2.1 DIGITAL PROCESSOR STATUS

All functions, except one, originally planned and designed into the processor are checked out and operating. The digital output from the 32-DOC correlator chips does not work properly. This appears to be caused by a malfunction in the chip itself. Four different chips were tested in the IPAR processor, but the digital output did not work on any of the four. Thus, the digital correlation output is not functional. Similarly, the digital detection output does not operate. The analog output also suffers from an error on the correlator chip itself in that the 32nd bit does not produce a correlation output. This error is fully explained in Reference [1]. Computer interfacing has been checked as much as possible without a computer.

The digital processor has been successfully interfaced to an X-band radar system and demonstrated both in the laboratory and in field tests.

2.2.2 CORRELATOR DESIGN THEORY

Figure 3 presents a block diagram of the 32-DOC correlators used in the IPAR digital processor. They consist essentially of two independent 32-bit shift registers. In use, the transmit, or reference, code is stored in the A register, and the quantized received signal is clocked through the B shift register. The maximum clock rate of either shift register in the IPAR processor is 100 MHz, yielding the minimum 10 ns subpulse length. The correlator

TABLE 1. IPAR DIGITAL PROCESSOR CAPABILITIES

Subpulse Length: 10 - 160 n
(100 - 6.25 MHz)

PRF: 500 - 8000 Hz Plus Manual

Any Binary Code Up To 32 Bits Long

Range Gate: 0 - 15 km,
0.75 m Maximum Accuracy

Correlation Processor

True Correlation For 32 Bit Code Length
Pseudo Correlation For 1 - 31 Bit Code Lengths

Adjustable Digital Threshold

Built-in Self Test/Calibration

Convenient Front Panel Data Display

Status Register
Reference Words
Digitized Received Signals

Designed For Computer Controlled Operation

Replay of Correlation function From Range Gate Location

TABLE 2. INPUTS AND OUTPUTS OF DIGITAL PROCESSOR

Radar Interfaces (Rear Panel BNC connectors)

Signal	Function
TWT 1 on and TWT 2 on	TWT's VDC when active. Enable high and low power TWT prior to transmit pulse and disable at end of transmit pulse.
MOD 1 PULSE	Small positive voltage (N1V) at 20 mA when active. Turns an isolation modulator/mixer during transmit pulse.
MOD 2 CODE	Low voltage (N±1V) bipolar signal at ± 20 mA when active. Drives coding modulator/mixer during transmit pulse.
LOCK 1 interval (XMCK) transmit	ECL level clock output coincident with subpulse coding occurring during transmit pulse. Used for controlling frequency.
LOCK 2	ECL level clock output coincident with subpulse coding interval occurring at the range gate time. Used to control the LO during receive.
VIDEO	Input phase detected video from radar ±0.250 V.

FRONT PANEL OUTPUTS (Front Panel BNC connectors)

Video Out	Correlated video signal. Real time video to range gate time. Replay of range gate correlation after that.
Det. Analog	Thresholded correlated video signal. Output goes to low state when threshold is exceeded.
Digital Det.	Not connected.
Sample clock	Not connected.

Range Gate	Not connected.
MSYNC	Master Sync. signal occurs prior to transmit.
Replay Sync	Sync signal coincident with replay interval.
XMIT Sync	Sync signal coincident with start of transmit pulse.

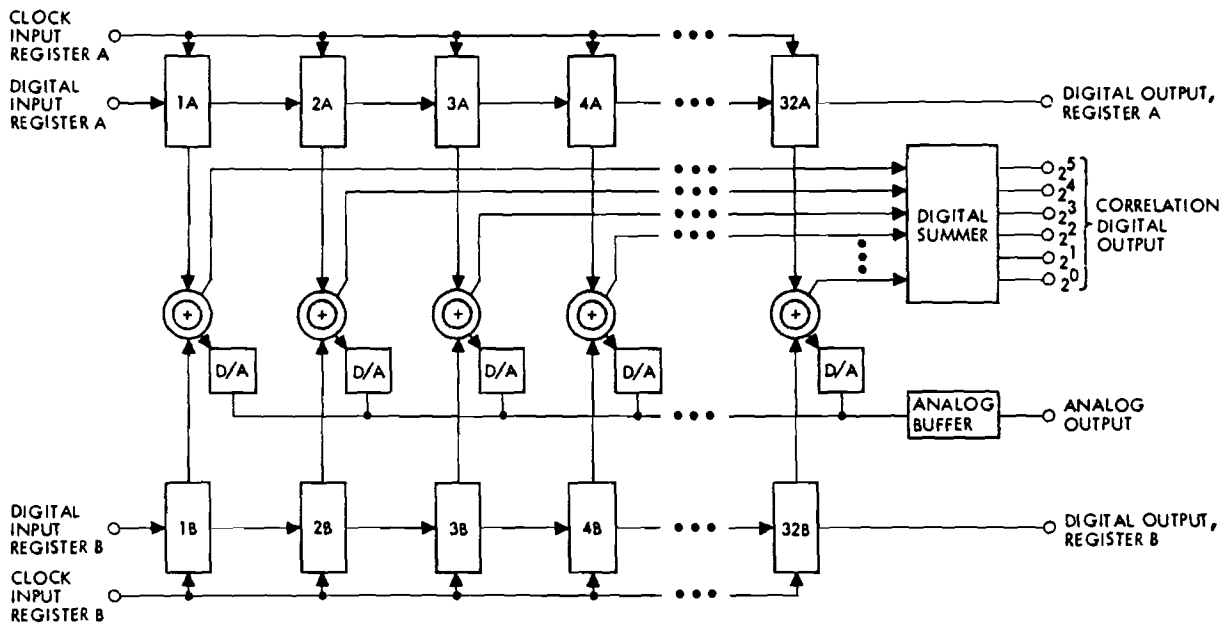

FIGURE 3. 32-DOC correlator block diagram.

compares the contents of each shift register, bit-by-bit in 32 exclusive-OR circuits. The digital summer then counts the number of zeroes (which indicate bit matches between the A and B registers) and theoretically outputs that number, which is between 0 and 32. Each exclusive-OR circuit controls a digital-to-analog (D/A) current source. The output currents are summed into a common mode to yield the output correlation function.

The IPAR concept requires that the received signal be quantized into three states: +1, 0, and -1. This is done as shown in Figure 4 through the use of two thresholds. Since digital circuitry quantizes data into only two levels, more than one correlator integrated circuit (IC) is required. It was originally anticipated that three binary correlator chips would suffice. Analysis indicated that two correlators are adequate for codes of maximum length (32) with no zeros in the code. For codes of less than 32 bits or with interspersed zeros, four correlator chips are required for perfect operation. However, the use of two binary correlators for codes of less than 32 bits provides a usable pseudo correlation, especially if an appropriate filler is employed in the unused bit positions. Future designs should use correlators that have a programmable word length. A brief derivation of these results is contained in the following paragraphs.

In general, a correlation function is composed of eight parts as illustrated below.

	Transmit Reference	Received Signal	
1.	+1	+1	plus terms
2.	-1	-1	
3.	+1	-1	negative
4.	-1	+1	terms
5.	0	-1	non-
6.	0	+1	contributing
7.	-1	0	terms
8.	+1	0	

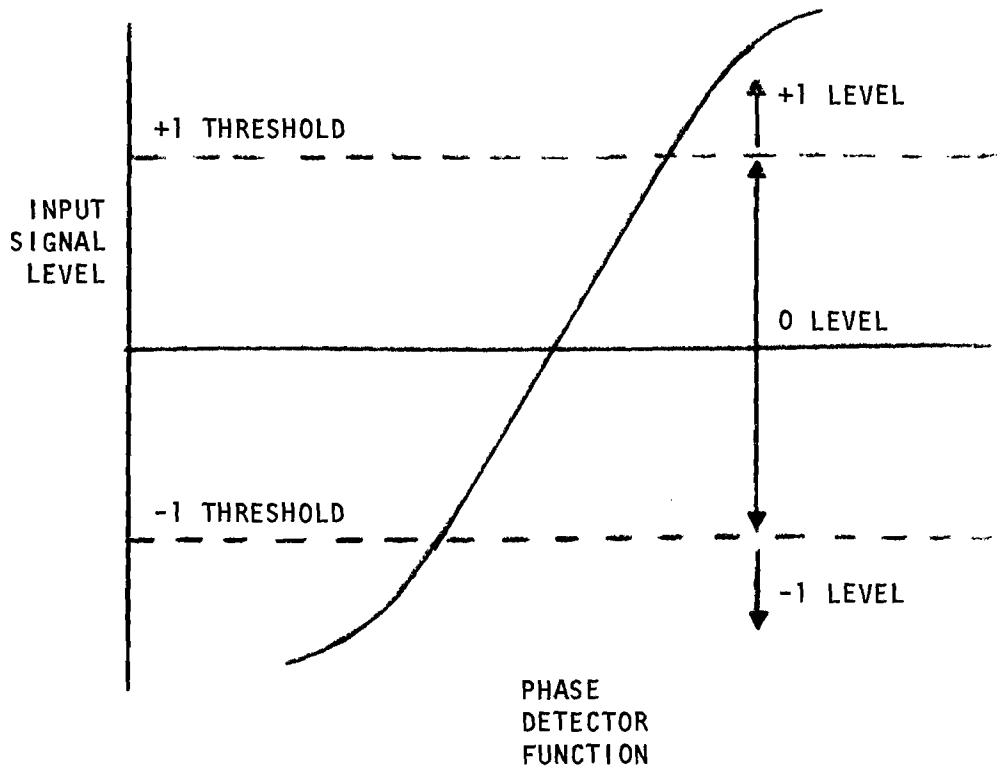

FIGURE 4. Received signal quantizations.

It is desired to quantize the transmitted and received signals to achieve the above results. There are six ways to quantize a three state signal into binary form:

1.	A:	(+1) →1;	(0, -1) →0
2.	$\overline{A}$:	(+1) →0;	(0, -1) →1
3.	B:	(+1, 0) →1;	(-1) →0
4.	$\overline{B}$:	(+1, 0) →0;	(-1) →1
5.	C:	(+1, -1) →0;	(0) →1
6.	$\overline{C}$:	(+1,-1) →1;	(0) →0

The minimum number of binary correlators required is two, because one is needed for positive correlations and one for anti-correlations. The output of the anti-correlation chip, or negative term, is subtracted from the positive correlation to yield the correct result. When the quantization schemes are correlated against each other, there are eight candidate positive terms and eight candidate negative terms, as listed below.

Candidate Correlation Terms

Positive	Negative
$A * A$	$A * \overline{A}$
$\overline{A} * \overline{A}$	$\overline{A} * A$
$A * B$	$A * \overline{B}$
$\overline{A} * \overline{B}$	$\overline{A} * B$
$B * B$	$B * \overline{A}$
$\overline{B} * \overline{B}$	$\overline{B} * A$
$B * A$	$B * \overline{B}$
$\overline{B} * \overline{A}$	$\overline{B} * B$

Where * indicates the correlation function.

Examination of the non-contributing terms indicates that it is not possible to obtain a perfect correlation function from only two correlator chips. In each case, a signal quantized as zero produces an output where none is desired.

Similar reasoning indicates that three correlators will fail for the same reasons. Only when four correlators are used will the perfect correlation function result. The use of four correlators was not justified, however, because of the extra circuit complexity and risk involved. As an alternative, various bit patterns were investigated to fill the unused bits. These patterns included all ones or zeros and alternating ones and zeros. The alternating pattern of ones and zeros with the transmit code right justified in the correlator seemed to yield the "best" results from the standpoints of lowest time sidelobes and similarity to the time correlation function. Thus, this technique was adopted for the IPAR processor.

The correlation functions and quantization schemes used in the IPAR processor are $A * A - \overline{B} * B$, where the first letter indicates the reference quantization scheme.

2.2.3 HARDWARE DESCRIPTION

The detailed block diagram of the IPAR digital processor shown in Figure 5 indicates the seven major components as well as the power supply connections to each of those components. The following subsections describe each of those parts in more detail.

2.2.3.1 Chassis, Power Supplies and Back Panel

The IPAR digital processor is contained in a 12-inch high, standard 19 inch wide, rack-mountable drawer. Side handles facilitate carrying the unit. Internal air circulation is provided by an AC powered "boxer" fan blowing across the wire-wrapped logic cards. Figure 6 illustrates the three individually fused power supplies which provide the four main voltages of +5 VDC at 8 amperes, - 5.2 VDC at 8 amperes, + 15 VDC at 3 amperes, and -15 VDC at 3 amperes. Two auxilliary TO-3 regulators mounted to the chassis provide -2 VDC used for ECL terminations and -6 VDC used for powering the 32-DOC correlators. Single-point grounding of the power supplies and input AC power

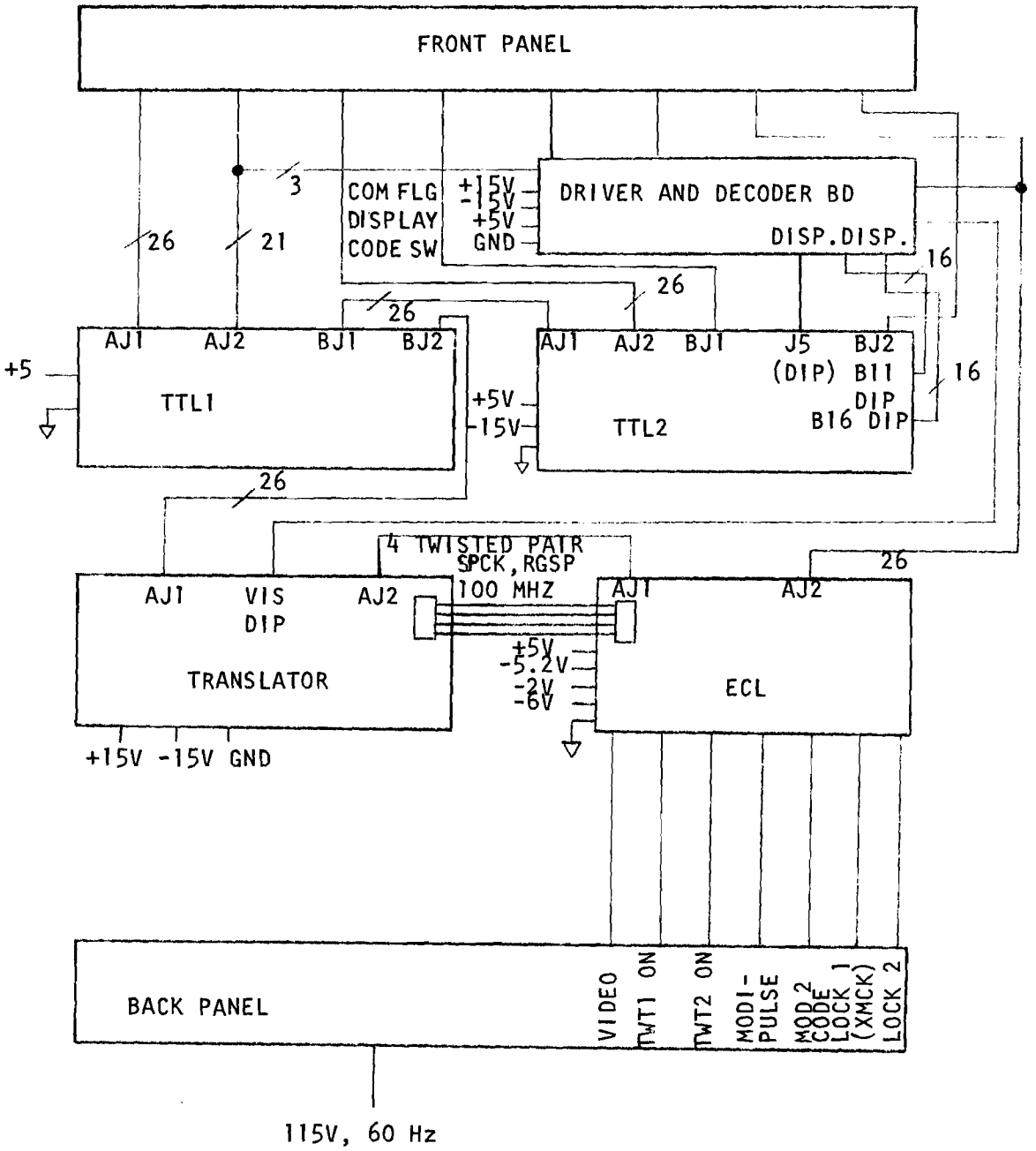

FIGURE 5. Digital processor detailed block diagram.

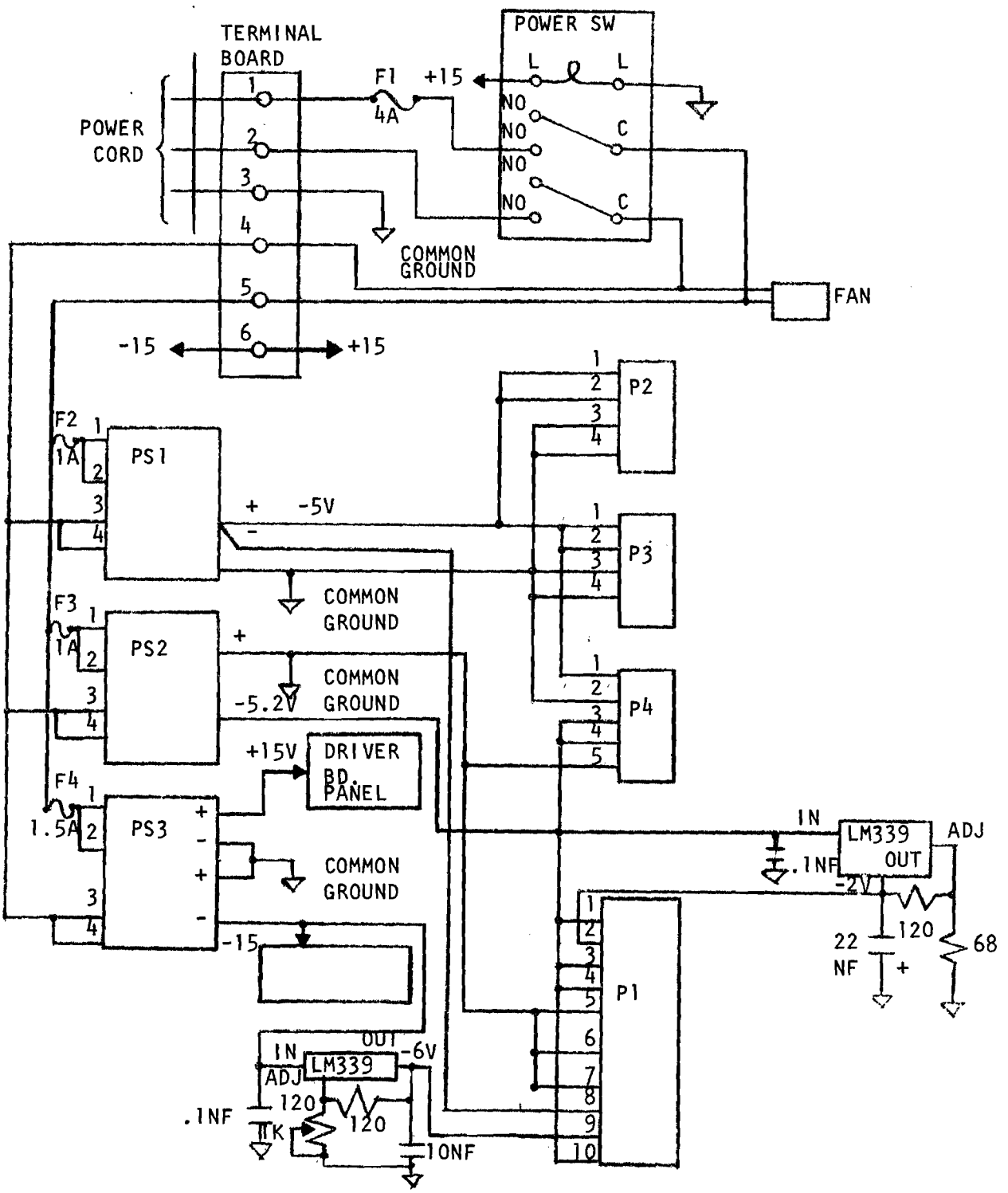

FIGURE 6. IPAR drawer power distribution.

eliminates the possibility of ground loops. Primary power is 115 V, 60 Hz AC at 4 amperes. All connections to the radar, as described in Table 2, are via back panel BNC connectors. The four main digital cards (TTL1, TTL2, the Translator and the ECL board) are mounted on stand-offs from the classic shelf. The TTL boards are mounted on the bottom. An aluminum shield separates the TTL board from the ECL boards and helps to eliminate noise pickup by the ECL circuits. All boards are of wire-wrap construction.

2.2.3.2 Front Panel

The IPAR digital processor front panel is illustrated in Figure 7. The function of each switch is noted below.

32 Code Input Switches: Used to input the desired transmit code and reference codes. The right-most switch is the first bit transmitted. Codes less than 32 bits should be entered right justified.

Code Length: Used to input the desired code length.

Three Reference Switches: Used to load the transmit and reference codes into the processor. The left most of these three switches is a momentary action switch; when this switch is moved upward from the AUTO position, the code is loaded into the A reference and $\overline{B}$ registers as selected by the Code Input and Code Length switches, and unused bit positions are automatically filled with alternating ones and zeros. The Load A and Load B switches have no effect when the third switch is in the AUTO position. When the left most switch is in the MAN position, the LOAD A switch loads the A Reference register exactly as the 32 Code Input switches are positioned. The transmitted signal will be the code input by the LOAD A switch with the length controlled by the Code Length switch. The LOAD $\overline{B}$ switch, with the AUTO/MAN switch in the MAN position, loads the $\overline{B}$ reference exactly as indicated by the 32 Code Input switches. Note that the Code Input and Code Length switches have no effect until loaded by one of the three reference switches.

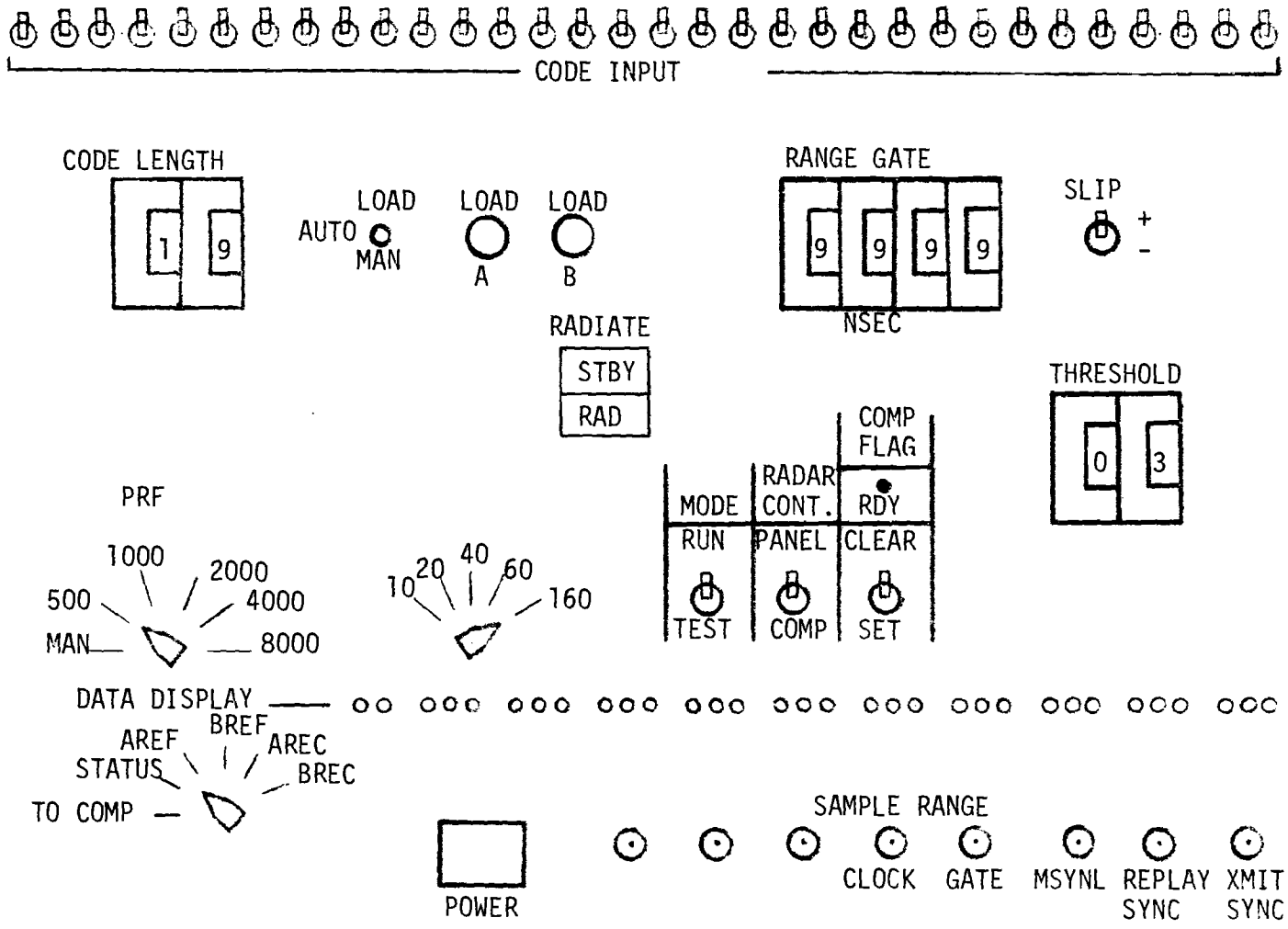

FIGURE 7. IPAR digital processor front panel.

Range Gate: The IPAR processor correlates the received signal in real-time until the range gate time (after the start of the transmit signal) is reached. At that point, 32 more samples are taken, at the subpulse clock rate, and stored. The 32 A quantized received samples are concatenated with 32 zeros and the 32 B received samples are concatenated with 32 ones. These 64 bit long sequences are then circularly shifted through the correlators to provide the replay function. The replay occurs at a slower rate than the real-time signal and continues until shortly before the next transmit pulse.

Slip: This switch changes ("slips") the range gate by one half the subpulse width. This prevents targets from "straddling" the range gates.

Radiate: Causes the digital processor to output the signals necessary to radiate coded RF energy.

PRF: Selects the pulse repetition frequency, from 500 Hz to 8000 Hz in powers of two. The MAN position allows a single transmission to occur each time the Radiate switch is depressed.

Subpulse Width: Selects the subpulse width from 10 n to 160 n in powers of two. Note that selecting the 160 n subpulse width automatically limits the PRF to be 4000 Hz maximum to prevent exceeding the duty cycle of the highpower TWT's.

Mode: Run position allows normal operation. The test position causes an all ones code of length 32 to be used as the A reference and A receive signal. Similarly, an all zeros code is used for the $\overline{B}$ reference and B receive signal. The resultant output is a triangle wave with maximum amplitude in both the positive and negative directions. Note that, if the radar is radiating, it will continue to do so in the test mode. Upon placing the switch to the Run position, the previously loaded code is again used.

Radar Control: Chooses either front Panel or Computer control.

Computer Flag and Ready LED: Has no effect when front panel control is selected. When Computer control is selected, this switch, when in the Set position, allows the computer to halt the processor by setting a flag bit. In the clear position, this flag bit is ignored. The RDY light emitting diode (LED) indicates that the computer is ready and has cleared the flag bit.

Threshold: Adjusts a positive threshold of a comparator circuit. A digital to analog converter changes the digital word to a voltage used by the analog output comparator. The range of useful thresholds is from zero to 32. The result of this thresholding operation is output on the Detected Analog and Digital Detection BNC connectors on the front panel.

Data Display: Controls data output from the digital processor. In the To Comp position, the control computer may select which data word is sent to the computer and simultaneously displayed on the 32 LED's. The five other positions display the data indicated below:

Status - displays a status word whose interpretation is indicated below:

Bit Position	Meaning				
0 - 15	not used				
16	Radar Control: 1 = Panel; 0 = Computer				
17	Computer Flag; 0 - Clear; 1 = Set				
18	Mode: 0 = Test; 1 = Run				
19	0	0	0	0	1
20	0	0	1	1	0
21	0	1	0	1	0
Subpulse Length	10	20	40	80	160

22		0	0	1	1	1	1
23		1	0	0	1	1	1
24		0	0	0	0	1	1
25		1	1	1	1	1	0
	PRF	MAN	500	1000	2000	4000	8000

26
27
28 Transmit Code Length
29 31 = LSB; 26= MSB
30
31

A Ref: Display A reference.

$\overline{B}$ Ref: Display $\overline{B}$ reference.

A Rec: Display the A receive signal stored by the range gate.

B Rec: Display the B receive signal stored by the range gate.

2.2.3.3 Driver and Decoder Board

This wire wrapped board is mounted to the back of the front panel and provides interface functions between the digital hardware and the front panel. A detailed block diagram is shown in Figure 8. Display drivers on this board are used for the 32 LED's of the data display, the Radiate switch lights and the Comp Rdy. LED. The two BCD to binary converters change the BCD thumbwheel switch output and convert it to binary for use in the following circuits. Finally, the D/A converter and buffer amplifier provide the analog threshold voltage to the analog comparator on the ECL board.

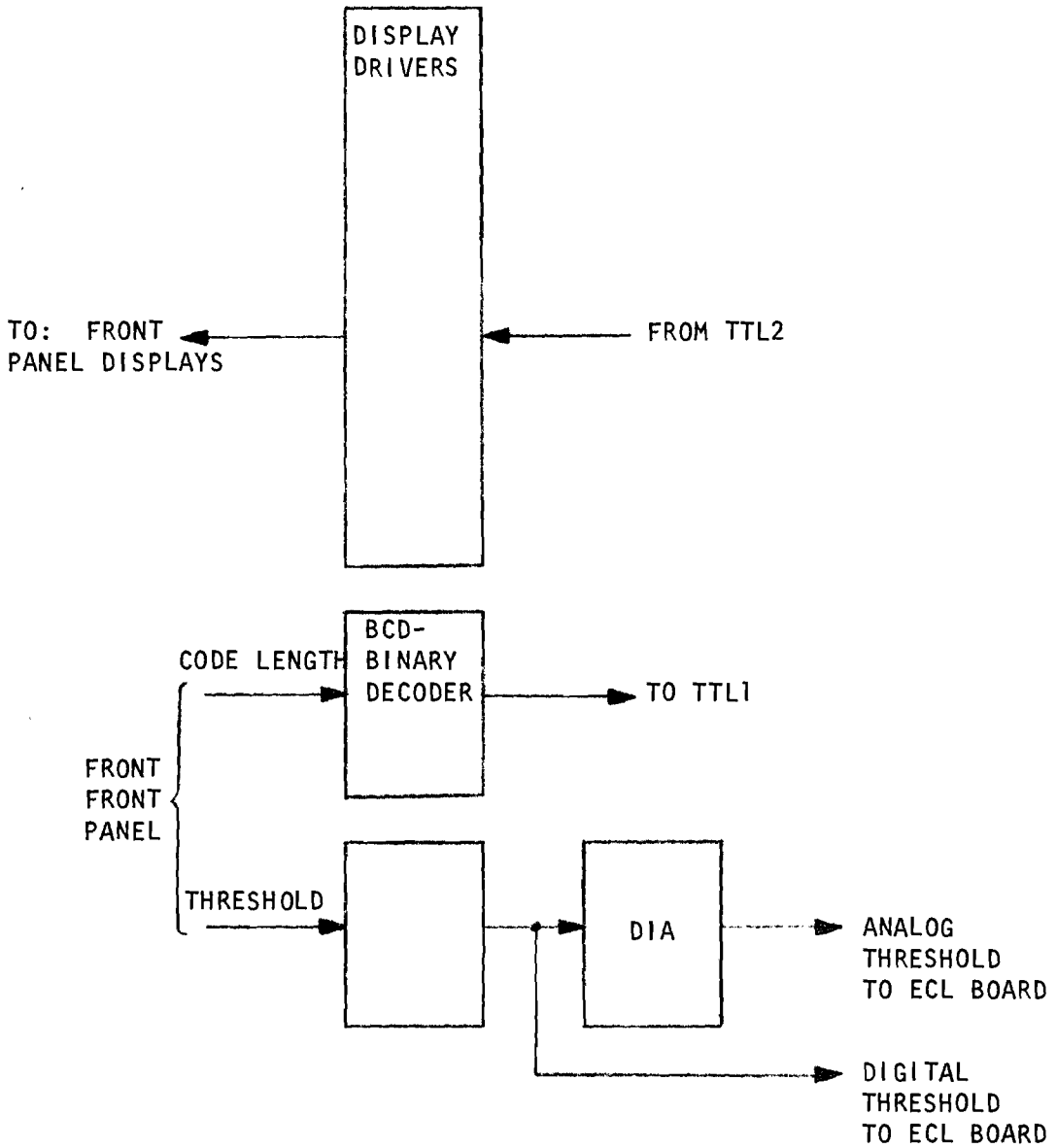

FIGURE 8. Driver and Decoder Board.

2.2.3.4 TTL 1

Constructed on a wire wrap board, this circuit generates most of the timing signals and performs most of the logical function required in the digital processor. A block diagram of the board is shown in Figure 9.

The MSYNC and clocks generator receive the 6.25 MHz continuous clock for the translator board and divides it by four to generate the internal 1.5 MHYz clock. MSYNC signals are continuously generated at a repetition rate determined by the PRF switch setting.

The replay clock and sync generator uses a DIP switch to program the replay clock frequency anywhere in the range from 94 kHz to 1.5 MHz. Also produced are replay syncs which occur once every 64 replay clock pulses and can be used to trigger an oscilloscope when viewing the replay correlation.

The transmitter enable logic accepts front panel switch inputs, status word inputs and control computer inputs, and combines them logically to enable the transmitter for the appropriate input conditions. Figure 10 is a flow chart of that logic. Note that, as a safety feature, the transmitter may only be enabled by, and may always be turned off by, the alternate action Radiate switch. A power-up clear circuit is included in the logic to insure that the transmitter is not enabled when power is initially turned on.

The internal timing generator produces most of the decoding clocks, latch strobes, etc., in the correct sequence for use in the IPAR digital processor.

The auto fill circuit uses the 32 Code Input switches as integral logic elements in its design to achieve automatic alternate +1 and -1 insertion into unused bit locations of the A and $\overline{B}$ reference words. Thirty-two pulses from the internal timing generator decode the binary code length word to determine the amount of fill required. This circuit does not operate when manual reference loading is chosen.

2.2.3.5 TTL 2

This circuit is also constructed on a wire wrap board. A block diagram of the circuit is given in Figure 11. The multiplexer and status latch chooses either front panel switch data or computer data to be used for the

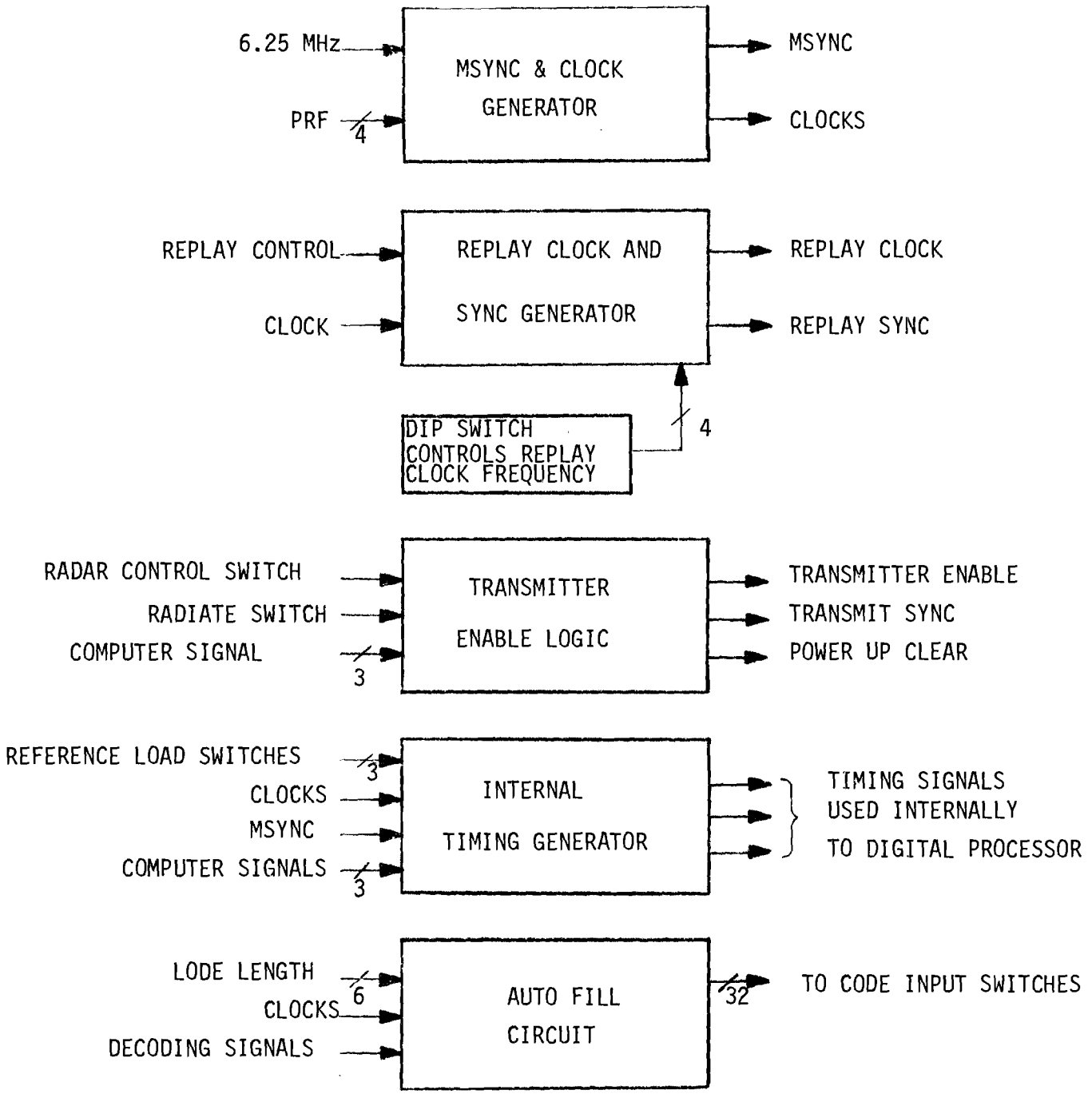

FIGURE 9. TTL1 block diagram.

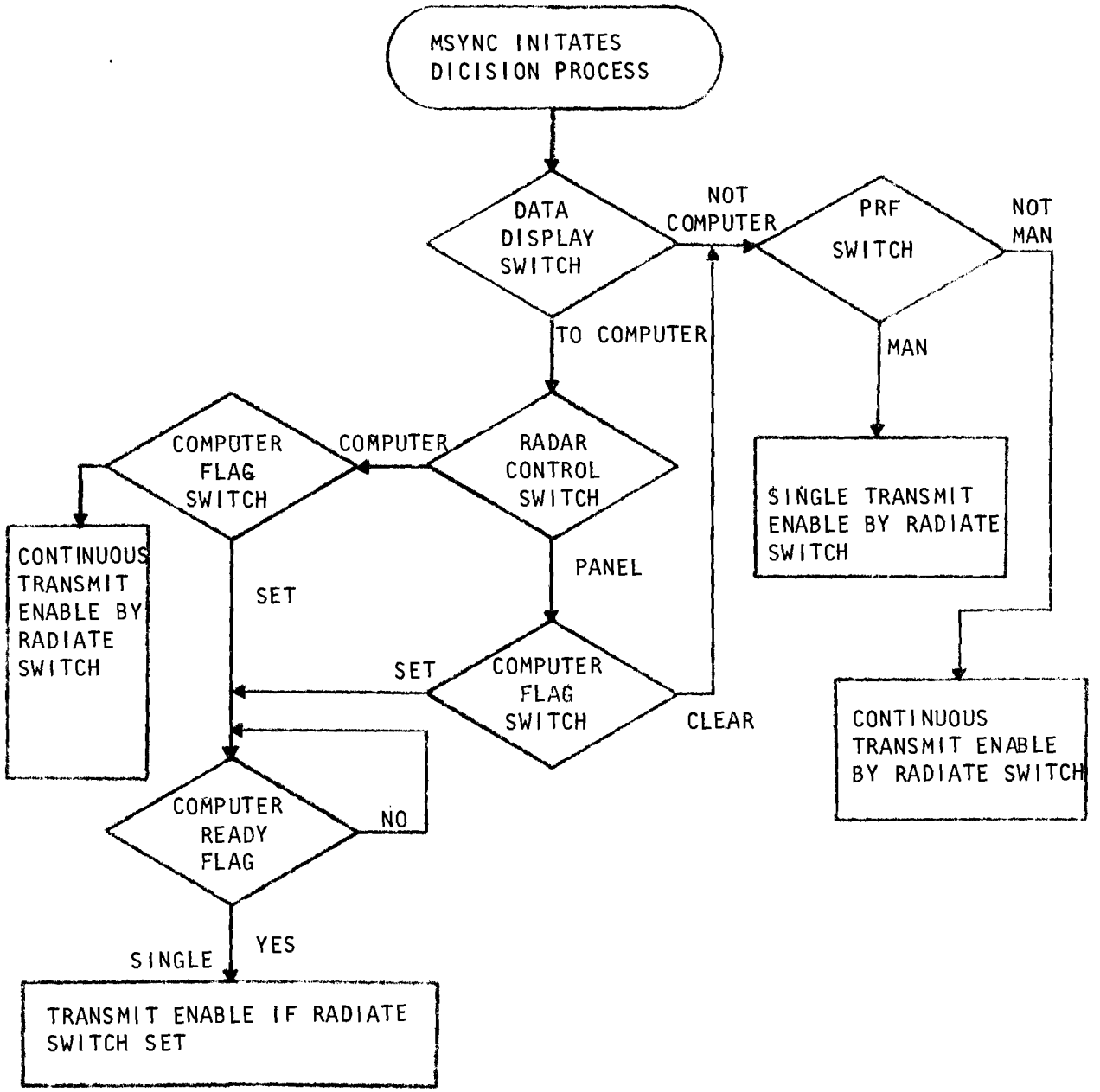

FIGURE 10. Transmit enable logic.

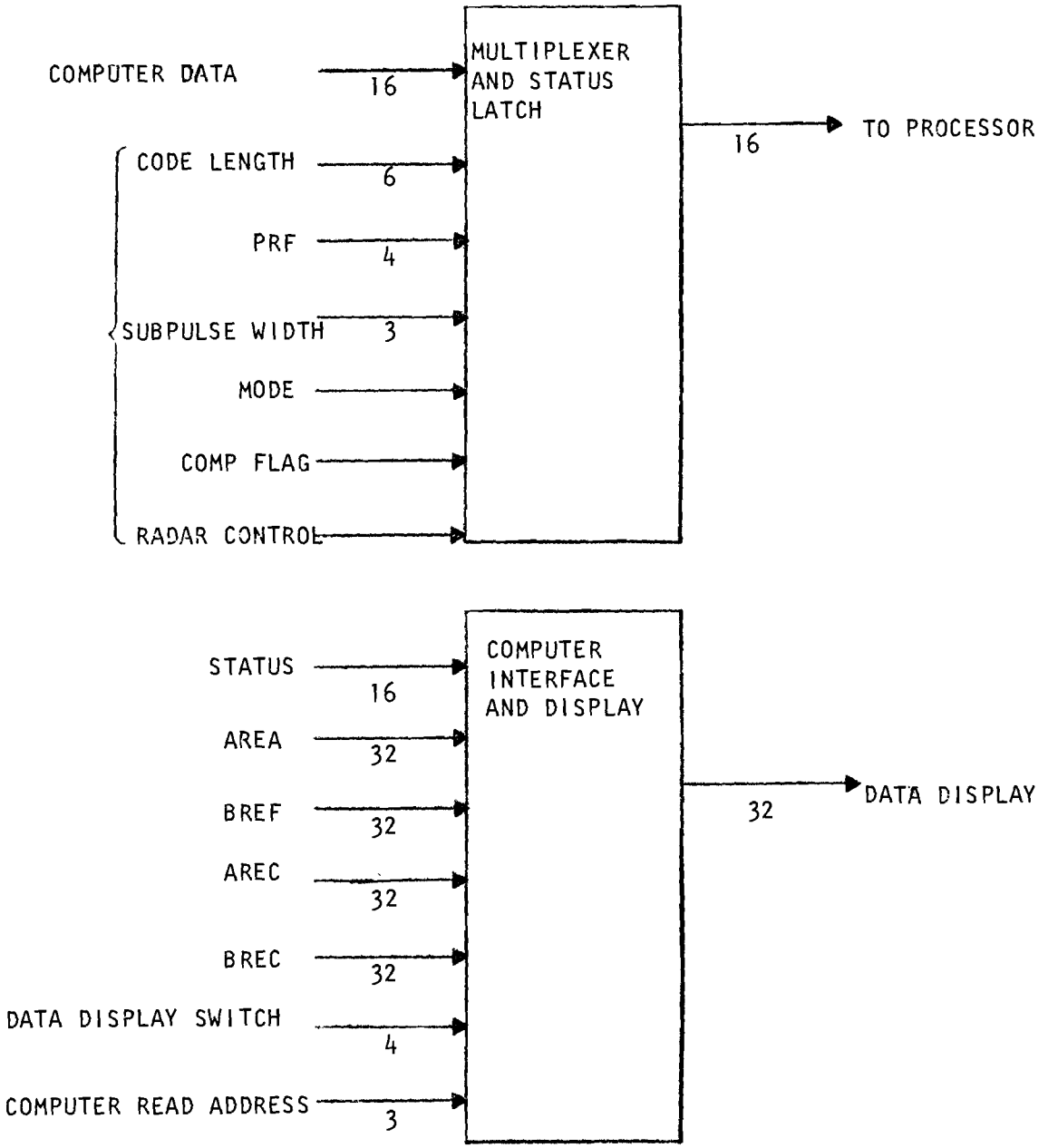

FIGURE 11. TTL2 block diagram.

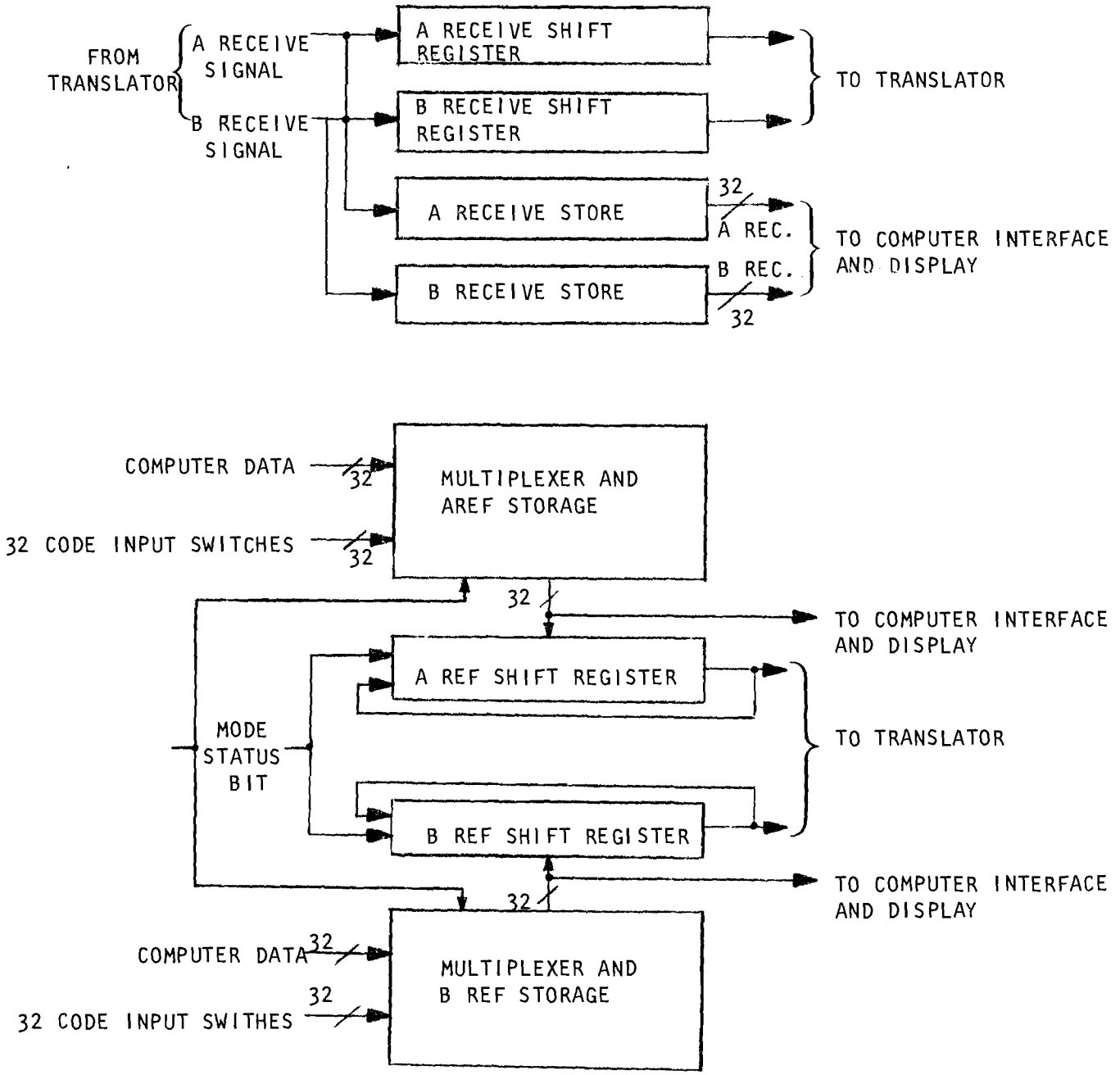

FIGURE 12. TTL2 block diagram (continued).

status word as determined by the Radar Control switch. The output of the status latch, designated the status word, is used to control the digital processor operation.

The computer interface and display circuit accepts the five inputs shown in Figure 11. The data displayed on the 32 LED's is determined by the position of the Data Display switch and, in the TO COMP position, by the read address specified by the control computer.

Quantized data received at the range gate time are stored and shifted through the A and B receive shift register and store circuit. The 32 bit shift registers are used in conjunction with the 32 bit shift registers of the 32-DOC correlator chip to provide the 64 bit shift register required during the replay function. The first time the range gated receive data is clocked into these shift registers, the A and B receive store circuits are enabled to gather the 32 bits of A and B data. These data are then stored, and may be examined until the next transmission occurs.

The final circuit of the TTL2 board chooses the appropriate source for the A and $\overline{B}$ reference words, stores this data and shifts it out serially to the Translator board. The radar control status bit determines whether computer data or the 32 code input switches are used for inputting the reference words.

2.2.3.6 Translator

The Translator wire wrap board serves two functions: first it translates signals to/from TTL voltage levels from/to ECL voltage levels; secondly, it generates the master clock signals used throughout the IPAR digital processor. Figure 13 presents a block diagram of this board. The translator functions are self-explanatory. The divider circuit uses the subpulse width selection to appropriately divide the 100 MHz master clock to obtain the subpulse clock. The range rate clock is the same frequency as the subpulse clock, but it may either be in phase or 180° out of phase with the subpulse clock depending on the position of the slip switch.

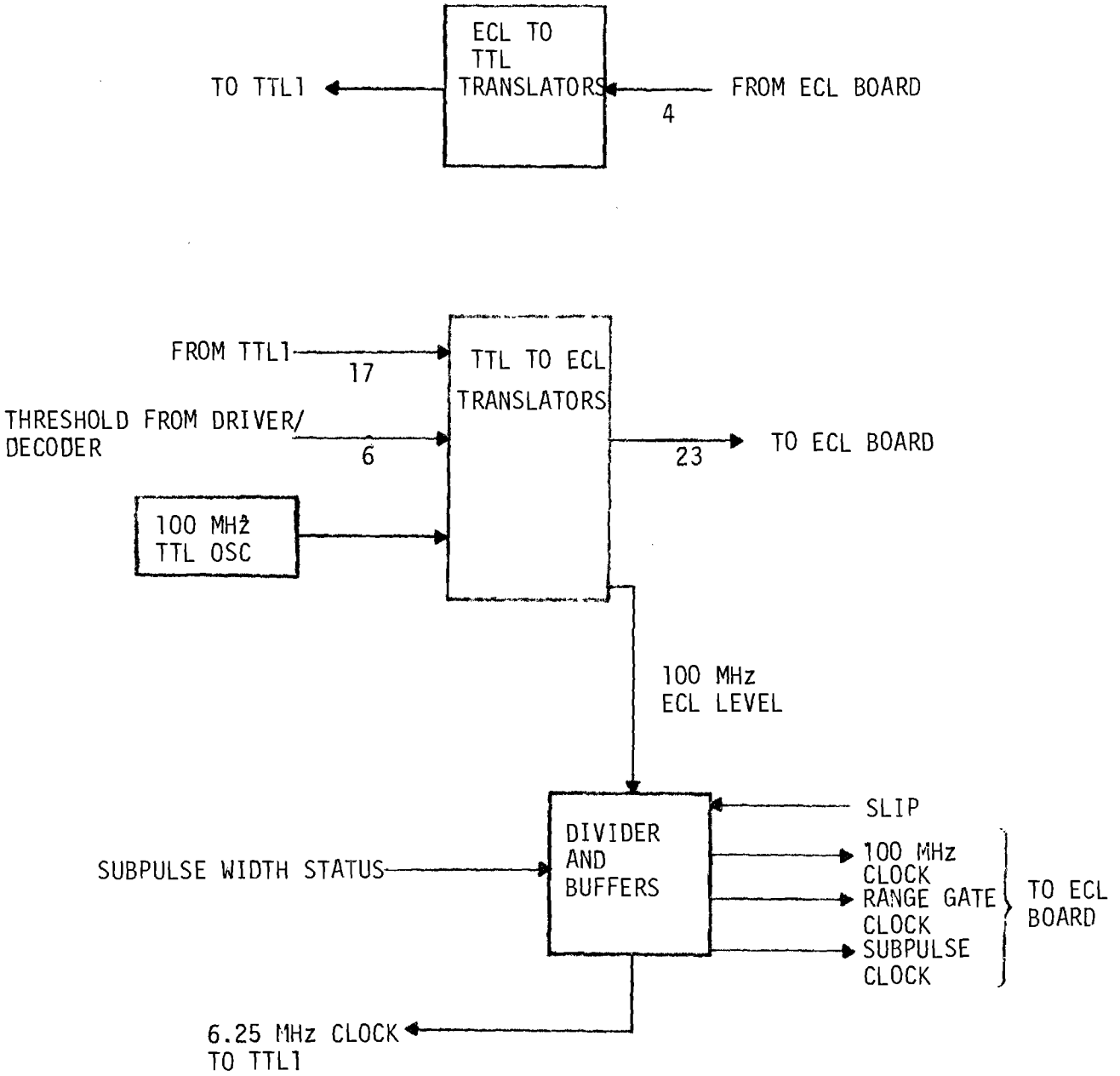

FIGURE 13. Translator block diagram.

2.2.3.7 ECL Board

The Emitter Coupled Logic (ECL) circuits are mounted on a wire wrap module and use the ECL 10,000 logic family. This board performs all of the high speed signal processing functions in the IPAR digital processor. Figure 14 is a block diagram of this board. As noted earlier, the heart of the signal processor is a pair of high speed 32 bit parallel correlators.

The high speed timing and control is slaved to the TTL logic which acts as the host unit. The A and $\overline{B}$ reference and code length are initially loaded into the timing unit and correlators shortly after the MSYNC signal. During this time, the reference multiplexer (Ref. Mux) at the input of correlator A selects the A reference input for loading the new code. After the TTL unit directs the ECL unit to transmit a pulse, the A correlator reference shift register is circularly shifted 32 places, through the reference multiplexer until it returns to its original location. This code is added with the code length signal and used to modulate the transmit signal. The B reference shift register in correlator B is not shifted at this time. The returning phase detected radar video signal is input to two comparator circuits with independent threshold voltages labeled VR1 and VR2. These comparators quantize the signal according to the A and B quantization schemes, respectively. The two correlators then sample the output from the comparators at times determined by the selected range gate clock width. As the quantized and sampled signal is clocked through the correlators, the correlation function is produced by subtracting the output of correlator B from that of correlator A. When the range gate setting after the transmit pulse is reached, 32 more samples are taken to fill the correlator with data from that range interval, and the sampling process is terminated. The stored data is then slowly circularly shifted out of the 32-DOC shift registers through the 32 bit A and B receive shift registers on TTL1 to produce the replay function. As noted earlier, the correlator digital outputs are not functional, but the analog output produces a usable signal. The threshold setting from the front panel thumbwheel switches is then applied to the complete correlation signal and may be reviewed on an oscilloscope as may the correlation signal itself.

In addition to the digital circuits on the ECL board, an input analog amplifier increases the level of the video signal from ±0.250 V to approxi-

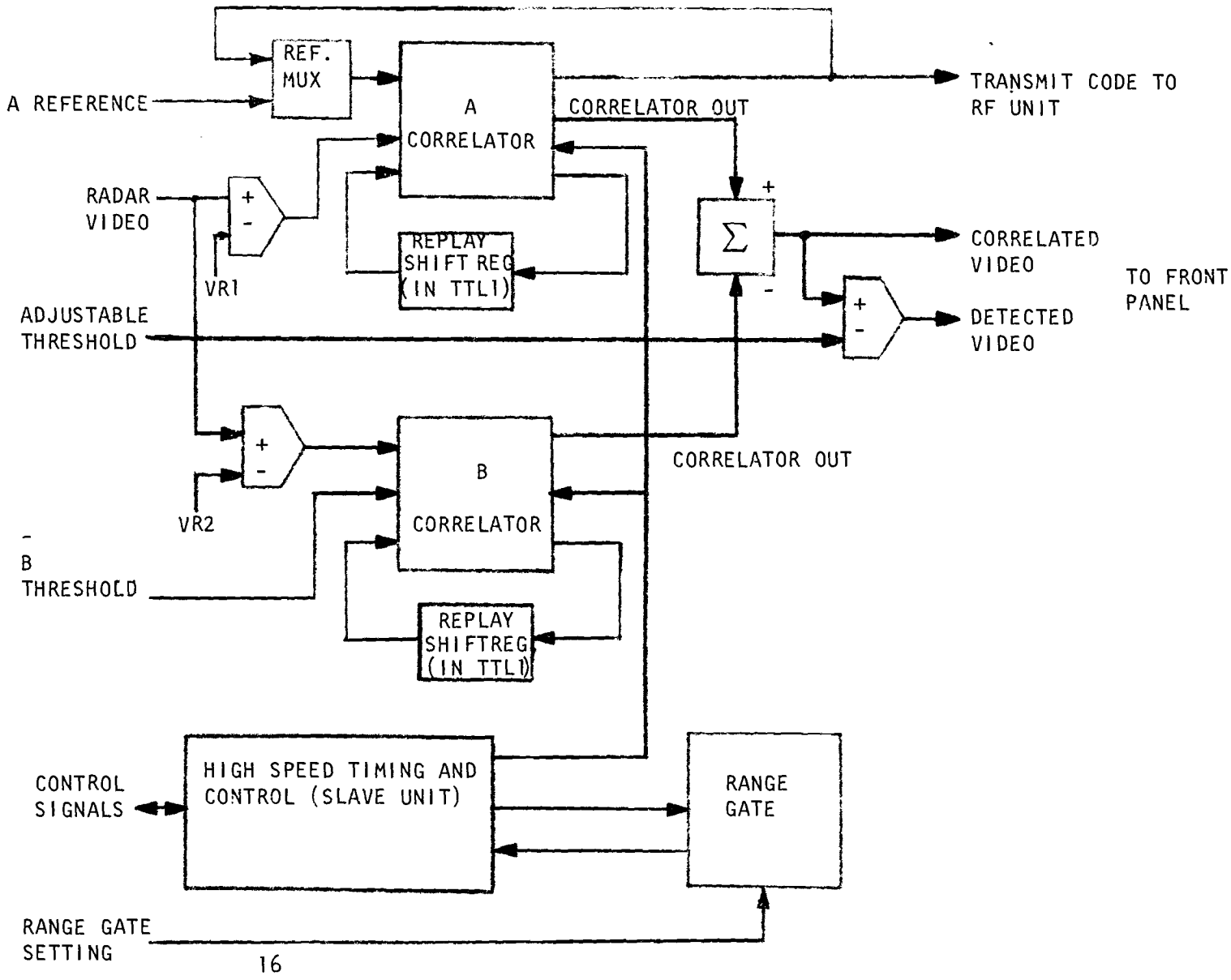

FIGURE 14. IPAR high speed (ECL) processor.

mately ± 1.7 V. Each of the signals to the radar (via the back panel) is also generated on the ECL board. The two TWT ON signals are level shifted by an ECL to TTL converter and amplified by an NPN transistor to the correct voltage level. The MOD 1 pulse signal is simply AC coupled through a 4.7 μf capacitor from an ECL buffer. The MOD 2 PULSE signal is transformer coupled.

2.3 IPAR RADAR

2.3.1 GENERAL

The IPAR concept requires that a polarization coded pulse be transmitted so that target reflection characteristics can be exploited in the detection process. The system described here uses a dual mode coupler at the antenna feed to combine two linear components of an X-band signal to generate a coded circularly-polarized signal. The two linear components of the radar return from a target are then compared in a phase detector to determine the phase between them. The output of the phase detector is used to determine the extent to which the target return is correlated with the original coded signal. A description of the transmitter and receiver sections of the IPAR radar is given below.

2.3.2 TRANSMITTER

The transmitter section of the IPAR radar consistsof a common oscillator source, power divider, two bi-phase modulators, a manual phase shifter, and two identical TWT amplifier chains. A block diagram of the transmitter-receiver is shown in Figure 15. The basic signal for the system is generated with a varactor tuned Gunn Oscillator. The oscillator typically has an output power level of 70 mW and is tuneable between 9.35 GHz and 9.75 GHz. An attenuator is included to adjust the power level into the bi-phase modulators to 7 mW. A 3 dB hybrid power divider supplies equal signal power to the two bi-phase modulators.

The polarization modulation is achieved by shifting the phase of one of the signals from a 90 degree leading phase angle to a 90 degree lagging phase

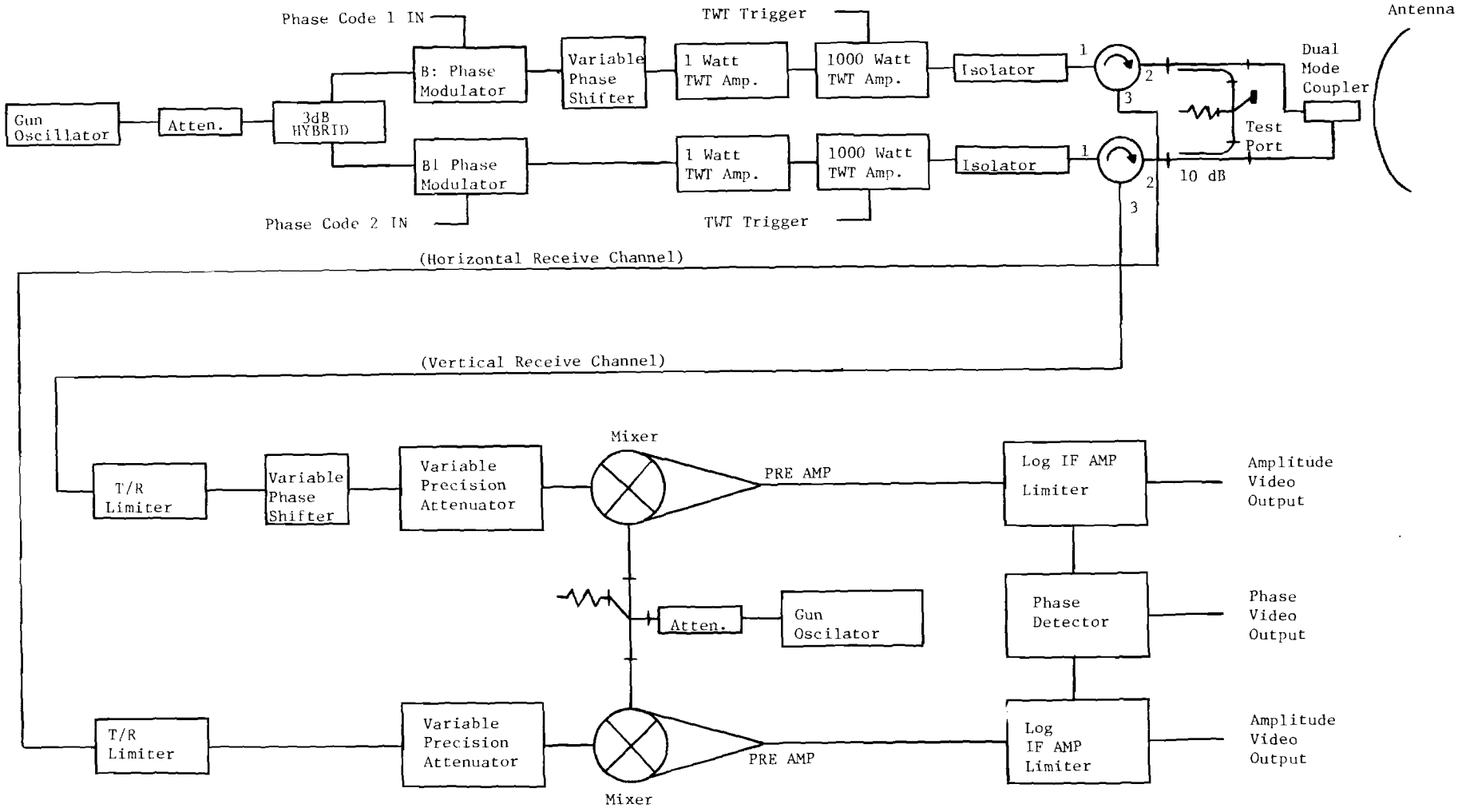

FIGURE 15. Transmitter receiver block diagram.

angle and recombining these two signals in a dual mode coupler located at the antenna feed horn. The required 180 degree phase shift is accomplished by supplying positive or negative currents, according to a predetermined code, to one of the bi-phase modulators. A constant current level is supplied to the other bi-phase modulator to generate a pulsed RF signal equal in length to the duration of the code. A phase shifter is included in the upper channel to aid in the initial set-up of the radar and to provide the required 90 degree phase difference between the two components of the radiated signal. Since the two components radiated from the dual mode coupler are spatially separated by 90 degrees, the resultant transmitted signal is right hand or left hand circularly polarized according to the code applied to the bi-phase modulator.

The two amplifier chains are composed of low power Traveling Wave Tube Amplifiers (TWTA) which boost the phase coded pair of signals to a level of approximately 1 watt, and high power pulsed TWTAs which further increase the signal power to a level of 1 kW. The low power TWTAs are Model 495A amplifiers manufactured by Hewlett Packard, Inc., and were purchased as standard stock items. The high power TWTAs were built for Georgia Tech by the Electron Tube Division of Litton Industries. Their amplifiers consist of type L-5655-59 Traveling Wave Tubes modulated by a Model M-624 modulator assembly. Specifications for these amplifiers are given in Table 3.

A four foot paraboloidal dish antenna is used in the IPAR Radar. This antenna has a dual mode coupler with a square linearly polarized feed horn located at the focus. The antenna can be rotated about its polarization axis so that any linear polarization can be generated by feeding one port of the dual mode coupler. The antenna is normally oriented so that the polarization of the transmitted signal is either horizontal or vertical, depending on which port of the dual mode coupler is selected as the signal path. The beamwidth and gain of the antenna are 1.8 degrees and 38 dB, respectively.

If both ports of the dual mode coupler are fed simultaneously, the signal radiated by the antenna can be generally described as elliptically polarized with either linear or circular polarizations being the limiting case. A rectangular waveguide port and video detector is provided at the center of the four foot dish to aid in the initial adjustment of the transmitter so that a circularly polarized signal results.

TABLE 3. TWT AMPLIFIER SPECIFICATIONS

Peak Power Output	1000 Watts
Frequency	8 - 12.5 GHz
Gain	35 dB minimum
Noise Figure	40 dB
Duty Cycle	2%
Pulse Width	0.2 to 15 μs
Input Gate Amplitude	+6 to +15 Volts
Input Gate Width	0.2 to 15 μs
Input Voltage	120 VAC ± 15%
Input Current	8 Amptere at 120 VAC

2.3.3 RECEIVER

The antenna is linearly polarized so that only the horizontal and vertical components of the reflected signal are received by the antenna. Two identical receivers are provided to detect these signals. Each receiver is equipped with a precision waveguide attenuator for calibration purposes, and one receiver channel has a phase shifter which is adjusted to compensate for any slight differences in path length between the two antenna ports. The mixer-preamplifiers operate at an intermediate frequency (IF) of 300 MHz and have a bandwidth of 100 MHz. The two (model DM8-12/300) mixers are fed with a common local oscillator similar to the oscillator source used in the transmitter. The detected 300 MHz IF signals are amplified by two (model 1CLT-300-B) logarithmic amplifiers. These amplifiers have both a detected video output and a limited IF output.

The amplitude outputs from the logarithmic amplifiers are used to measure the radar cross section of radar targets. The two limited IF outputs from the logarithmic amplifiers contain the phase information which is used in the IPAR correlation processor to determine the degree of correlation between the transmitted code and the received signal. A double balanced mixer is used to detect the phase difference between the horizontal and vertical components of the received signal.

2.3.4 DATA COLLECTION SYSTEM

The radar system was designed for the purpose of collecting data which would allow a theoretical evaluation of the IPAR technique. For this purpose, a bank of five range gated sample and hold circuits are used to collect amplitude and phase data and to sample the correlation function. The output of the sample and hold unit represents the time history of the radar signal received from a given range cell. This unit is capable of capturing and reproducing events which occur in times as short as 20 ns. The outputs from the sample and hold circuits are recorded along with the radar PRF on a 7 track FM tape recorder. These recorded data can then be returned to the laboratory for analysis.

SECTION 3
IPAR DEMONSTRATION

The IPAR system was successfully demonstrated during the first quarter of calendar year 1981. The official observer was Mr. Charles Jedrey of the Naval Sea Systems Command (Code 62 R 13). A briefing was provided prior to the demonstration in which the purpose of the demonstration, and what was to be demonstrated, were discusssed. A detailed functional block diagram similar to Figure 14 was used to explain system operation. The operation and function of each control on the equipment was explained.

Several simple targets (e.g., corners) were positioned at various relative geometries during the demonstration. Different types of targets were shown to have expected correlation characteristics. The nature of the correlation function was demonstrated. It was also demonstrated that right and left circular polarization coding rates up to 100 MHz were being transmitted, received, and decoded.

A general measurements plan for gathering quantitative data in the next program phase was presented.

SECTION 4
ANALYSIS

The methodology for the Signal-to-Noise (S/N) and Signal-to-Clutter (S/C) improvement analysis was to derive analytical equations which represent the probability distributions for various radar signal processing techniques; in particular IPAR. A simplified method of specifying the improvement of IPAR as compared to other techniques was used so that repeated interpretation of graphical data would not be necessary in comparing various techniques. The techniques considered included the following:

(a) Square Law Detection with constant false alarm rate (CFAR) and without Frequency Agility (SLD wo FA).

(b) Square Law Detection with CFAR, with Frequency Agility and multiple pulse integration (SLD w FA).

(c) Polarimetric phase processing wherein signal amplitude data is retained; commonly referred to as Pseudo Coherent Detection (PCD) with Frequency Agility and integration (PCD w FA).

(d) PCD processing with Instantaneous Automatic Gain Control, Frequency Agility, and integration (PCD w FA and IAGC).

(e) PCD/IAGC based IPAR processing.

The analysis is quite general and must be considered preliminary in nature. Conventional mathematical expressions were used when convenient and available. Due to the preliminary nature of the analysis, extensive referencing is not provided in this report though several were used. It is expected that a proper list of references can be made available in future reports.

4.1 SQUARE LAW DETECTION (SLD wo FA)

This title is used to represent a conventional radar which performance may be approximated by the square law mathematical radar model. Certain simplifying assumptions are made. The probability density functions for noise and target plus noise are assumed to be Gaussian. Noise is assumed to be independent in time quadrature.

4.1.1 SINGLE PULSE PROBABILITY DENSITY FUNCTIONS

The single pulse probability density functions for the target plus interference may be written as

$$\overline{Z}_1 = A^2 + 2\sigma^2$$

and

$$\sigma_{Z1}^2 = 4\sigma^4 + 4A^2\sigma^2$$

where: $\overline{Z}_1$ is the mean value for target plus interference.

A is the target signal amplitude.

σ is the interference rms amplitude.

σ_{Z1} is the standard deviation of the resultant density function.

The derivation is shown in the Appendix.

For interference alone, the above equations reduce to

$$\overline{Z}_0 = 2\sigma^2$$

and

$$\sigma_{Z0}^2 = 4\sigma^4$$

where: $\overline{Z}0$ is the mean value of the interference alone.

σ_{Z0} is the standard deviation of the interference alone.

In the case where the interference is noise, the above expressions are valid. In the case where the interference is clutter, the above expressions seldom apply completely. They will be assumed to apply for clutter however, for two reasons. First, this analysis is simplified and strictly theoretical, and it is beyond the scope of this work to develop a detailed clutter model. Second, such assumption will prove advantageous to the SLD technique, in terms of its expected performance. As a result, any improvements in other techniques, when stated in terms relative to the SLD technique, will be at least as good as, and probably better than, the computed improvement. Often σ is replaced by σ_c to denote clutter specifically, rather than an unspecified interference.

4.1.2 MULTIPLE PULSE PROBABILITY DENSITY FUNCTIONS

The multiple pulse probability density functions for noise may be written as

$$\overline{Z}_{1N} = N(A^2 + 2\sigma^2)$$

$$\sigma^2_{Z1N} = 4N\ (\sigma^4 + A^2\sigma^2)$$

where: $\overline{Z}_{1N}$ is the mean value for signal plus noise after integrating N pulses non-coherently.

σ_{Z1N} is the standard deviation after N pulses have been integrated non-coherently.

In the case where clutter is the interference, there is no independence from pulse to pulse without frequency agility, assuming that the clutter is not decorrelated during the pulse integration time interval. If the clutter is not decorrelated over the integration time, the probability density function is not affected on a normalized basis by the number of pulses integrated. Mathematically, this is equivalent to writing

$$\sigma_{Z1N} \text{ for clutter} = N\sigma_{Z1} \text{ for clutter}$$

or

$$\sigma^2_{Z1N} = 4N^2\ (\sigma^4_c + A^2\ \sigma^2_c\ )$$

and

$$\sigma^2_{Z0N} = 4N^2\sigma^4_c\ .$$

Hence,

$$\overline{Z}_{1N} = N(A^2 + 2\sigma^2_c\ ),$$

$$\sigma^2_{Z1N} = 4N^2(\sigma^4_c + A^2\ \sigma^2_c\ ),$$

$$\overline{Z}_{0N} = 2N\sigma^2_c,$$

and

$$\sigma^2_{Z0N} = 4N^2\sigma^4_c.$$

4.2 SQUARE LAW DETECTION WITH FREQUENCY AGILITY (SLD w FA)

4.2.1 MULTIPLE PULSE DISTRIBUTIONS

As was the case for SLD wo FA, the multiple pulse density functions for WLD w FA may be described by

$$\bar{Z}_{1N} = N(A^2 + 2\sigma^2),$$

$$\sigma_{Z1N} = 4N\ (\sigma^4 + A^2\ \sigma^2),$$

$$\bar{Z}_{0N} = 2N\sigma^2,$$

and

$$\sigma^2_{Z0N} = 4N\sigma^4.$$

For the first time there is a difference between the SLD w FA and SLD wo FA techniques. This difference occurs in the case of clutter. If we assume that the clutter is decorrelated pulse-to-pulse for the integration time interval, due to FA, the above equations apply in the clutter case, and σ_c may be substituted for σ. This was not true for SLD wo FA.

4.3 PSEUDO COHERENT DETECTION WITH FREQUENCY AGILITY (PCD w FA)

This technique, often referred to as the "dot product" PCD technique, or simply "dot product" technique, is the first of the polarization processing techniques to be considered. Generally, when the expression PCD is used herein, it will refer to a system having the following characteristics:

(a) The transmissions are circularly polarized and the polarization may be switched on a pulse-to-pulse basis.

(b) Frequency agility is employed pulse-to-pulse.

(c) Linear receivers are employed.

(d) The two orthogonal linear components of the received signal are processed.

(e) Phase detection is performed with the two polarization components (dot product).

(f) The single pulse results from the phase detection process are integrated for N pulses.

(g) A threshold decision is made which permits a specified false alarm level (i.e., a constant false alarm rate, CFAR).

4.3.1 SINGLE PULSE DISTRIBUTIONS

The probability density functions characteristics for the PCD techniques are derived in the Appendix. They are:

$$\overline{Z}_1 = A^2,$$

$$\sigma_{Z1}^2 = 2\sigma^4 + 2A^2\sigma^2,$$

$$\overline{Z}_0 = 0,$$

and

$$\sigma_{Z0}^2 = 2\sigma^4 .$$

These expressions differ from those of SLD w FA and SLD wo FA, but are very similar in two respects. The importance of these similarities will be seen later and are summarized in the two following sentences. First, the difference between the mean values of target plus interference and interference alone is the same as for the SLD techniques. Secondly, the variances are one-half the values for the SLD techniques. The above expressions also include the additional assumption of independence between the two orthogonal polarization components in the case of interference and a unity cross correlation between the two components in the case of targets. In reality, neither of these convenient assumptions are entirely true. In the above expressions, σ may be replaced by σ_c under such assumptions.

4.3.2 MULTIPLE PULSE DISTRIBUTIONS

For multiple pulses, both the means and variances are increased by a factor of N with respect to the single pulse case for clutter and noise interference. Hence, the resulting distributions are:

$$\overline{Z}_1 = NA^2,$$

$$\sigma_{Z1}^2 = 2N(\sigma^4 + A^2\sigma^2),$$

and

$$\sigma_{Z0}^2 = 2N\sigma^4 .$$

Note that the two similarities mentioned above for the single pulse case still exist.

4.4 PSEUDO COHERENT DETECTION WITH FREQUENCY AGILITY AND INSTANTANEOUS AUTOMATIC GAIN CONTROL (PCD w FA AND IAGC)

This technique was chosen as a mathematical convenience. The other common method of implementing the PCD technique is to employ limiting amplifiers on receive and to perform phase only detection with the two polarization components. Unfortunately, the Phase Only PCD technique (POP CD) is cumbersome mathematically. The PCD w IAGC has very similar characteristics to the POP CD technique and in some circumstances is identical in performance. The greater simplicity of PCD w IAGC as compared to POP CD encourages its use as an indicator of PO PCD performance.

The basic difference between the PCD w IAGC and the normal dot product PCD techniques is that the amplitude of each signal is normalized on a pulse by pulse basis before integration in the PCD w IAGC technique.

4.4.1 SINGLE PULSE DISTRIBUTION

The characteristics of the single pulse probability density function for the PCD w IAGC technique is identical to that for the conventional PCD techniques discussed in section 4.3, except for the amplitude normalization. The process of the normalization results in the following means and variances for the PCD w IAGC technique:

$$\overline{Z}_1 = \left[\frac{A^4}{A^4 + 2A^2\sigma^2 + 2\sigma^4} \right]^{1/2}$$

$$\sigma^2_{Z1} = 1 - \frac{A^4}{A^4 + 2A^2\sigma^2 + 2\sigma^4}$$

$$\overline{Z}_0 = 0$$

$$\sigma^2_{Z0} = 1$$

In the above equations, σ may be replaced by σ_c under previously related assumptions. The equations for the PCD w IAGC technique have some interesting characteristics. Notice that the maximum value for $\overline{Z}_1$ and the maximum

difference between $\overline{Z}_1$ and $\overline{Z}_0$ is unity as $\sigma \to 0$. Also notice that the variance for target plus interference approaches zero for $A \gg \sigma$ and approaches unity for $A \ll \sigma$. Very significant and advantageous is the fact that the variance for interference alone is unity, regardless of the signal-to-interference (S/I) ratio. The physical interpretation of these mathematical characteristics is that this technique has an automatic, cell-by-cell, CFAR capability. This is an important conclusion in that the performance of this technique is dependent only on the S/I ratio for each individual cell and does not depend on the average interference for different cells.

4.4.2 MULTIPLE PULSE DISTRIBUTION

The multiple pulse density functions may be represented as the single pulse means and variances multipled by N.

4.5 INTRAPULSE POLARIZATION AGILE RADAR (IPAR)

The IPAR configuration and technique is described more extensively in Section 2 of this report. Each subpulse interval, called spulse for convenience, may be based on the PCD or PO PCD approaches, where the PO PCD approach is approximated by the PCD w IAGC model. The model analyzed here is one based on the PCD w IAGC model.

4.5.1 SINGLE PULSE DISTRIBUTION

It is shown in the Appendix that the following expressions apply to the IPAR technique for a single pulse:

$$\overline{Z}_1 = C\left[\frac{A^4}{A^4 + 2A^2\sigma^2 + 2\sigma^4} \right]^{1/2}$$

$$\sigma_{Z1}^2 = \frac{C}{4}\left[1 - \frac{A^4}{A^4 + 2A^2\sigma^2 + 2\sigma^4} \right]$$

$$\overline{Z}_0 = 0$$

and

$$\sigma_{Z0}^2 = \frac{C}{4}$$

where C refers to the compression ratio. In the Appendix, these equations are written as

$$\overline{Z}_{11C}\ ,\quad \sigma^2_{11C},\ \overline{Z}_{10C},\ \text{and}\ \sigma^2_{10C}$$

as this notation was advantageous during the development of the equations. The above equations take into account the binomial distributions resulting from the binary decisions on an spulse-by-spulse basis, the code auto-correlation of target like backscatter signals vs. the lack of auto-correlation in noise like interference signals, and the effects of compression. The results are that the means are multiplied by C and the variances by C/4, compared to the PCD w IAGC technique.

4.5.2 MULTIPLE PULSE DISTRIBUTION

After multiple pulses, the mean and variances expressions for IPAR become

$$\overline{Z}_1 = NC\ \left[\ \frac{A^4}{A^4 + 2A^2\ \sigma^2 + 2\sigma^4}\ \right]^{1/2}$$

$$\sigma^2_{Z1} = \frac{NC}{4}\ \left[\ 1 - \frac{A^4}{A^4 + 2A^2\sigma^2 + 2\sigma^4}\ \right]$$

$$\overline{Z}_0 = 0$$

$$\sigma^2_{Z0} = \frac{CN}{4}\ .$$

4.6 COMPARISON OF TECHNIQUES

One method of comparing various processing techniques is to plot detection probability vs required S/I ratios. One can then look for the difference in S/I between two techniques required to give the same detection probability. This difference applies for only one specified false alarm probability, however. In general, the curves for the various technique have different slopes and characteristics. Therefore, an improvement determined under one set of conditions does not apply under another set. Graphical data such as that discussed above is shown in the Appendix. Also shown in the Appendix are the equations for computing probability of false alarm, P_{FA}, and probability of detection, P_D. By making use of the characteristics of these equations and what we know about reasonable operational constraints normally placed on P_{FA} and P_D, we can derive expressions which permit a more

consistent, if approximate, method of stating improvement.

Let k_o equal the multiple of standard deviations above the mean interference level which the threshold must be set for an acceptable P_{FA}. Let k_1 equal the multiple of standard deviations below the target plus interference distributions where the same threshold must be for an acceptable P_D.

From the Appendix, the form of the P_D equation shows that the detection probability is indicated by

$$k_1 = \frac{\overline{Z}_1 - Z_{TH}}{\sigma_{Z1}}$$

where:

$$Z_{TH} = \overline{Z}_0 + k_0 \sigma_{Z0} \ .$$

Therefore

$$k_1 = \frac{\overline{Z}_1 - \overline{Z}_0 - k_0 \sigma_{Z0}}{\sigma_{Z1}}$$

or

$$k_0 = \frac{\overline{Z}_1 - Z_0 - k_1 \sigma_{Z1}}{\sigma_{Z0}} \ .$$

Whenever two techniques are compared and a common P_{FA} is specified (i.e., specific k_0), a different P_D will result from the two techniques (i.e., different k_1's). Conversely, if a common P_D is specified, different P_{FA}'s will result (i.e., different k_0's). In either case, the preprocessed S/I must be changed for one technique compared to another until the same P_{FA} and P_D exists for the two techniques. In other words, the apparent improvement for one technique as compared to another is a function of both P_D and P_{FA}, and a specified value of improvement in general applies to only one specified P_D, P_{FA} pair. In any approach, the ratio of the difference between the means to a standard deviation is a measure of the relative "goodness." As an example, assume that a value 0.5 is specified for P_D. This corresponds to $k_1 = 0$. The corresponding value for k_0 would be;

$$k_0 = \frac{\overline{Z}_1 - \overline{Z}_0}{\sigma_{Z0}} \ .$$

For the same preprocessed S/I's, the different processing would result in

different Z_1's, Z_0's, as we have seen. As result, different S/I's must be specified if equal k_0's are to result. The amount by which different S/I's must be changed to bring the k_0's into agreement is a measure of the improvement. Hence, k_o is a measure of improvement.

It is a common requirement that P_{FA} be a very low value, and this implies a large value for k_0. Acceptable values for P_D seldom fall below 0.1 and seldom above 0.99, with more typical values being closer to 0.5 than either of these extremes. Hence, the absolute value of k_1 is normally not very far from zero. By selecting $k_1 = 0$, we have set the P_D equal to 0.5, and k_0 becomes a relative measure of improvement.

4.6.1 SUMMARY OF PDF EQUATIONS

Table 4 is a summary of the means and variances for the various techniques. The SLD wo FA distributions were unchanged for the multiple pulse case because of the normalization considerations discussed earlier.

4.6.2 RELATIVE PERFORMANCE EQUATIONS

Table 5 is a summary of the equations which describe the relative performance of the various techniques as derived from the expression

$$k = \frac{\bar{z}_1 - \bar{z}_0}{\sigma_{Z0}}$$

Table 6 shows the performance improvement values for the various techniques for various S/I ratios, number of pulses integrated, and compression ratios.

TABLE 4. MULTIPLE PULSE PERFORMANCE EQUATIONS

	$\overline{Z}_1$	σ^2_{Z1}	$\overline{Z}_0$	σ^2_{Z0}
SLD W/O FA	$A^2 + 2\sigma_C^2$	$4\sigma_c^4 + 4A^2\sigma_c^{\leftarrow 2}$	$2\sigma_c^2$	$4\sigma_C^4$
SLD WITH FA	$N(A^2+2\sigma_c^{\leftarrow 2})$	$N(4\sigma_c^4 + 4A^2\sigma_c^{\leftarrow 2})$	$2N\sigma_c^{\ 2}$	$4N\sigma_c^{\ 4}$
PCD WITH FA	NA^2	$N(2\sigma_c^4 + 2A^2\sigma_c^{\leftarrow 2}$	0	$2N\sigma_c^4$
PCD WITH FA & IAGC	$N\left[\dfrac{1}{1 + \dfrac{2A^2\sigma_c^{\leftarrow 2} + 2\sigma_c^{\leftarrow 4}}{A^4}}\right]^{1/2}$	$N\left[1 - \dfrac{1}{1 + \dfrac{2A^2\sigma_c^{\leftarrow 2} + 2\sigma_c^{\leftarrow 4}}{A^4}}\right]$	0	N
IPAR	$NC\left[\dfrac{1}{1 + \dfrac{2A^2\sigma_c^{\leftarrow 2} + 2\sigma_c^{\leftarrow 4}}{A^4}}\right]^{1/2}$	$\dfrac{NC}{4}\left[1 - \dfrac{1}{1 + \dfrac{2A^2\sigma_c + 2\sigma_c^{\leftarrow 4}}{A^4}}\right]$	0	$\dfrac{CN}{4}$

TABLE 5. RELATIVE PERFORMANCE EQUATIONS

SLD W/O FA	$\frac{A^2}{2\sigma_c^{\leftarrow 2}}$
SLD WITH FA	$\frac{\sqrt{N}\,A^2}{2\,\sigma_c^{\leftarrow 2}}$
PCD WITH FA	$\frac{\sqrt{N}\,A^2}{\sqrt{2}\,\sigma_c^{\leftarrow 2}}$
PCD WITH	$\sqrt{N}\left[\frac{1}{1+\frac{2A^2\sigma_c+2\sigma_c^{\leftarrow 4}}{A^4}}\right]^{1/2}$
IPAR	$2\sqrt{NC}\left[\frac{1}{1+\frac{2A^2\sigma_c+2\,\sigma_c^{\leftarrow 4}}{A^4}}\right]^{1/2}$

TABLE 6. PERFORMANCE IMPROVEMENT

No. Pulses	Compres-sion	SLD W/O FA	SLD W FA	PCD W FA	PCD W FA 7 IAGC	IPAR
1	1	1	1.	1.414	.632	1.265
1	10	1	1.	1.414	.632	4.000
1	100	1	1.	1.414	.632	12.649
10	1	1	3.162	4.472	2.000	4.000
10	10	1	3.162	4.472	2.000	12.649
10	100	1	3.162	4.472	2.000	40.000
100	1	1	10.000	14.142	6.325	12.649
100	10	1	10.000	14.142	6.325	40.000
100	100	1	10.000	14.142	6.325	126.491
1	1	.1	0.100	0.141	0.128	0.256
1	10	.1	0.100	0.141	0.128	0.810
1	100	.1	0.100	0.141	0.128	2.561
10	1	.1	0.316	0.447	0.405	0.810
10	10	.1	0.316	0.447	0.405	2.561
10	100	.1	0.316	0.447	0.405	8.098
100	1	.1	1.000	1.414	1.280	2.561
100	10	.1	1.000	1.414	1.280	8.098
100	100	.1	1.000	1.414	1.280	25.607
1	1	10	10.000	14.142	0.951	1.903
1	10	10	10.000	14.142	0.951	6.017
1	100	10	10.000	14.142	0.951	19.026
10	1	10	31.623	44.721	3.008	6.017
10	10	10	31.623	44.721	3.008	19.026
10	100	10	31.623	44.721	3.008	60.166
100	1	10	100.	141.421	9.513	19.026
100	10	10	100.	141.421	9.513	60.166
100	100	10	100.	141.421	9.513	190.260

SECTION 5
CONCLUSIONS AND RECOMMENDATIONS

5.1 HARDWARE

The IPAR hardware was constructed as proposed and functions as anticipated.

5.2 DEMONSTRATION

The IPAR hardware was successfully demonstrated to function as proposed and was shown to possess the general characteristics and capabilities suggested by the analysis contained herein.

5.3 ANALYSIS

The analysis compares the signal-to-interference (S/I) improvement of the IPAR technique to various other radar signal processing techniques. IPAR is shown to provide an improvement in S/I relative to all the other techniques. Although an accurate methodology of comparing system approaches in terms of relative S/I improvement was demonstrated (see Appendix), an approximate method was identified from which an estimate of improvement could be determined. IPAR was shown to provide the potential for considerable performance improvement over all other techniques with which it was compared in S/I ratio improvement. In addition to the basic improvement for an advantageous clutter model, IPAR also provides improvement in non-ideal clutter, which is distributed. Additional analyses conducted in the Appendix shows additional characteristics of the various techniques such as their behavior under various "in cell" to "out of cell" clutter or interference. In general, the performance of an IPAR technique in S/I improvement may be derived from the "dot product" or "phase only" PCD techniques and accounting for the additional improvement deriving from the correlation and compression. Whatever basic polarimetric phase processing technique is incorporated prior to correlation and compression processing, the IPAR S/I improvement performance is roughly twice the square root of the compression ratio greater or for non-target-like clutter or interference. For target-like interference (clutter) which is

distributed, IPAR retains its improvement, whereas the other polarimetric phase processing techniques lose their advantage over conventional amplitude techniques.

5.4 RECOMMENDATIONS

The following recommendations are made in regard the system.

1. Continue the analysis of the advantages of IPAR under multipath conditions for surveillance and track radars.
2. Perform a measurements program to gather data from which a quantitative determination of S/I and multipath advantages can be made.
3. Plan for follow on improvements, modifications, and growth in the present system to take advantage of current observations and planned automation.
   (a) Automated pulse-to-pulse code control by a processor for time side lobe cancellations, etc.
   (b) Increased correlation length.
   (c) Multiple pulse correlations integrator.
   (d) Analyze the LPI, ECCM, and target recognition (identification) potential of IPAR.

REFERENCES

[1] Final Report "High Speed Low-Power Correlator Development."
David Breuer — Diogenes Cordero
Albert Cosand — Alan Templin
Wayne Current
Contract No. N00014-73-C-0034; TRW Systems Group, One Space Park, Redondo Beach, California 90278; for NRL, Code 5260, Washington, D.C. 20375.

[2] Skolnik, Merrill I. Radar Handbook, McGraw-Hill Book Co., New York.

[3] Long, Maurice W. Radar Reflectivity of Land and Sea, Lexington Books, Lexington, Massachusetts.

APPENDIX

DEVELOPMENT OF SQUARE LAW EQUATIONS

$a = A\cos\phi + x$ $\qquad$ $b = A\sin\phi + y$

$$Z = (a + jb)\,(a - jb)$$

$$Z = (A\cos\phi + x)^2 + (A\sin\phi + y)^2$$

$$Z = A^2 + 2Ax\cos\phi = 2Ay\sin\phi + x^2 + y^2$$

$$\overline{y} = \overline{x} = 0$$

$$\sigma_x^2 = \sigma_y^2 = \sigma_c^2$$

$$\overline{Z^2} = A^4 + 4A^2\sigma_c^4 + 4A^2\sigma_c^2 = A^4 + B\sigma_c^4 + 8A^2\sigma_c^2$$

$$\overline{Z} = A^2 + x^2 + y^2 = A^2 + 2\sigma_c^2$$

$$\overline{Z}^2 = A^4 + 4A^2\sigma_c^2 + 4\sigma_c^4$$

$$\overline{Z^2} - \overline{Z}^2 = \sigma_Z^2 = 4\sigma_c^4 + 4A^2\sigma_c^2$$

Therefore:

$$\overline{Z} = A^2 + 2\sigma_c^2$$

$$\sigma_Z^2 = 4\sigma_c^4 + 4A^2\sigma_c^2$$

DEVELOPMENT OF DOT PRODUCT EQUATIONS

$$Z = \mathrm{Re}\ [S_h\ S_V^*]$$

$$S_h = A_H \cos\ \phi_H + X_H + j\ (A_H \sin\ \phi_H + Y_H)$$

$$S_V^* = A_V \cos\ \phi_V + X_V - j\ (A_V \sin\ \phi_V + y_v)$$

$$Z = (A_H \cos\ \phi_H + x_H)\ (A_V \cos\ \phi_V + x_V) + A_H \sin\ \phi_H + y_H)\ (A_V \sin\ \phi_V + y_V)$$

$$\overline{Z} = A_H\ A_V \cos\ \phi_H \cos\ \phi_V + A_H \sin\ \phi_H\ A_V \sin\ \phi_V$$

$$\overline{Z} = A_H A_V = A^2 \text{ for } A_H = A_V$$

$$\overline{Z^2} = A^4 + 2\sigma^4 + 2A^2\ \sigma^2$$

$$\overline{Z}^2 = A^4$$

$$\overline{Z^2} - \overline{Z}^2 = 2\ \sigma^4 + 2\ A^2\ \sigma^2 = \sigma_Z^2$$

Square Law with FA and CFAR

Clutter Discrimination Performance with Ideal Clutter and Ideal Target

$$Z = A^2 + 2A_x \cos\phi + 2A_y \sin\phi + x^2 + y^2$$

$$\bar{x} = \bar{y} = 0 \quad \sigma_x^2 = \sigma_y^2 = \sigma_c^2$$

<u>Target + Clutter</u>

$$\bar{Z} = A^2 + 2\sigma_C^2$$

$$\sigma^2 = 4\sigma_C^4 + 4A^2 \sigma_C^2$$

<u>Clutter Alone</u>

$$\bar{Z} = 2\sigma_C^2$$

$$\sigma_Z^2 = 4\sigma_C^4$$

COMPUTATION OF PROBABILITY OF DETECTION (PD)

$$Z_{TH} = Z_o + ko\ \sigma_{ZO} \quad \text{Threshold Voltage}$$

$$PD = \int_{Z_{TH}}^{\infty} P(Z_1)\, d_Z$$

$$\bar{Z}_o = 2\sigma_C^2$$

$$k_o\ \sigma_{zo} = k_o\ 2\sigma_c^2$$

$$P(Z_1) = \frac{1}{2\pi\ \sigma_{Z1}} e^{-\frac{(Z-\bar{Z}_1)^2}{2\sigma_{Z1}^2}}$$

A gaussian distribution with mean

$$\bar{Z}_1 = A^2 + 2\ \sigma_C^2$$

and variance

$$\sigma_{Z1}^{2} = 4\sigma_c^{4} + 4A^2 \sigma_c^{2}$$

$$PD = \int_{2\sigma^2(-1 + k_o)} \left[\frac{1}{2\pi\,(40c^4 + 4A^2\sigma c^2)^{1/2}} e^{-\frac{(Z-A^2-2\sigma_c 2)^2}{8\sigma_c^4 + 8A\,\sigma_c^2}} \right] dZ$$

$$2\sigma_c^{2}\,(-1 + ko)$$

where k_o = number of std deviations above mean clutter where threshold is set corresponding to allowed false alarm rate.

The ratio $\dfrac{\bar{Z}_1 = Z_{TH}}{\sigma_{Z_1}}$ determines the detection probability

Therefore the detection probability for a particular false alarm is indicated by

$$\frac{2\sigma_c^{2} - ko}{\left(1 + \frac{A^2}{\sigma_c^2}\right)^{1/2}} = \frac{A^2 - 2\,ko\,\sigma_c^{2}}{(4\sigma_c^{4} + 4A^2\sigma_c^{2})^{1/2}}$$

$$= \frac{A^2 + 2\sigma_c^2 - 2\sigma_c^2 - 2ko\sigma_c^2}{(4\sigma_c^{4} + 4A^2\sigma_c^{2})^{1/2}}$$

$$k_1 = \frac{\frac{A^2}{2\sigma_c^{2}} - ko}{\left(1 + \frac{A^2}{\sigma_c^2}\right)^{1/2}}$$

where k_1 is the number of standard deviations of the threshold is below the mean target plus clutter, when set k_o standard deviations above the mean clutter. With these definitions for k_o and k_1, standard normalized Gaussian distributions may be used in the computation of PFA and PD and the relative performance of various techniques k_1 may be mathematically compared directly, without the need to compute probabilities.

k_o	P_{FA}	$\frac{A^2}{2\sigma_c^2}$ (db)	k_1	P_D
1	.1587	0	0	.50000
2	.0228	0	-.58	.2710
3	.0013	0	-1.15	.1251
2	.0228	-3	-1.06	.1446
3	.0013	-3	-1.76	.0392
2	.0228	-10	-1.73	.0418
3	.0013	-10	-2.65	.0040
2	.0228	+10	1.75	.9599
3	.0013	+10	1.53	.9370
2	.0228	3	-0.00	.5000
3	.0013	3	-0.45	.3264
		6	.66	.7454
		6	.33	.6293

PCD with FA

Clutter Discrimination Performance with Ideal Clutter and Ideal Target

$$Z = (A_H \text{ Cos } \phi_H + x_H)(A_V \text{ Cos } \phi_V + x_V)$$

$$+ (A_H \text{ Sin } \phi_H + y_H)(A_V \text{ Sin } \phi_V + y_V)$$

Target plus clutter

$$\overline{Z}_1 = A^2$$

$$\sigma^2_{Z_1} = 2\sigma_c^4 + 2A^2 \sigma_c^2$$

Clutter alone

$$\overline{Z}_o = 0$$

$$k_1 = \frac{\overline{Z}_1 - Z_{TH}}{\sigma_{Z_1}} = \frac{A^2 - \sqrt{2}\, ko\, \sigma_c^2}{(2\sigma_c^4 + 2A^2\sigma_c^2)^{1/2}}$$

$$k_1 = \frac{\dfrac{A^2}{2\sigma_c^2} - \dfrac{ko}{\sqrt{2}}}{\left(\dfrac{1}{2} + \dfrac{A^2}{2\sigma_c^2}\right)^{1/2}}$$

k_o	P_{FA}	$\frac{A^2}{2\sigma_c^2}$ [db]	k_1	P_D
2	.0228	-10	-1.70	.04
3	.0013	-10	-2.61	.01
2	.0228	-6	-1.34	.09
3	.0013	-6	-2.16	.02
2	.0228	-3	-0.91	.18
3	.0013	-3	-1.62	.05
2	.0228	0	-0.34	.37
3	.0013	0	-0.92	.18
2	.0228	3	0.37	.64
3	.0013	3	-0.08	.47
2	.0228	6	1.21	.89
3	.0013	6	0.88	.81
2	.0228	10	2.65	1.00
3	.0013	10	2.43	.99

MULTIPULSE

SLD WITH FA AND CFAR

Clutter Discrimination Performance with Ideal Clutter and Ideal Target - Multipulse

$$\overline{Z}_{MULTI} = N\,\overline{Z}_{SING}$$

$$\sigma^2_{MULTI} = B\,\sigma^2_{SING}$$

N = Number of pulses

$$\overline{Z} = N\,(A^2 + 2\sigma_c^{\,2})$$

$$\sigma_z^{\,2} = 4N\sigma_c^{\,4} + 4N\,A^2\sigma_c^{\,2}$$

PCD with FA

$$\overline{Z} = NA^2$$

$$\sigma^2 = N\,(2\sigma_c^{\,4} + 2A^2\sigma_c^{\,2})$$

$$\frac{\overline{Z_1} - Z_{TH}}{\sigma_{Z_1}} = k_1$$

$$Z_{TH} = \overline{Z}_o + ko\,\sigma_{Z0}$$

k_1 for SLD

$$\sigma_{Z1MULTI} = \sqrt{N}\,\sigma_{Z1SINGLE}$$

$$\overline{Z}_{1MULTI} = N\,Z_{1\ SINGLE}$$

$$\sigma_{Z0\ MULTI} = \sqrt{N}\ \sigma_{Z0\ SINGLE}$$

$$\overline{Z}_1 = N\ (A^2 + 2\sigma_c{}^2)$$

$$\overline{Z} = 1N\sigma_c^2$$

$$\sigma_{Z1} = (4N\sigma_c{}^4 + 4NA^2\sigma_c{}^2)^{1/2}$$

$$Z_{TH} = NA^2 + ko\ [4n\sigma_c{}^4 + 4\ NA^2\sigma_c{}^2]^{1/2}$$

$$\sigma_{Z0} = (4n\sigma_c{}^4)^{1/2}$$

$$k_1 = \frac{N\ (A^2+2\sigma_c{}^2) - 2N\sigma_c 2 - ko\ (4n\sigma_c{}^4)^{1/2}}{(4n\sigma_c^4 + 4NA\ \sigma_c^2\ )^{1/2}}$$

SLD

$$k_1 = \frac{\sqrt{N}\,\frac{A^2}{2\sigma_c^2} - ko}{\left[\,1 + \frac{A^2}{\sigma_c^2}\,\right]^{1/2}}$$

PCD

$$k_1 = \frac{\sqrt{N}\,\frac{A^2}{2\sigma_c^2} - ko}{\left[\,\frac{1}{2} + \frac{A^2}{2\sigma_c^2}\,\right]^{1/2}}$$

SLD

k_o	P_{fa}	$\frac{A^2}{2\sigma_c^2}$	N	k_1	P_D
3	.0013	-10	10	-2.45	.01
3	.0013	-15	100	-2.60	.00
3	.0013	-6	10	-1.80	.04
3	.0013	-10	100	-1.83	.04
3	.0013	-3	10	-1.00	.16
3	.0013	-6	100	-0.40	.35
3	.0013	0	10	0.09	.54
3	.0013	-3	100	1.42	.92
3	.0013	3	10	1.48	.93
3	.0013	0	100	4.04	1.00
3	.0013	6	10	3.20	1.00

PCD

k_o	P_{fa}	$\frac{A^2}{2\sigma_c^2}$	N	k_1	P_D
3	.0013	-1	10	-2.33	.01
3	.0013	-6	10	-1.53	.06
3	.0013	-3	10	-0.54	.30
3	.0013	0	10	0.85	.80
3	.0013	3	10	2.65	1.00
3	.0013	-15	100	-2.48	.01
3	.0013	-10	100	-1.45	.07
3	.0013	-6	100	0.45	.67
3	.0013	-3	100	2.89	1.00

INTERCELL VS. INTRACELL CONSIDERATIONS

When the intracell clutter differs from the clutter in adjacent cells:

SLD:

$$Z_{TH} = 2N\sigma^2_{CINTER} + k_o(4N\sigma^4_{CINTER})^{1/2}$$

$$\overline{Z}_1 = N\ (A^2 + 2\sigma^2_{CINTRA})$$

$$\sigma_{Z1} = \left(4N\sigma^4_{CINTRA} + 4NA^2\sigma^2_{CINTRA}\right)^{1/2}$$

$$k_1 = \frac{NA^2 + 2N\sigma^2_{CINTRA} - 2N\sigma^2_{CINTER} - k_o(4N\sigma^4_{CINTER})^{1/2}}{\left(4N\sigma^4_{CINTRA} + 4NA^2\sigma^2_{CINTRA}\right)^{1/2}}$$

$$k_1 = \frac{N\ \dfrac{A^2}{2\sigma^2_{CINTER}} - N + N\ \dfrac{\sigma^2_{CINTRA}}{\sigma^2_{CINTER}} - k_o\sqrt{N}}{\left(N\ \dfrac{\sigma^4_{CINTRA}}{\sigma^4_{CINTER}} + N\ A^2\ \dfrac{\sigma^2_{INTRA}}{\sigma^4_{CINTER}}\right)^{1/2}}$$

$$k_1 = \frac{\sqrt{N}\ \dfrac{A^2}{2\sigma^2_{CINTER}} - \sqrt{N}\left(1 - \dfrac{\sigma^2_{CINTRA}}{\sigma^2_{CINTER}}\right) - k_o}{\left(\dfrac{\sigma^4_{CINTRA}}{\sigma^4_{CINTER}} + \dfrac{A^2}{2\sigma^2_{CINTER}}\ \dfrac{2\sigma^2_{CINTRA}}{\sigma^2_{CINTER}}\right)^{1/2}}$$

PCD:

$$Z_{TH} = k_o\sqrt{2N}\ \sigma^2_{CINTER}$$

$$\overline{Z}_1 = NA^2$$

$$\sigma_{Z1} = [2N^4_{CINTRA} + 2NA^2 \ \sigma^2_{CINTRA}]^{1/2}$$

$$k_1 = \frac{\overline{Z}_1 = Z_{TH}}{\sigma_{Z_1}}$$

$$k_1 \quad \frac{NA^2 - k_o \sqrt{2N} \ \sigma^2_{CINTER}}{(2N\sigma^4_{CINTRA} + 2NA^2 \sigma^2_{CINTRA})^{1/2}}$$

$$k_1 = \frac{\sqrt{NA^2} - k_o \sqrt{2N} \ \sigma^2_{CINTER}}{(2\sigma^4_{INTRA} + 2A^2 \sigma^2_{CINTRA})^{1/2}}$$

$$k_1 = \frac{\sqrt{N} \ \frac{A^2}{2\sigma^4_{CINTRA}} - k_o \frac{1}{\sqrt{2}}}{\left(\frac{\sigma^4_{CINTRA}}{2\sigma^4_{CINTER}} + \frac{A^2}{2\sigma^2_{CINTER}} \ \frac{\sigma^2_{CINTRA}}{\sigma^2_{CINTER}}\right)^{1/2}}$$

Dot Product with IAGC

$$Z_{IAGC} = \frac{Z_{PCD}}{Z_{PCD}}$$

$$\left(\overline{\frac{Z_{PCD}}{Z_{PCD}}}\right) = \frac{\overline{Z_{PCD}}}{\overline{Z_{PCD}}}$$

$$\overline{Z}_{1AGC} = \frac{\overline{Z}_{PCD}}{\overline{Z_{PCD}}} \cong \frac{\overline{Z}_{PCD}}{\sqrt{\overline{Z^2_{PCD}}}}$$

$$\overline{Z^2_{CD}} = \overline{Z}^2_{PCD} + \sigma^2_{PCD}$$

$$\overline{Z}^2_{1AGC} = \frac{\overline{Z}^2_{PCD}}{\overline{Z}^2_{PCD} + \sigma^2_{PCD}} = \frac{1}{1 + \left(\frac{\sigma_{PCD}}{\overline{Z}_{PCD}}\right)^2}$$

$$Z^2_{1AGC} = \frac{Z^2_{PCD}}{(Z_{PCD})^2} = 1 = \overline{Z^2_{1AGC}}$$

$$\overline{Z^2}_{1AGC} - \overline{Z}^2_{1AGC} = \sigma^2_{1AGC} = 1 - \frac{1}{1 + \left(\frac{\sigma_{PCD}}{\overline{Z}_{PCD}}\right)^2}$$

$$\overline{Z}_{1AGC} = \left[\frac{1}{1+\left(\frac{\sigma_{PCD}}{Z_{PCD}}\right)^2}\right]^{1/2} \qquad \sigma^2_{1AGC} = 1 - \frac{1}{1+\left(\frac{\sigma_{PCD}}{\overline{Z}_{PCD}}\right)^2}$$

$$\sigma^2_{o1AGC} = 1$$

$$\sigma_1{}^2{}_{1AGC} = N\left[\left(1 - \frac{1}{1 + \left(\frac{\sigma_{PCD}}{\overline{Z}_{PCD}}\right)^2}\right)\right]$$

$$\sigma_1{}^2{}_{1AGC} = N\left[1 - \left[\frac{1}{1 + \frac{2A_C^2\sigma^2 + 2\sigma_c^4}{A^4}}\right]\right]$$

$$\overline{Z} = N\left[\frac{1}{\frac{1 + 2A^2\sigma_c + 2\sigma_c{}^4}{A^4}}\right]^{1/2}$$

$$k_1 = \frac{\overline{Z}_1 - Z_{TH\ 1AGC}}{\sigma_{1\ 1AGC}} \qquad Z_{TH\ 1AGC} = Z_{o\ 1AGC} + k_o\ \sigma_{o\ 1AGC}$$

$$0 + \sqrt{N}\, k_o$$

$$= k_o \sqrt{N}$$

$$k_1 = \frac{N \left[1 + \dfrac{2A^2\sigma_c^{\,2} + 2\sigma_c^{\,4}}{A^4}\right]^{1/2}}{\sqrt{N}\left[1 - \dfrac{1}{1 + 2A^2\sigma_c^{\,2} + 2\sigma_c^{\,4} \;/\; A^4}\right]^{1/2}}$$

SLD

k_o	P_{fa}	$\frac{A^2}{2\sigma^2_{CINTER}}$ [db]	$\frac{\sigma^2_{CINTRA}}{\sigma^2_{CINTER}}$ [db]	N	k_1	P_D
3	.0013	-6	-3	10	-5.33	0.00
3	.0013	-3	-3	10	-3.45	0.00
3	.0013	0	-3	10	-1.26	0.10
3	.0013	3	-3	10	1.15	0.88
3	.0013	6	-3	10	3.89	1.00
3	.0013	-6	-3	100	-7.72	0.00
3	.0013	-3	-3	100	-3.43	0.00
3	.0013	0	-3	100	1.80	0.96
3	.0013	3	-3	100	7.97	1.00
3	.0013	-3	-6	10	-6.74	0.00
3	.0013	0	-3	10	-2.93	0.00
3	.0013	3	-3	10	0.91	0.82
3	.0013	6	-3	10	5.03	1.00
3	.0013	-3	-3	100	-9.76	0.00
3	.0013	0	-3	100	-0.65	0.25
3	.0013	3	-3	100	9.17	1.00
3	.0013	1	-3	10	-1.66	0.05
3	.0013	2	-3	10	-0.38	0.35
3	.0013	1	-2	100	2.52	0.99

PCD

k_o	P_{fa}	$\frac{A^2}{2\sigma^2_{CINTER}}$	$\frac{\sigma^2_{CINTRA}}{\sigma^2_{CINTER}}$	N	k_1	P_D
3	.0013	-3	-3	10	-0.87	0.19
3	.0013	0	-3	10	1.31	0.91
3	.0013	-2	-3	10	-0.19	0.42
3	.0013	-1	-3	10	0.54	0.71
3	.0013	1	-3	10	2.14	0.98
3	.0013	2	-3	10	3.01	1.00
3	.0013	-3	-3	100	4.71	1.00
3	.0013	-4	-3	100	3.26	1.00
3	.0013	-5	-3	100	1.95	0.97
3	.0013	-6	-3	100	0.78	0.78
3	.0013	-7	-3	100	-0.27	0.40
3	.0013	-8	-3	100	-1.18	0.12
3	.0013	-6	-6	10	-4.31	0.00
3	.0013	-3	-6	10	-1.35	0.09
3	.0013	-2	-6	10	-0.29	.039
3	.0013	-1	-6	10	0.81	0.79
3	.0013	0	-6	10	1.95	0.97
3	.0013	1	-6	10	3.15	1.00
3	.0013	-3	-6	100	7.28	1.00
3	.0013	-6	-6	100	1.27	0.90
3	.0013	-7	-6	100	-0.44	0.33
3	.0013	-8	-6	100	-2.01	0.02

PCD WITH IAGC

k_o	P_{fa}	$\frac{A^2}{2\sigma^2_{CINTER}}$	$\frac{\sigma^2_{CINTRA}}{\sigma^2_{CINTER}}$	N	k_1	P_D
3	.0013	-3	-3	10	-1.29	0.10
3	.0013	-2	-3	10	-1.13	0.13
3	.0013	-1	-3	10	-0.98	0.16
3	.0013	0	-3	10	-0.84	0.20
3	.0013	3	-3	10	-0.44	0.33
3	.0013	6	-3	10	-0.08	0.46
3	.0013	10	-3	10	0.38	0.65
3	.0013	15	-3	10	1.10	0.86
3	.0013	20	-3	10	2.18	0.99
3	.0013	-3	-3	100	4.29	1.00
3	.0013	-4	-3	100	3.32	1.00
3	.0013	-6	-3	100	1.65	0.95
3	.0013	-7	-3	100	0.94	0.82
3	.0013	-10	-3	100	-0.70	0.24
3	.0013	-15	-3	100	-2.17	0.02
3	.0013	0	-6	10	-0.44	0.32
3	.0013	-3	-6	10	-0.84	0.20
3	.0013	-6	-6	10	-1.29	0.10
3	.0013	3	-6	10	-0.09	-0.46
3	.0013	6	-6	10	0.26	0.60
3	.0013	10	-6	10	0.78	0.78
3	.0013	15	-6	10	1.68	0.95
3	.0013	-3	-6	100	7.80	1.00
3	.0013	-10	-6	100	0.95	0.83
3	.0013	-15	-6	100	-1.45	0.07
3	.0013	-12	-6	100	-0.23	0.41

COMPLEX TARGETS

Long shows (Ref. 1) that if circular polarization is transmitted, on the average, 50% of the backscattered energy will be of the same sense circular and 50% will be of opposite sense circular. With the rotation of the e-field as viewed along the axis of propagation as the convention, the polarization of circular polarization is reversed upon striking a perfectly conducting flat plate. Upon striking a diplane, the circular polarization is reversed twice, with the resultant being the same as the original before the first bounce. Hence the return of an ensemble of randomly oriented dipole, or an ensemble of randomly positioned single and double bounce plates, will result in a return which is a mixture of some sense and opposite sense circular polarizations, though only one sense is transmitted. The following phasor diagrams show that an ensemble of right circular returns will result in a right circular resultant, as though there was a singular single bounce reflector. Whenever the ensemble is spatially distributed, the apparent centroid location of the resultant will move randomly, in a manner similar to target tracking glint error phenomena.

Either the dipole or combined diplane-plate models would produce the results assumed for the uniformly distributed probability density function for clutter polarimetric phase.

The composite return from two ensembles of different (i.e., odd bounce and even bounce) scatterers in general results in an ellipse. If the two ensembles are of different magnitudes the returns will be predominantly one sense elliptical. If the relative magnitudes of the two ensembles are reversed, the returns will be predominantly of the opposite sense. Under some conditions, a randomly oriented linear will result.

For clutter, we assume that both ensembles are distributed such that the apparent position of the resultants of the two ensembles have variable position. When the two scatterer equivalents are used to represent targets, we will assume that they are less distributed and the relative positions of the limited number of scatterers in an ensemble are fixed.

Square Law Reponse to single type one (1 bounce) scatterer:

$$S = A\, e^{j\phi_A}$$

$$Z = SS^* = Ae^{j\phi_A} Ae^{-j\phi_A}$$

$$Z = A^2$$

Square Law Response to single type two (2 bounce) scatterer:

$$S = Be^{j\phi_B}$$

$$Z = SS^* \; Be^{j\phi_B} Be^{-j\phi_B}$$

$$Z = B^2$$

Square Law Response to one type one and one type two scatterer:

$$S = Ae^{j\phi_A} + Be^{j\phi_B}$$

$$Z = SS^* = (Ae^{j\phi_A} = Be^{j\phi_B})(Ae^{-j\phi_A} + Be^{-j\phi_B})$$

$$Z = A^2 + B^2 + AB\{e^{j(\phi_A \phi_B)} + e^{j(\phi_B - \phi_A)}\}$$

$$\overline{Z^2} = A^4 + B^4 + 4A^2B^2$$

$$\overline{Z} = A^2 + B^2 \qquad \sigma^2 = \overline{Z^2} - \overline{Z}^2 = 2A^2B^2$$

$$\text{Vertical} = Ae^{j\phi_A} + Be^{j\phi_B}$$

$$\text{Horizontal} = j\,Ae^{j\phi_A} - jBe^{j\phi_B}$$

$$\text{Phase shift horizontal } (-j) = Ae^{j\phi_A} - Be^{j\phi_B}$$

$$\text{Conjugate} = Ae^{-j\phi_A} - Be^{-j\phi_B}$$

$$Z = \text{Re}\,[(Ae^{j\phi_A} + Be^{j\phi_B})(Ae^{-j\phi_A} - Be^{-j\phi_B})]$$

$$Z = \text{Re}\,[A^2 - B^2 + AB\,e^{j(\phi B - \phi A)} - e^{j(\phi A - \phi A)}]$$

$$Z = \text{Re}\,[A^2 - B^2 + AB\cos(\phi_B - \phi_A) + j\sin(\phi_B - \phi_A) - \cos(\phi_A - \phi_B) - j\sin(\phi_A - \phi_B)]$$

$$Z = \text{Re}\,[A^2 - B^2 + AB\,2j\sin(\phi_B - \phi_A)]$$

$$Z = A^2 - B^2$$

$$\overline{Z} = A^2 - B^2$$

$$\sigma_Z^2 = 0$$

<u>IAGC</u> $\overline{Z} = 1$ or -1

$$\sigma_2^2 = 0$$

A great number of scatterers of both types randomly distributed over the entire resolution cell would result in phase quadrature independence. However, the polarimetric phase between vertical and horizontal components would not necessarily be independent. Both the phase quadrature and polarimetric phases component would be independent in the case or many randomly oriented and randomly distributed dipoles. For a limited number of

fixed scatterers of type one and type two, neither the phase quadrature nor the polarimetric phase components are independent but are related in the manner illustrated by the equations developed above.

IPAR

In the case of IPAR both the direction of circularity as well as the frequency, in general, is changed from one sub pulse interval (hereinafter called spulse) to the next spulse. Hence, ϕA becomes,

$$\phi_A \rightarrow \phi_A(t)$$

and ϕ_B becomes,

$$\phi_B \rightarrow \phi_B\ (t) + 2\pi f\ \frac{2\Delta R}{C}$$

where,

ΔR is the difference in range between the type A and type B scatterer centroid. In the case of a clutter component which can be described as a type B ensemble the ΔR will be variable. In the case of a single discrete type B scatterer the ΔR will be fixed. The function of t will be understood and the functional notation dropped. For one sense circular:

$$\text{Vertical} = Ae^{j(\phi_A)} + Be^{j(\phi_B + 2\pi f\ \frac{\Delta R}{C})}$$

$$\text{Horizontal} = jA\ e^{j\phi_A} - j\ Be^{j(\phi_B\ +\ 4\pi f\frac{\Delta R}{C})}$$

$$\text{Phase shifted horizontal} = Ae^{j\phi_A} - Be^{j(\phi_B + 4\pi f\frac{\Delta R}{C})}$$

$$\text{Conjugate} = Ae^{-j\phi_A} - Be^{-j(\phi_B + 4\pi f\ \frac{\Delta R}{C})}$$

$$Z = \mathrm{Re}\ [Ae^{j\phi_A} + Be^{j(\phi_B + 4\pi f\frac{\Delta R}{C})}\ Ae^{-j\phi_A} - Be^{-j(\phi_B + 4\pi f\frac{\Delta R}{C})}]$$

$$Z = \mathrm{Re}\ [A^2 - B^2 = AB\ e^{(\phi_B - \phi_A + 4\pi f\frac{\Delta R}{C})} - e^{j(\phi_A - \phi_B - 4\pi f\frac{\Delta R}{C})}]$$

$$Z = A^2 - B^2$$

For the opposite sense circular:

$$Z = B^2 - A^2$$

Whenever the sense of circularity is mixed:

$$V = Ae^{j\phi_A} + Be^{j(\phi_B + 4\pi f\frac{\Delta R}{C})}$$

$$H_{Conj} = Ae^{-j\phi_A} + Be^{-j(\phi_B + 4\pi f\frac{\Delta f}{C})}$$

$$Z = \mathrm{Re}\ (V\ H_{Conj})$$

$$Z = \mathrm{Re}\ [\ Ae^{j\phi_A} + Be^{j(\phi_B + 4\pi f\frac{\Delta R}{C})}\ Ae^{-j(\phi_A +}\ Be^{-j\phi_B + 4\pi f\frac{\Delta R}{C})}]$$

$$Z = \mathrm{Re}\ [A^2 + B^2 + AB\ e^{j(\phi_A - \phi_B - 4\pi f\frac{\Delta R}{C})} + e^{-j(\phi_A - \phi_B - 4\pi f\frac{\Delta R}{C})}]$$

$$Z = A^2 + B^2 + 2AB\ \cos(\phi_A - \phi_B - 4\pi f\frac{\Delta R}{C})$$

The difference in circularity is accounted for by the coefficient sign change for B. The phase change due to range change is accounted for by the $4\pi f\frac{\Delta R}{C}$ exponent term. Therefore, since B and A are illuminated by the same signal $\phi_A = \phi_B$ and,

$$Z = A^2 + B^2 + 2AB \cos(4\pi f \frac{\Delta R}{C})$$

where f is the average frequency during the time lapse corresponding to the difference in range between scatterer A and scatterer B. If Δf from spulse-to-spulse is greater than or equal to

$$\Delta f \geq \frac{C}{4\Delta R_{\tau_p}} = \frac{1}{4\tau_p}$$

the returns from many scatterers over the pulse width will be decorrelated and the apparent ΔR will vary from spulse-to-spulse. If at the same time

$$\Delta f \ll \frac{C}{4\Delta R_{\tau s}} = \frac{k}{4\ \tau s}$$

where k is the number of spulse intervals between scatterers and the ΔR between fixed target scattering centers are greater than or equal to a spulse, the target scatterers will be highly correlated. As an example, if:

$\tau_p = 100$ ns $\qquad R_{\tau_p} = C\ \tau_p$

$\tau_s = 10$ ns

then, $2.5 \leq \Delta f \ll 25$ MHz

Frequency agility of this amount from spulse to spulse will cause the A and B ensembles of clutter to decorrelate while the individual A and B discrete target scatterers will remain auto-correlated. In other words, A and B for clutter will assume an independent random distribution as assumed in earlier analyses, except on a single pulse basis. The condition for two discrete scatterers on a target are as follows.

During the sub-pulse intervals where the signal is being returned only from A, the value for Z is,

$$Z = A^2.$$

The number of intervals for which this valid is,

$$N_1 = \frac{\Delta R}{\Delta R_{\tau s}}$$

$$\Delta R_{\tau s} = \frac{C\tau s}{2\tau}$$

$$N_1 = \frac{2\Delta R}{C\tau s}$$

So if $\tau s = 10$ ns

and $\Delta R = 1.5$ m

$$N_1 = \frac{2\ (1.5)}{(3x10^8)(10x10^{-9}} = 1$$

During spulse intervals when returns are received only from B the value for Z is,

$$Z = -B^2$$

During spulse intervals where returns are received from both A and B the value for Z is

$$Z = A^2 - B^2$$

where circularity was the same or

$$Z = A^2 + B^2 + 2AB\ \cos(4\pi f\frac{\Delta R}{C})$$

for spulses where circularity was different. Statistically, for most codes having low sidelobes, the number of spulses during which the circularity was different for one spulse compared to a different spulse, would approximately equal the number of spulses for which the circularity was the same. The number of spulses for each case is,

$$\frac{N_{TOTAL} - 2N_1}{2}$$

$A^2 = 1$ Normalized

$A^2 - B^2$ Same sense = 1 for $A > B$, for A Band -1 for $A < B$

$A^2 + B^2 + 2AB \cos\left(4\pi f \frac{\Delta R}{C}\right)$ opposite sense = 1 Normalized

$-B^2 = -1$ Normalized

The compressed correlation value for normalized amplitude for AB will be,

$$N_1 + \frac{(N_s - N_1)}{2} \text{ for A}$$

$$\text{and } - N_1 - \frac{(N_s - N_1)}{2} \text{ for B}$$

The compressed correlated value for normalized amplitudes for $A > B$ will be,

Ns for A

and $-N_1$ for B

Figures A-14 through A-17 show some of the effects.

Only rarely will two discrete scatterers be identical in size, so the correlated compressed returns from a dominate and subordinate scatterer will normally be Ns and Nl in magnitude respectively.

The success of IPAR in discriminating targets from clutter will depend on the clutter. The more homogeneous, isotropic and random the clutter is, the

better IPAR will discriminate on a single pulse basis. The greater the granularity the less the discrimination. The success also depends on the target scatterer being larger in magnitude on a spulse basis, though it may be smaller on a pulse basis. The discrimination ability will be affected by whether the dominant characteristic of the clutter is the same or the opposite of the dominant target characteristic.

For truly random clutter, which results in phase quadrature and polarimetric independence on a spulse by spulse basis, the peak correlated compressed amplitude will seldom exceed unity compared to a target amplitude of the code length.

For target like clutter, there will still be an improvement, even when the target is less than the integral pulse clutter. The mean value for the clutter in this case will be equal to the granularity of the clutter expressed in multiples of spulses between major scattering centers. These higher clutter correlations must be subtracted from Ns to determine the relative target to clutter signal improvement potential. If the target like clutter is homogenous the improvement would be similar to that achievable in the random clutter case. If the clutter is a typical of the target, (i.e. opposite bounce characteristic), the improvement will actually be greater than for random clutter. For target like clutter the target return must always be larger than the single spulse clutter level unless it is an typical case.

IPAR is a great deal like PCD with IAGC on a single spulse basis hence,

$$\overline{Z}_{1S} = \left[\frac{1}{1 + \dfrac{2A^2\sigma_c^2 + 2\sigma_c^4}{A^4}} \right]^{1/2}$$

$$\overline{Z}_{0S} = 0$$

$$\sigma^2_{Z1S} = 1 - \frac{1}{1 + \dfrac{2A^2\sigma_c^2 + 2\sigma_c^4}{A^4}}$$

$$\sigma^2_{Z0S} = 1$$

A majority of spulse polarities in one direction (i.e. + or −) establishes that polarity, same or opposite sense, as the preferred direction. Additional polarities of the same sense will increase the correlation while those of opposite sense will decrease the correlation. A perfect target would result in each spulse having the same polarity whether positive or negative. Random clutter would result in random positives and negatives. This condition is represented by a Binomial Distribution. Having a preferred direction which can be of either sense is not the same as taking the absolute value on a single spulse basis. The absolute value approach does not require a correlation of successive spulses with previous ones.

The favored direction (i.e., correlation) binary decision processing results in the following distributions which have been modified according to binomial statistics on a single spulse basis:

$$\overline{Z}_{11} = \left[\frac{1}{1 + \dfrac{2A^2\sigma_c^2 + 2\sigma_c^4}{A^4}} \right]^{1/2}$$

$$\sigma_{11}^2 = \frac{1}{4} \left[1 - \frac{1}{1 + \dfrac{2A^2\sigma_c^2 + 2\sigma_c^4}{A^4}} \right]$$

$$\overline{Z}_{10} = 0$$

$$\sigma_{10}^2 = \frac{1}{4}$$

After C spulses are correlated and compressed;

$$\overline{Z}_{11C} = C\,\overline{Z}_{11} = C \left[\frac{1}{1 + \dfrac{2A^2\sigma_c^2 + 2\sigma_c^4}{A^4}} \right]^{1/2}$$

$$\sigma_{11C}^2 = \frac{C}{4} \left[1 - \frac{1}{1 + \frac{2A^2\sigma_c^2 + 2\sigma_c^4}{A^4}}\right]$$

$$Z_{10C} = C\,\overline{Z}_{10} = 0$$

$$\sigma_{10C}^2 = C\,\sigma_{10}^2 = \frac{C}{4}$$

After multiple pulses the distributions become,

$$\overline{Z}_1 = NC \left[\frac{1}{1 + \frac{2A^2\sigma_c^2 + 2\sigma_c^4}{A^4}}\right]^{1/2}$$

$$\sigma_{Z1}^2 = \frac{NC}{4} \left[1 - \frac{1}{1 + \frac{2A^2\sigma_c^2 + 2\sigma_c^4}{A^4}}\right]$$

$$\overline{Z}_0 = 0$$

$$\sigma_{Z0}^2 = \frac{CN}{4}$$

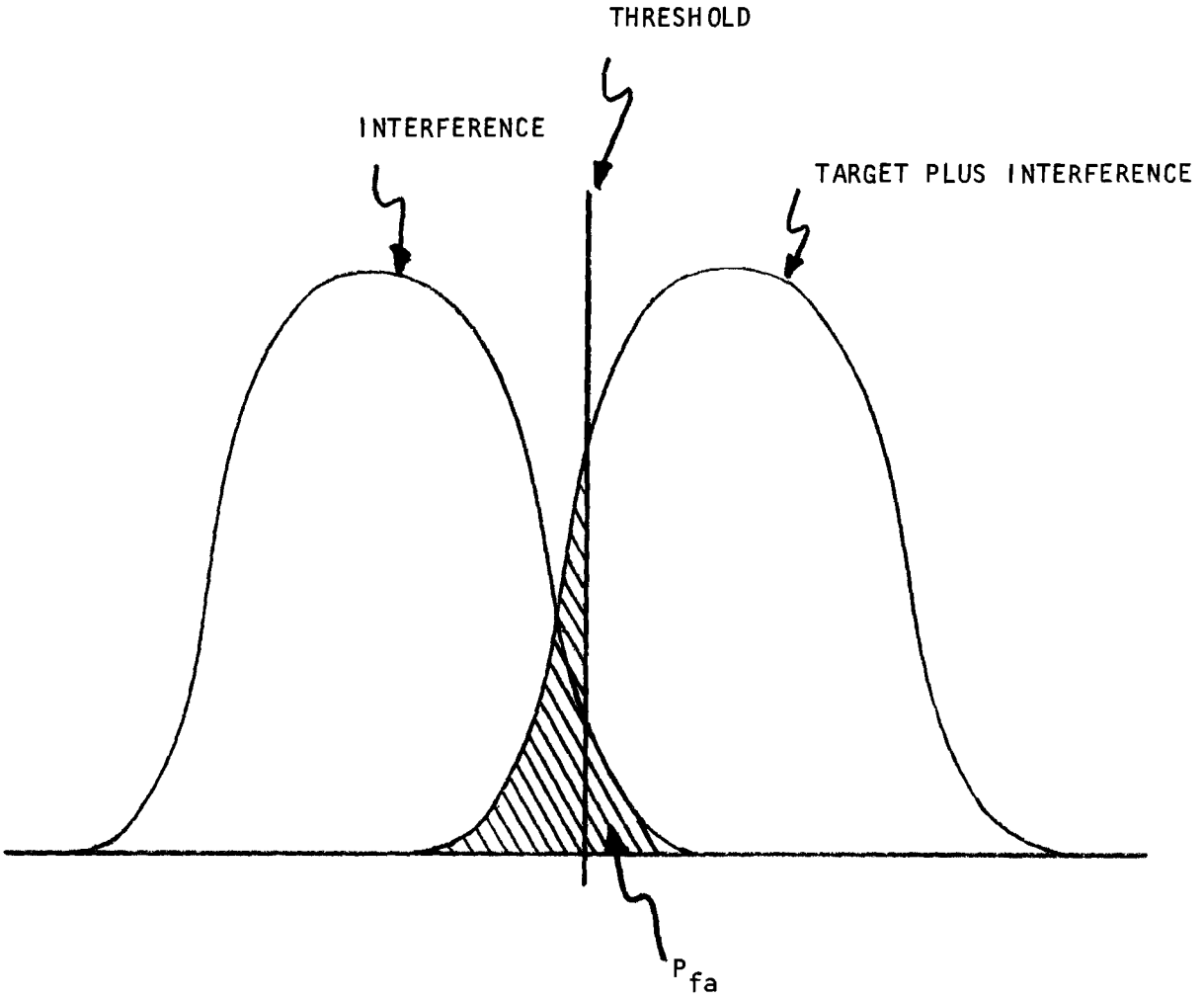

FIGURE A-1. Probability density functions.

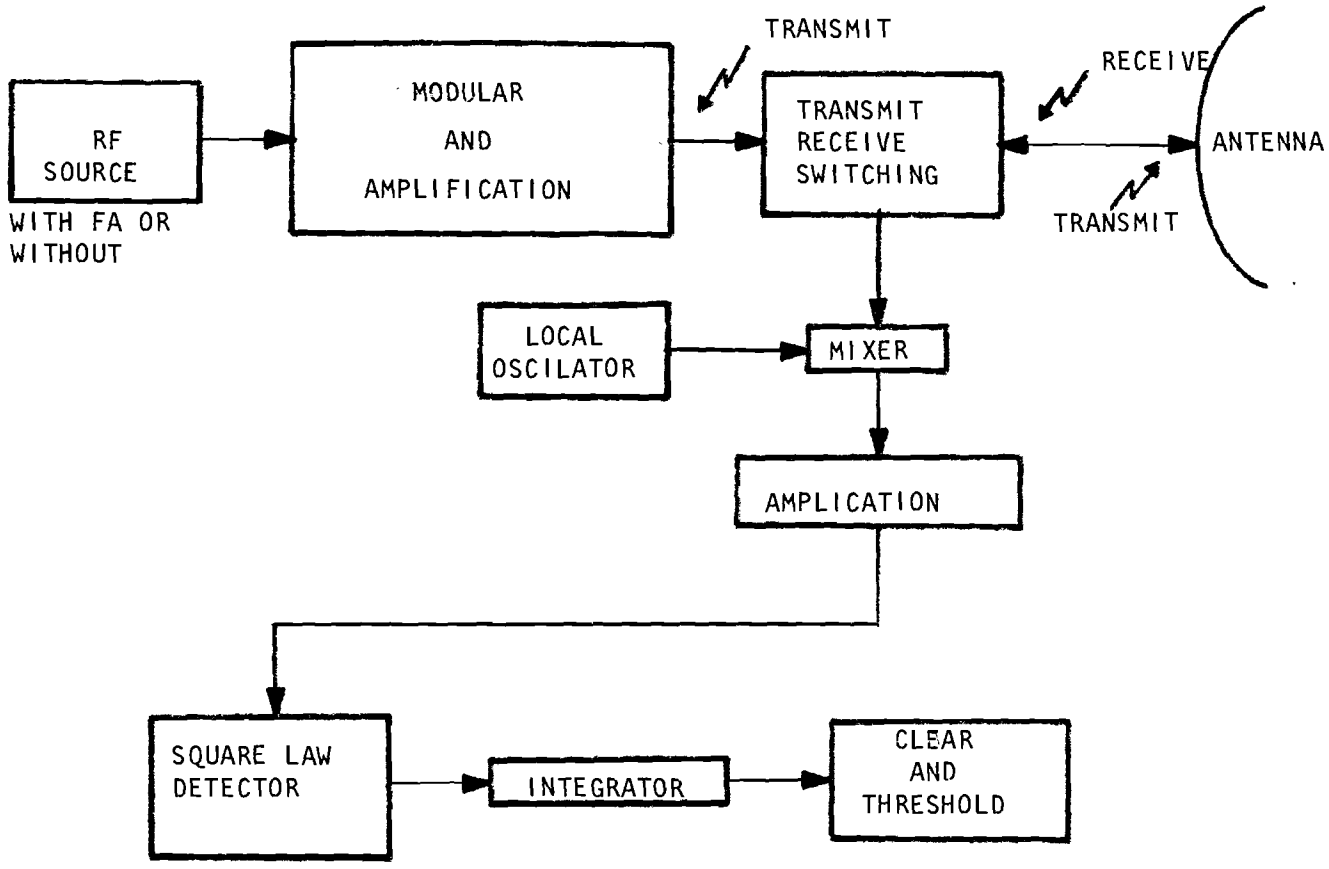

FIGURE A-2. Square law configurations.

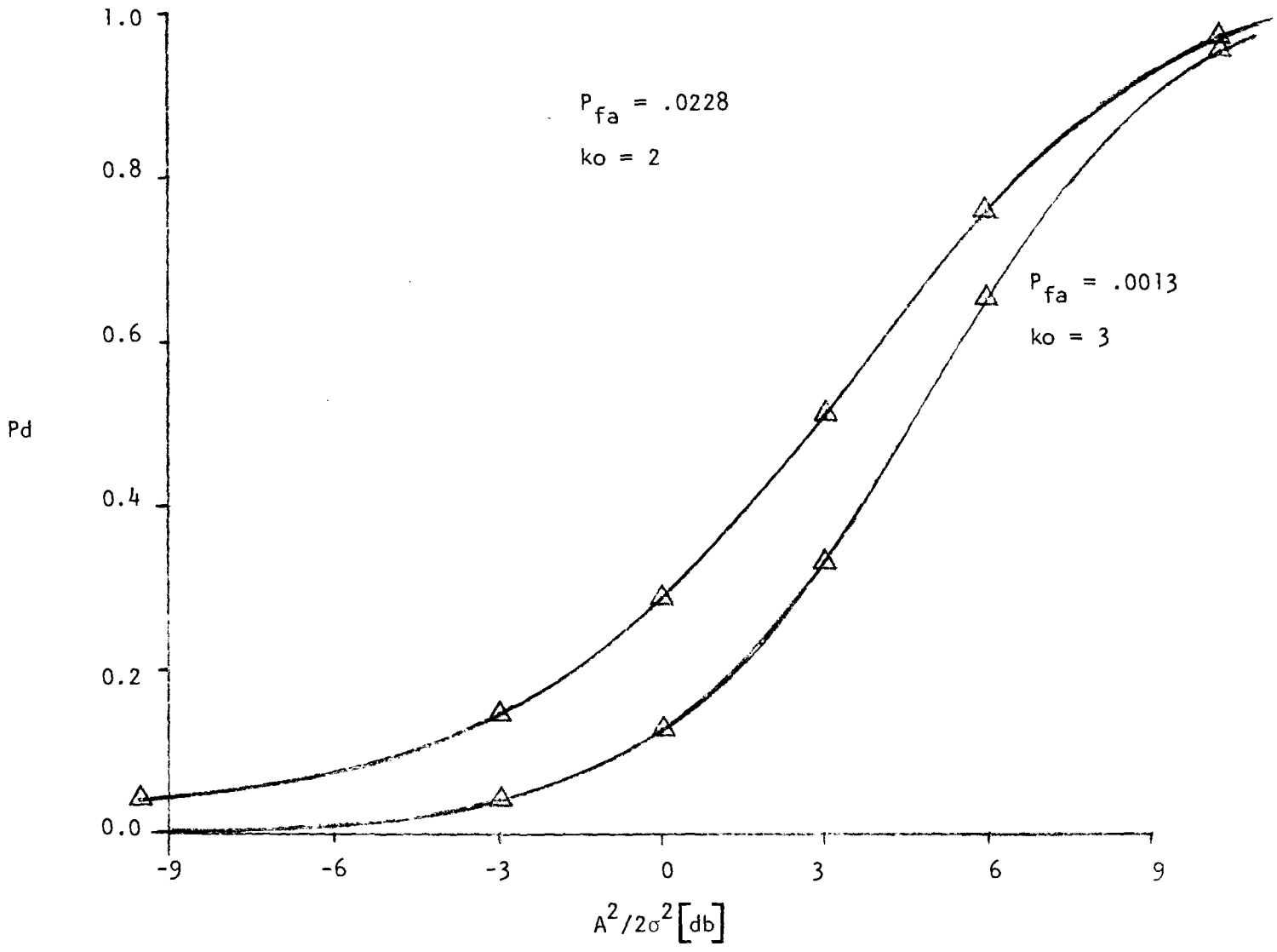

FIGURE A-3. SLD with CFAR and FA single pulse (statistical equivalent).

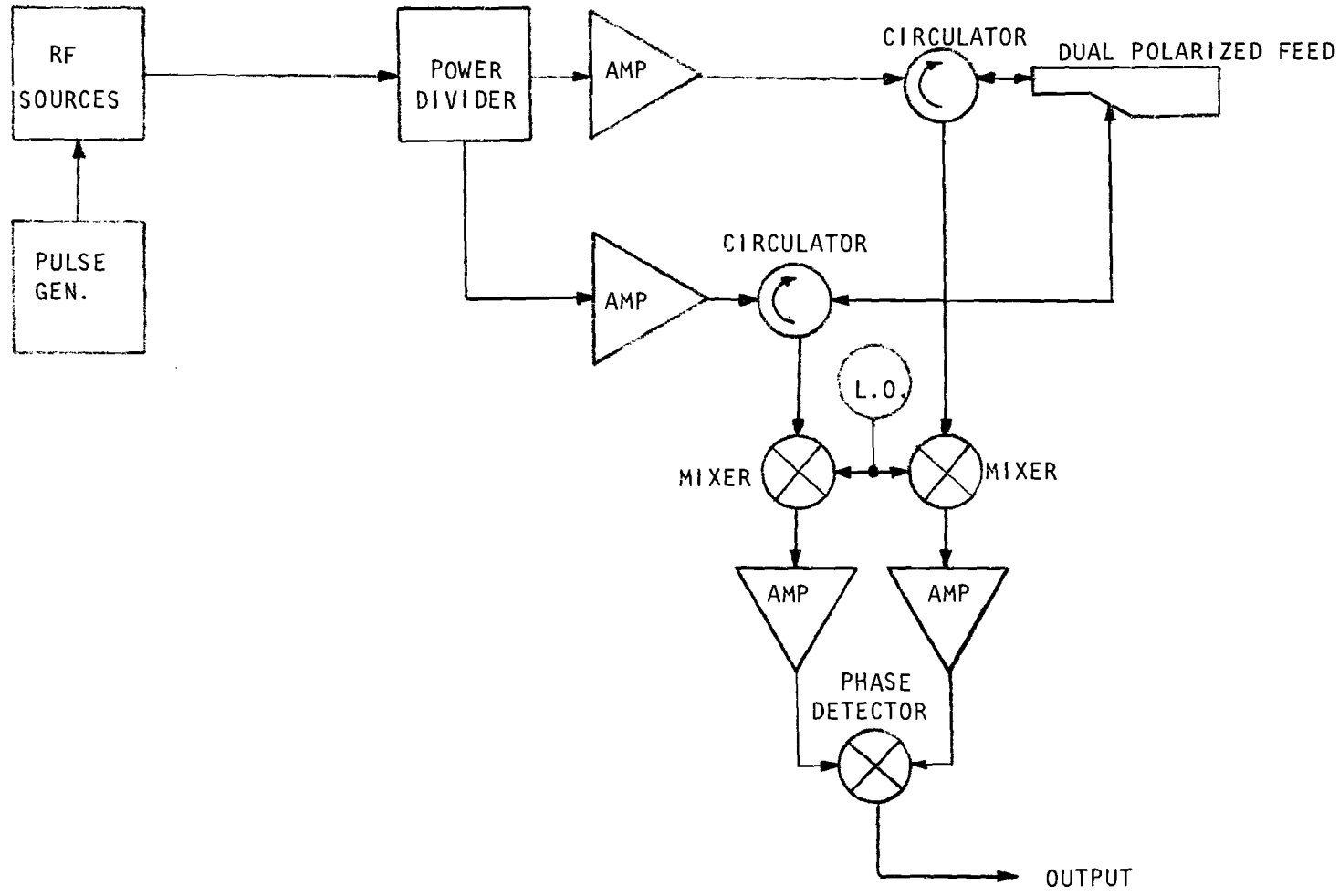

FIGURE A-4. PCD configurations.

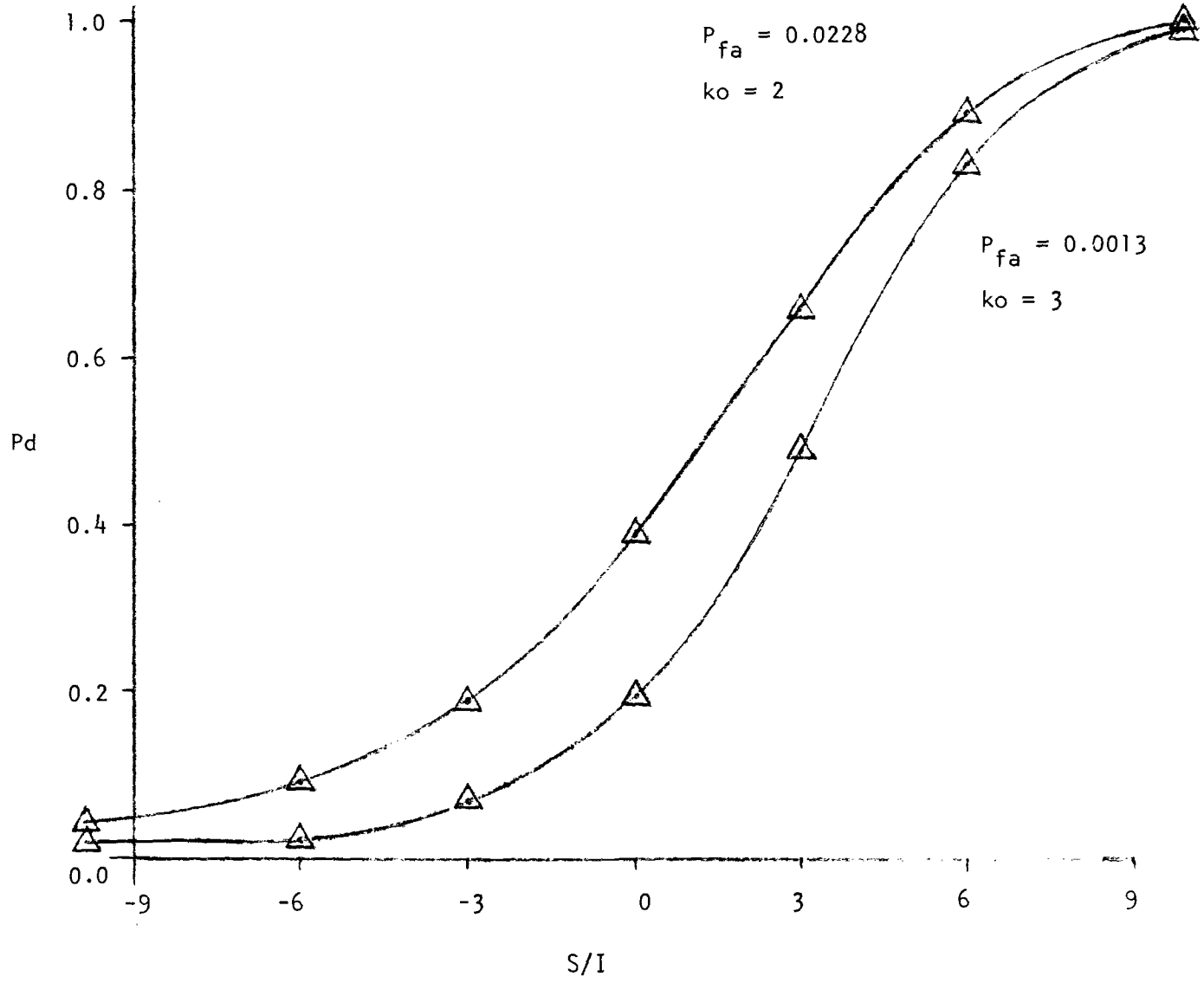

FIGURE A-5. PCD with FA single pulse (statistical equivalent).

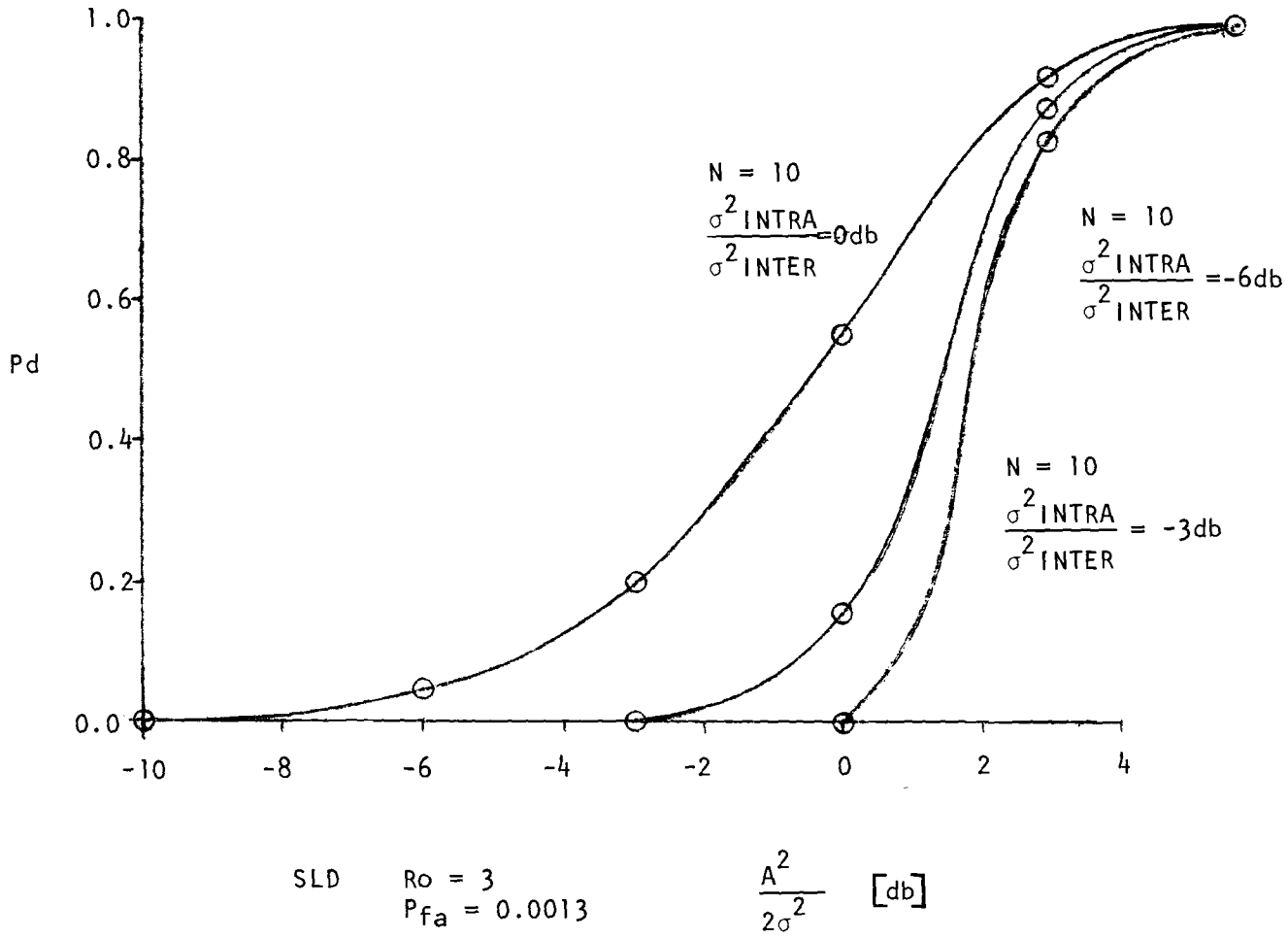

FIGURE A-6. Ten pulse SLD performance.

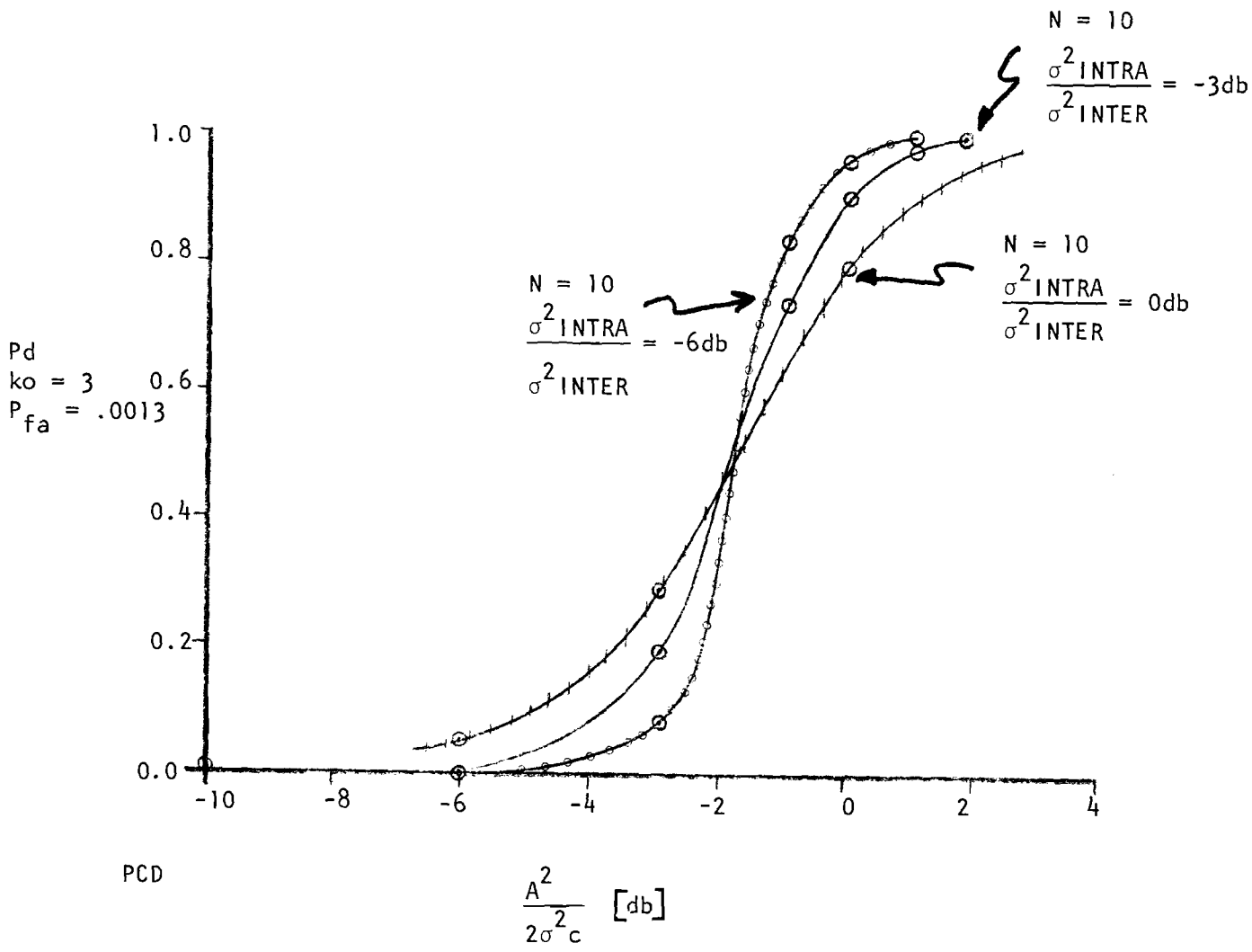

FIGURE A-7. Ten pulse PCD performance.

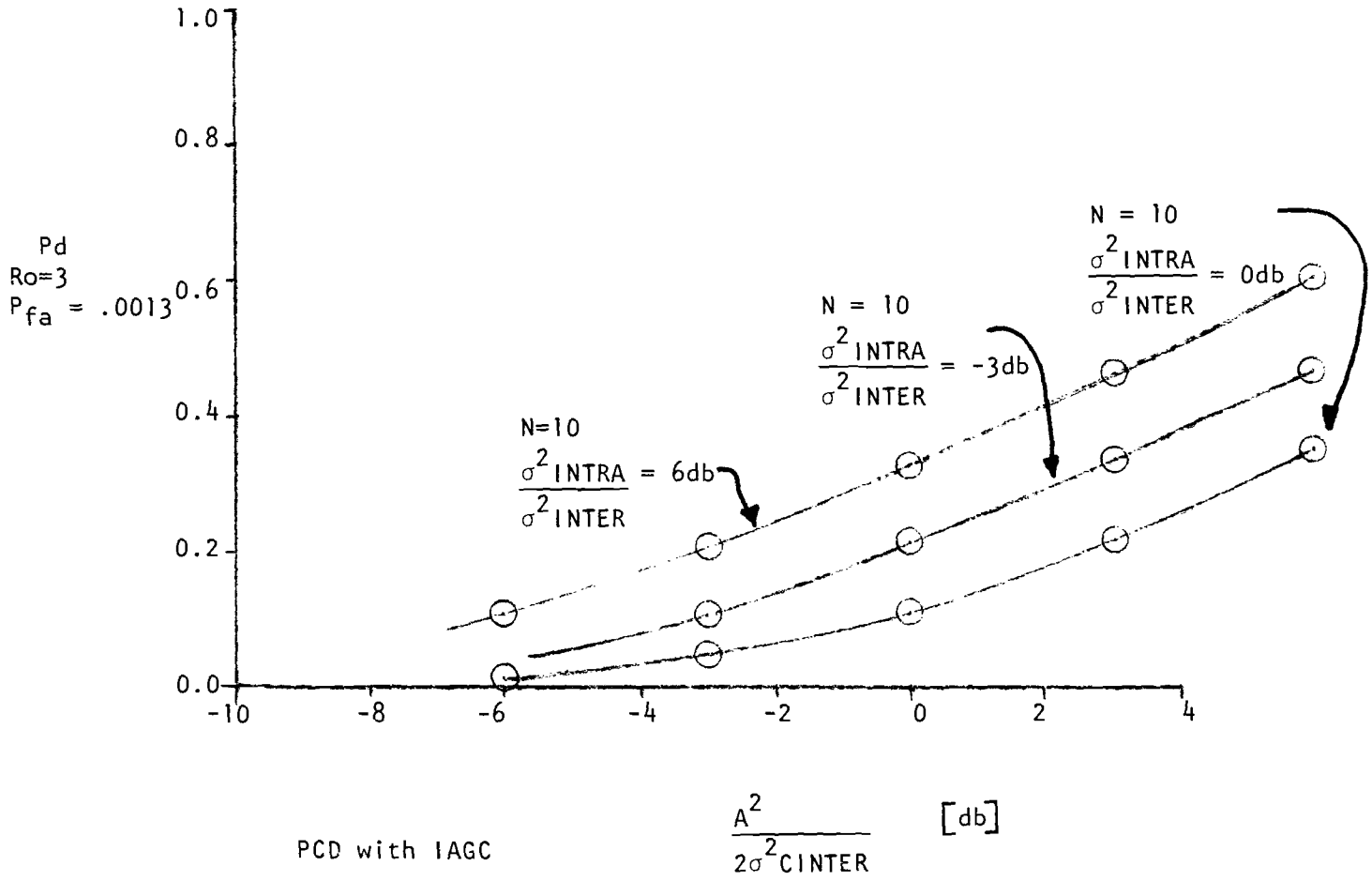

FIGURE A-8. Ten pulse PCD w IAGC performance.

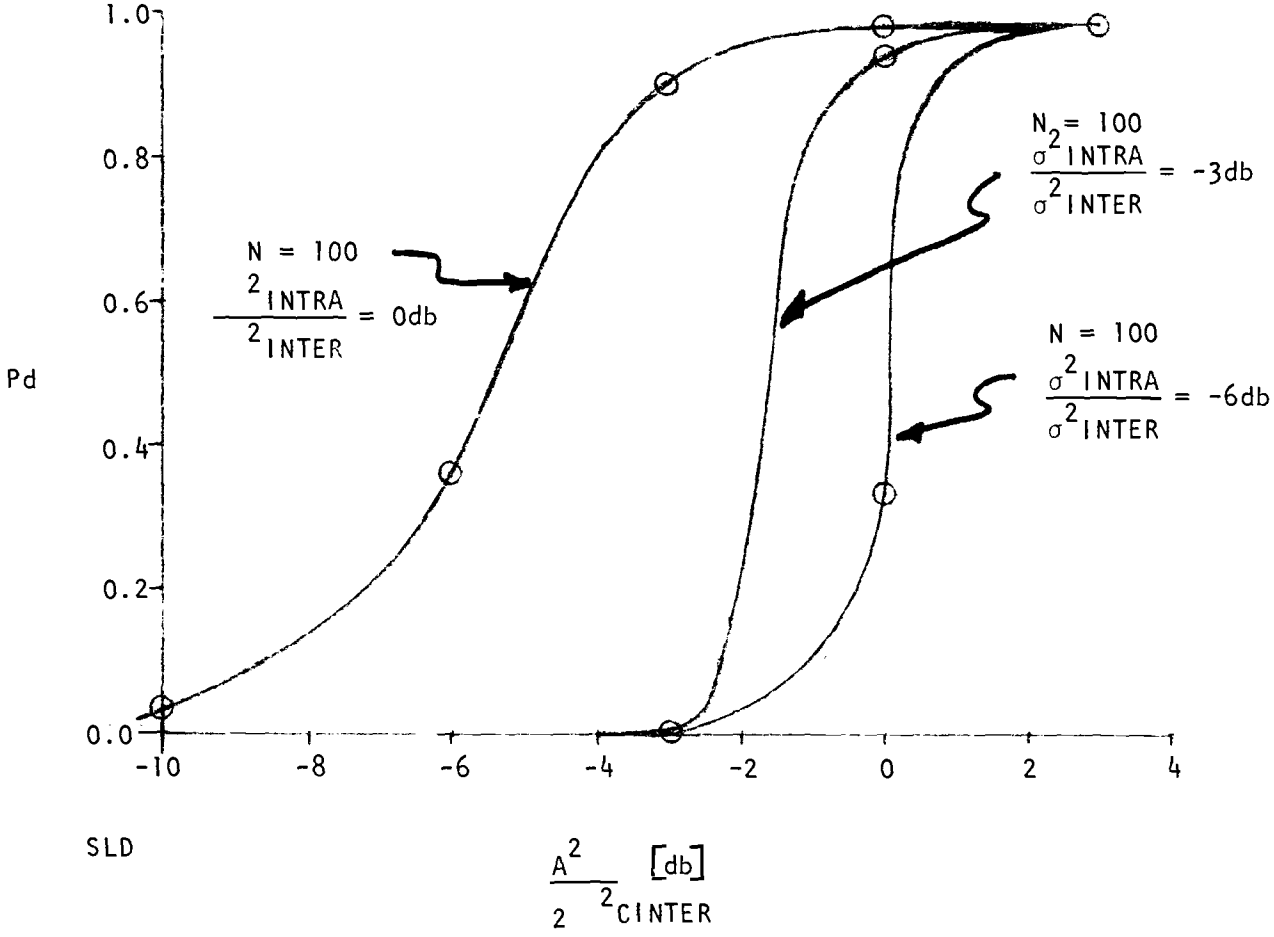

FIGURE A-9. One hundred pulse SLD performance.

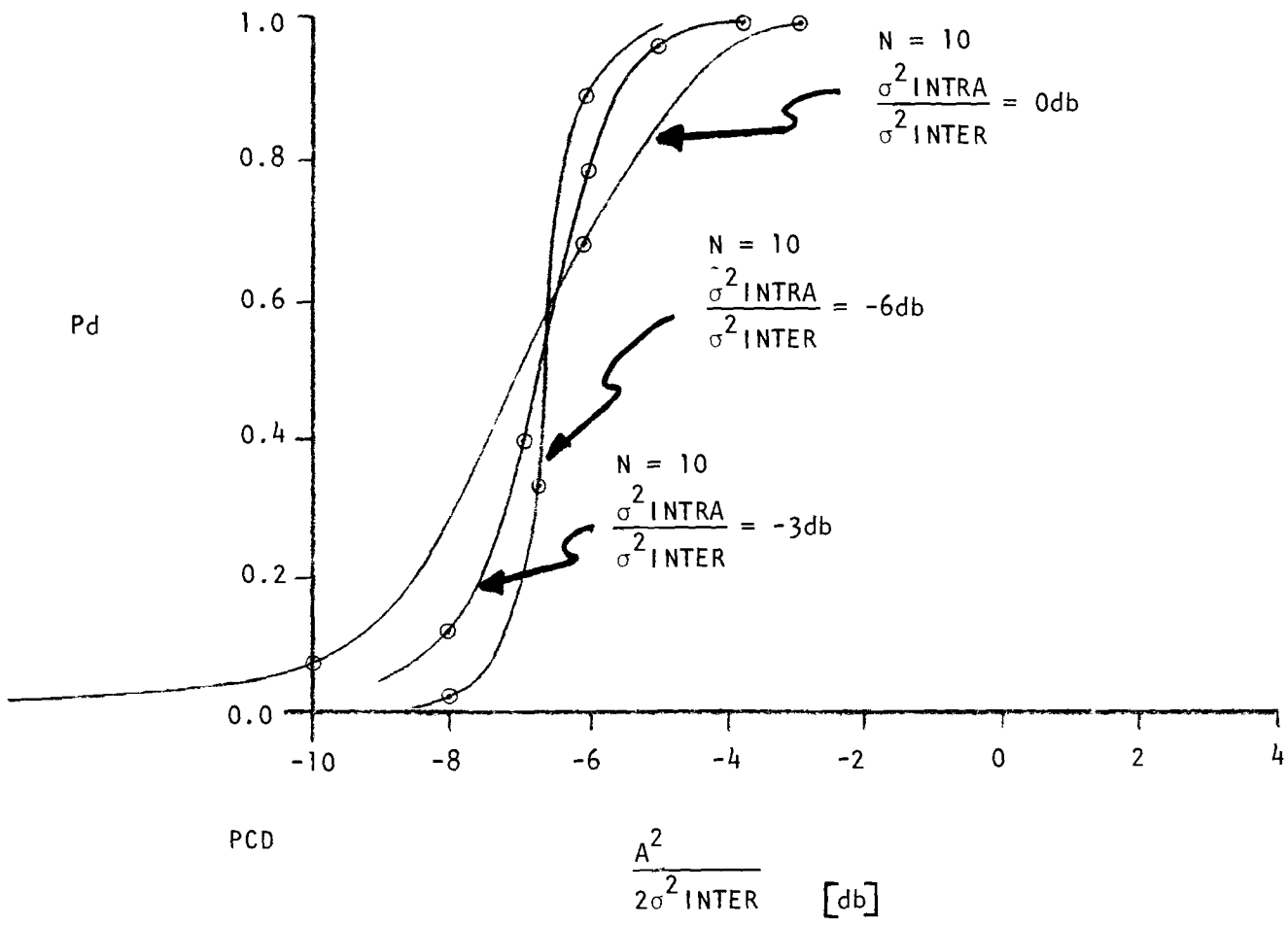

FIGURE A-10. One hundred pulse PCD performance.

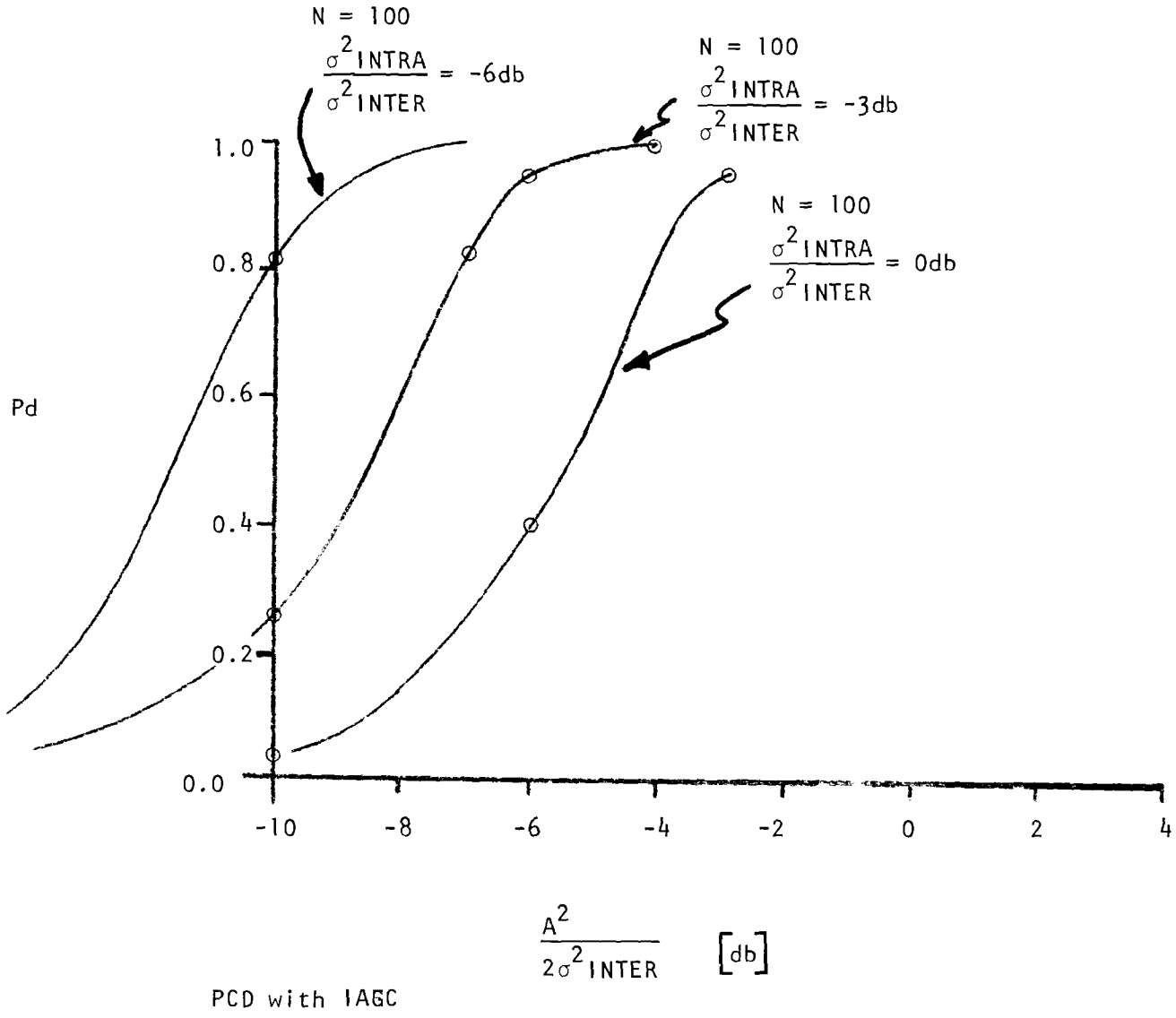

FIGURE A-11. One hundred pulse PCD with IAGC performance.

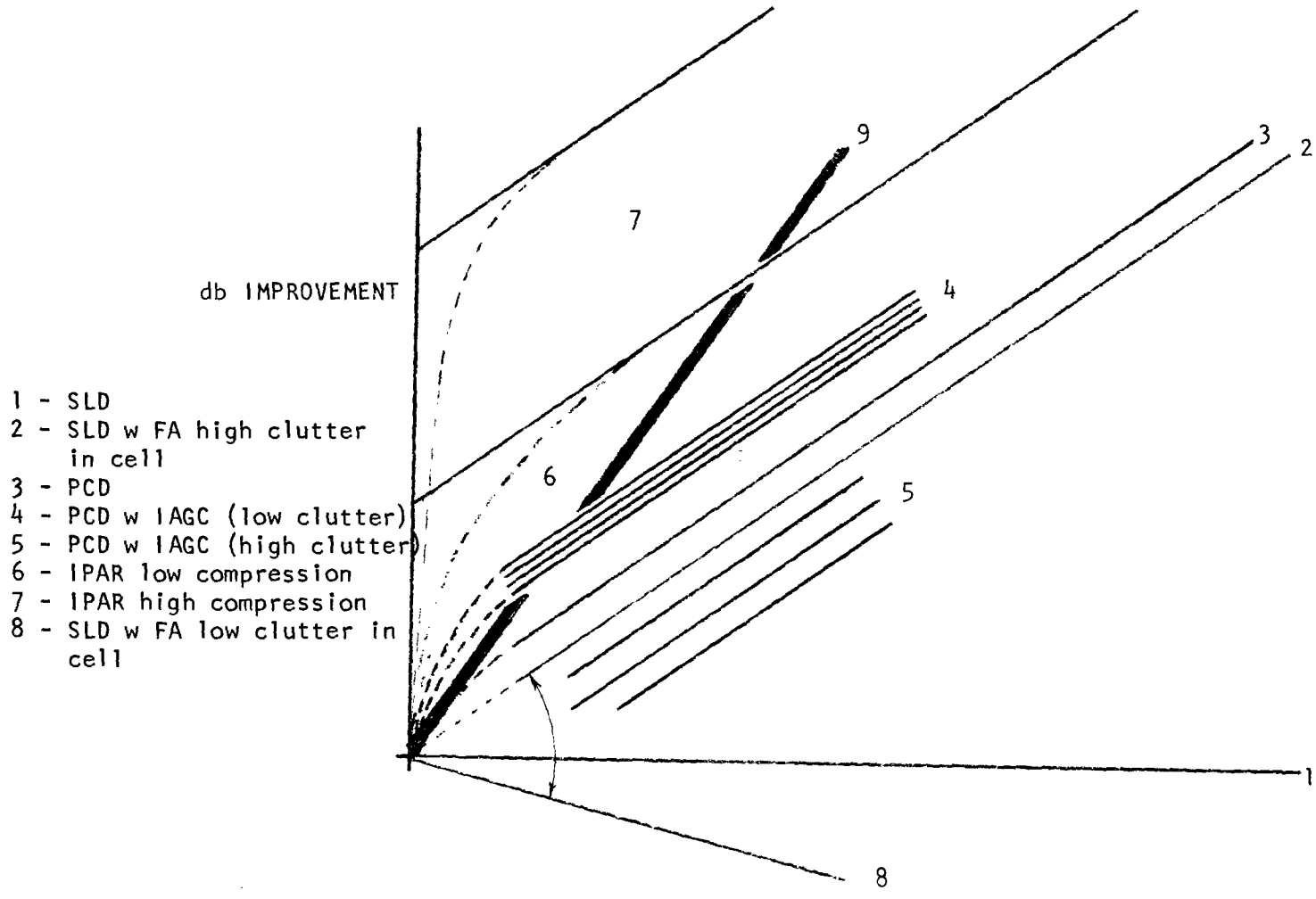

Number of pulses.

FIGURE A-12. Qualitative performance summary.

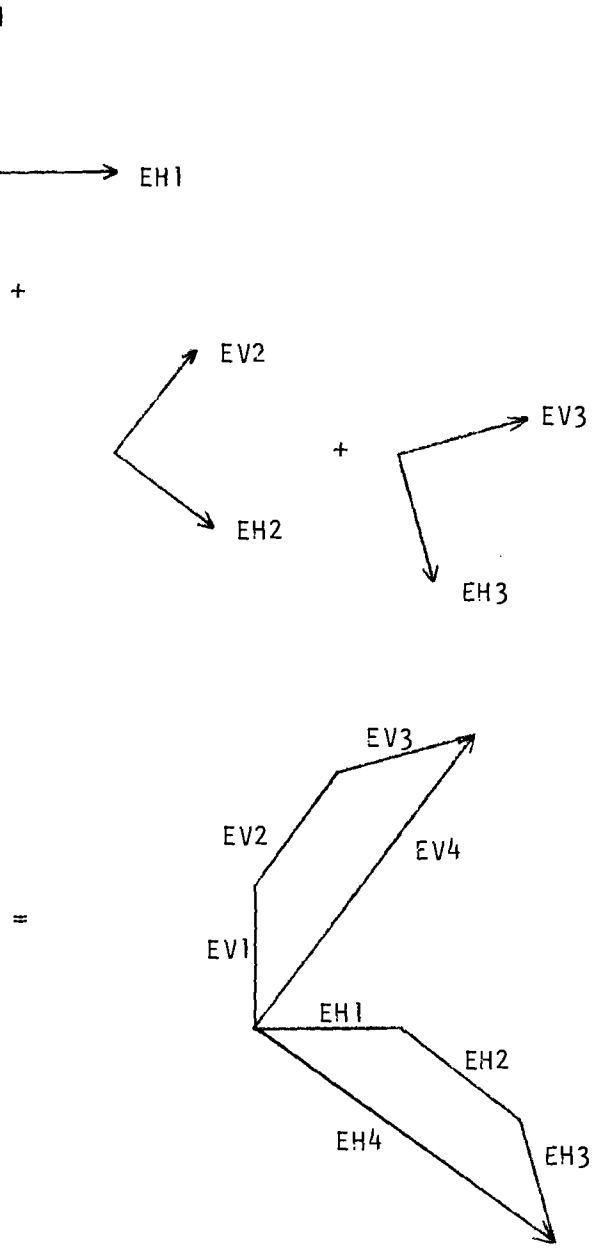

FIGURE A-13. Resultant of aggregate of similar scatterers.

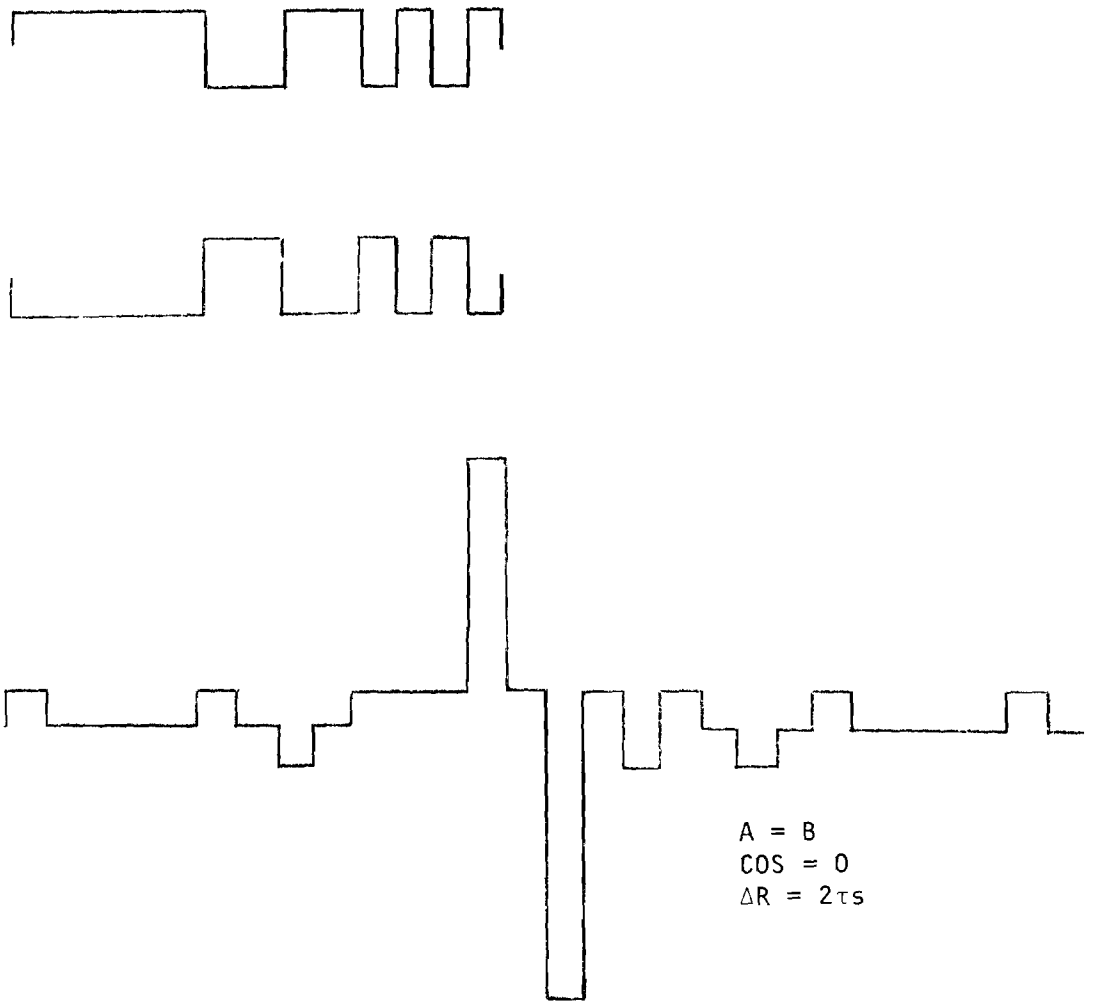

FIGURE A-14. Interference of two scatterers of equal amplitude.

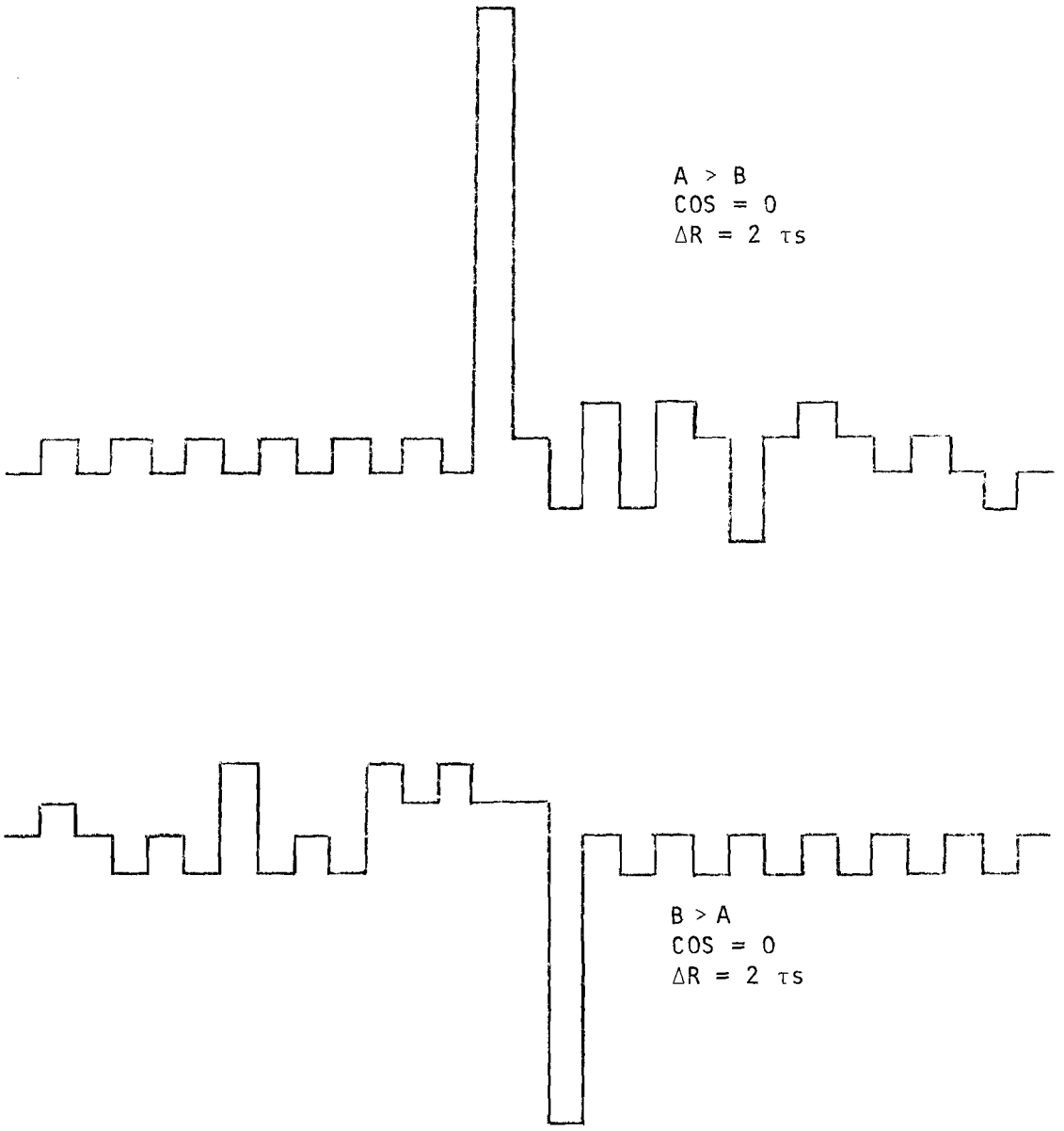

FIGURE A-15. Interference of unequal scatterers.

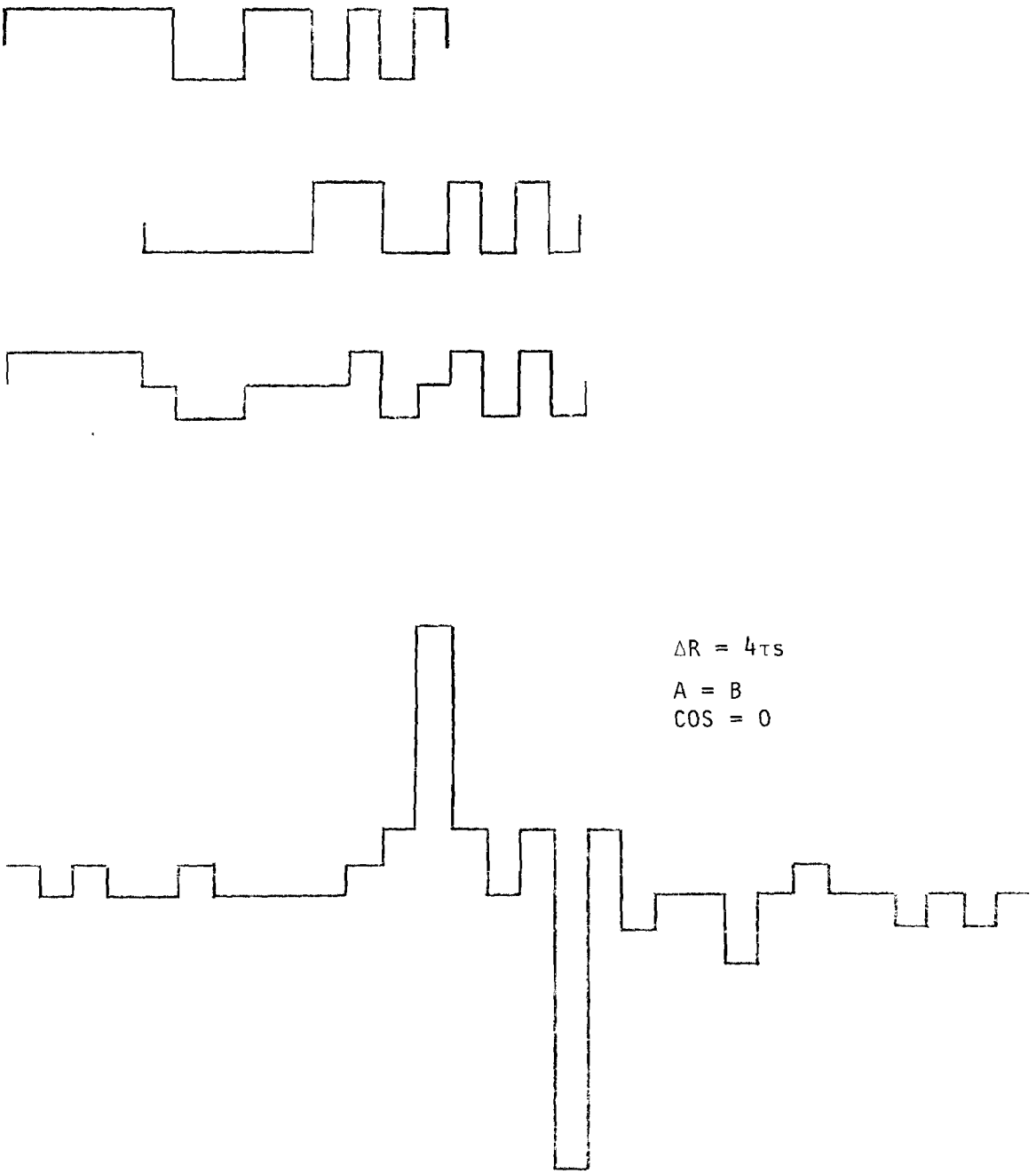

FIGURE A-16. Equal scatterers; Four cell separation.

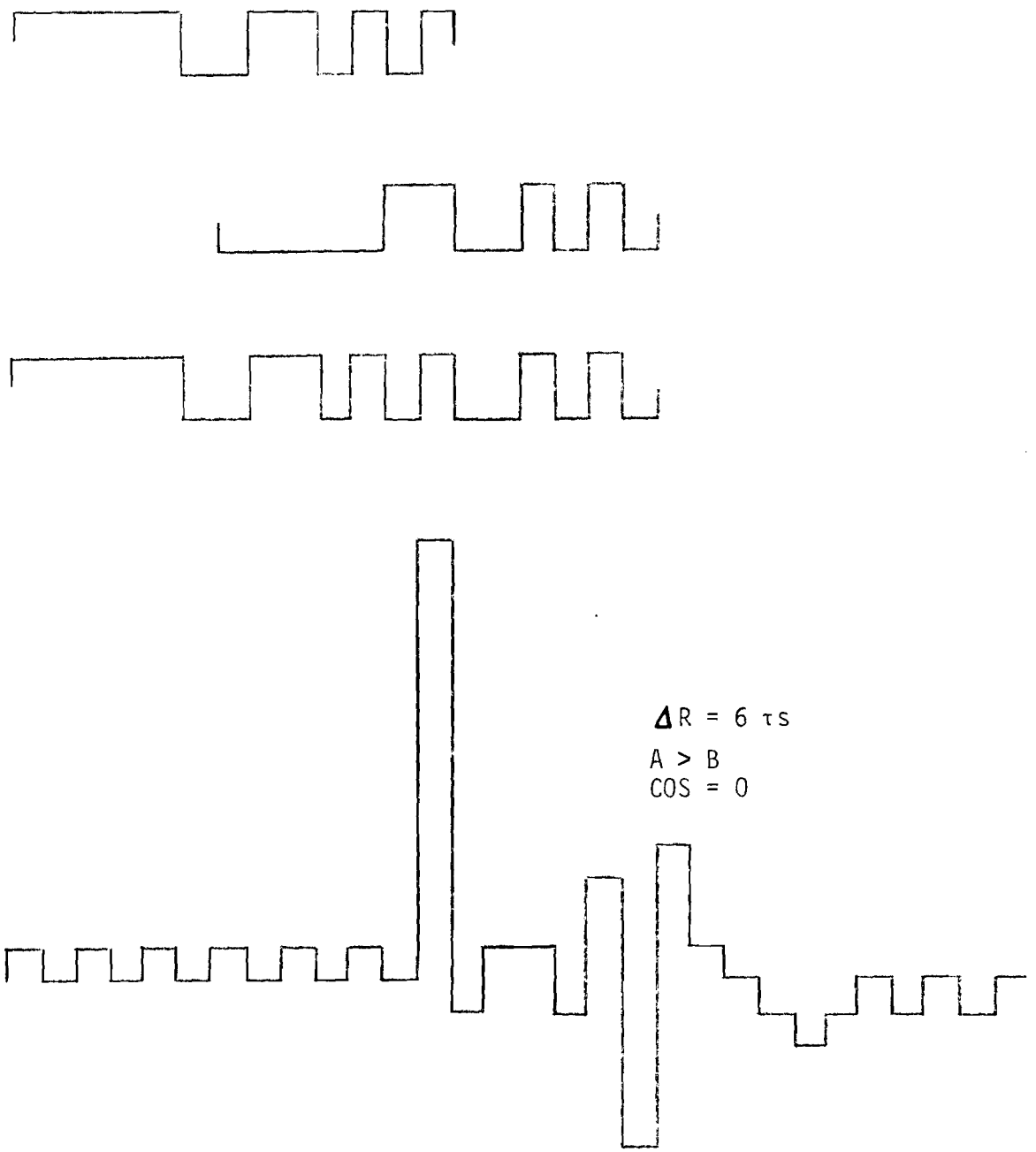

FIGURE A-17. Unequal scatterers; 6 cell separation.

FINAL TECHNICAL REPORT
GIT/EES PROJECT A–2343

INTRAPULSE POLARIZATION AGILE RADAR DEVELOPMENT PROGRAM

By

M. N. Cohen
E. E. Martin
E. S. Sjoberg

Prepared for

SOUTHEASTERN CENTER for
ELECTRICAL ENGINEERING EDUCATION
ST. CLOUD, FLORIDA

Under

Contract No. SCEEE/81–2
Prime Contract No. N00024–78–C–5338

December 1981

GEORGIA INSTITUTE OF TECHNOLOGY
A Unit of the University System of Georgia
Engineering Experiment Station
Atlanta, Georgia 30332

UNCLASSIFIED

SECURITY CLASSIFICATION OF THIS PAGE (When Data Entered)

REPORT DOCUMENTATION PAGE

READ INSTRUCTIONS BEFORE COMPLETING FORM

1. REPORT NUMBER

2. GOVT ACCESSION NO.

3. RECIPIENT'S CATALOG NUMBER

4. TITLE (and Subtitle)

Intrapulse Polarization Agile Radar Development Program

5. TYPE OF REPORT & PERIOD COVERED

Final Technical Report

6. PERFORMING ORG. REPORT NUMBER

GIT/EES No. A-2343 FTR

7. AUTHOR(s)

Marvin N. Cohen, Eugene E. Martin, and Eric S. Sjoberg

8. CONTRACT OR GRANT NUMBER(s)

N00024-78-C-5338
SCEE/79-2 and SCEEE/81-2

9. PERFORMING ORGANIZATION NAME AND ADDRESS

Georgia Institute of Technology
Engineering Experiment Station
Atlanta, Georgia 30332

10. PROGRAM ELEMENT, PROJECT, TASK AREA & WORK UNIT NUMBERS

11. CONTROLLING OFFICE NAME AND ADDRESS

SCEEE, Management Office, Central Florida Facility
11 and Massachusetts Avenue
St. Cloud, Florida 32769

12. REPORT DATE

December 1981

13. NUMBER OF PAGES

54

14. MONITORING AGENCY NAME & ADDRESS (if different from Controlling Office)

United States Navy
Sea Systems Command (NAVSEA)
Washington, D.C. 20362

15. SECURITY CLASS. (of this report)

UNCLASSIFIED

15a. DECLASSIFICATION/DOWNGRADING SCHEDULE

16. DISTRIBUTION STATEMENT (of this Report)

17. DISTRIBUTION STATEMENT (of the abstract entered in Block 20, if different from Report)

18. SUPPLEMENTARY NOTES

19. KEY WORDS (Continue on reverse side if necessary and identify by block number)

Clutter Suppression
Doppler Invariance
ECCM
LPI
Multipath Reduction
Polarization
Polarization Agility
Polarization Compression
Polarization Processing
Radar
Target Enhancement

20. ABSTRACT (Continue on reverse side if necessary and identify by block number)

The Intrapulse Polarization Agile Radar (IPAR) has been successfully field tested, thus proof of the concept of pulse compression on polarization modulation has been established. This report documents the field testing, hardware modifications, and the generation of a preliminary test and data collection plan that were undertaken in fulfillment of the current contract.

DD FORM 1 JAN 73 1473 EDITION OF 1 NOV 65 IS OBSOLETE

UNCLASSIFIED

SECURITY CLASSIFICATION OF THIS PAGE (When Data Entered)

TABLE OF CONTENTS

TABLE OF CONTENTS

(continued)

LIST OF FIGURES

LIST OF TABLES

SECTION 1
INTRODUCTION

1.1 OVERVIEW AND BACKGROUND

The Intrapulse Polarization Agile Radar (IPAR) has been successfully field tested; thus proof of the concept of pulse compression on polarization modulation has been established. The radar/processor has also been enhanced so as to form a capable and complete data collection system. These goals have been achieved under Southeastern Center for Engineering Education, Contract Number SCEE/81-2 (under prime Contract Number N00024-78-C-5338), for which this document is the final technical report.

This report documents the Lake Lanier field operation, local system testing, hardware modifications, and the generation of a preliminary test and data collection plan that were undertaken in the fulfillment of the current contract. The local system testing and Lake Lanier field operation established proof-of-concept for various predicted IPAR properties, and served as "shakedown" outings for the delineation and correction of any system problems or deficiencies. The hardware RF and digital modifications to IPAR included those that: (1) were mandated as a result of the Lanier field operation, and (2) have transformed the IPAR radar/processor from a demonstration radar to a fully capable data collection unit. The testing and data collection plans will be used as a basis for the data collection field operation that comprises the first part of the next phase of the ongoing IPAR program.

Under contract to the Air Force six to seven years ago, GIT/EES was tasked to investigate stationary target indication techniques. During this project (A-1686), the relative usefulness of employing frequency agility and polarization agility, independently and together, to simulate clutter decorrelation was tested.[1,2,3] Two processors were constructed to discriminate between clutter and hard targets: Dynamic Threshold Gating (DTG) and Correlation Coefficient Discrimination (CCD) processors. Some success was achieved, but it was difficult to state the degree of improvement in quantitative terms. Of greater significance were two observations made by project personnel during the final phase of that program. The processors were designed to work primarily with amplitude discriminants, but discriminants (i.e., difference between clutter and targets) were also observed in the relative phase characteristics of the two orthogonal polarizations.

Subsequent to project A-1686, several field experiments and demonstrations were conducted. One of the more notable demonstrations, in terms of technique exposure, was conducted at Missile Command (MICOM), Huntsville, Alabama. GIT/EES personnel were positioned on a hill with Radar Van GT-2. The radar (AN/APQ-126) which had been used in project A-1686 was used. Normal amplitude, phase detected, and threshold gated integrated digital video were simultaneously displayed. Targets included corner reflectors and tanks. MICOM personnel were given briefings and they observed the simultaneous A-scope presentation of amplitude, phase and integrated digital video. The tank was moved around during the demonstration so that the observers could be certain of what they were viewing. Polarization, frequency agility, threshold setting and integration time were all variable and were varied during the demonstration. Photographs (i.e., both Army and GIT/EES) were made during the demonstration. Attenuators were used to attenuate the clutter signal until its amplitude matched the unattenuated target amplitude. The relative clutter-to-target amplitude was found to be approximately 20 dB, yet the target could still be detected and displayed without clutter false alarms. In addition, project personnel who had been involved in project A-1686 made observations that performance varied between inter-cell and intra-cell conditions.

In 1978, an analysis of Pseudo-Coherent Detection (PCD) techniques was conducted. This analysis is documented by report DELCS-TR-76-0961-F, entitled "Stationary Target Detection and Classification Studies," dated April, 1979.[4] The analysis did not predict the performance which had already been demonstrated. Subsequently, it was learned that the analysis did not include the considerations which would have been representative of the conditions under which the demonstration was conducted. For the demonstration, the average clutter in the vicinity of the target was tens of dB larger than the target, whereas the clutter in the exact resolution cell containing the target was nil. For that particular technique, lower in-cell clutter (which reduces the combined target plus in-cell clutter amplitude relative to the average regional clutter) increases the detection probability.

The first phase of the IPAR program was begun by the Georgia Institute of Technology in March 1979 under the auspices of the Southeastern Center for Electrical Engineering Education (SCEE), subcontract SCEE-NAVSEA/79-2, Contract Number N00024-78-C-5338, with Mr. Charles Jedrey of NAVSEA acting as Technical Monitor. During this program (Georgia Tech Project Number A-2343), a demonstration state-of-the-art IPAR radar/processor was designed, built, and demonstrated. In addition, a

detailed paper-and-pencil analysis of PCD was conducted to better understand this technique, which lies at the heart of the IPAR process, and to attempt to clarify the apparent lack of consistency (as noted above) between the predicted and observed effects of PCD. The results of the program are documented in the project final report dated July 1981.[5] In summary, the system was designed, assembled, and successfully demonstrated. Essentially perfect intrapulse polarization coding and compression of the radar waveform was achieved at real-time rates of up to 50 MHz, and somewhat degraded compression was achieved at rates up to 100 MHz. Thus, the concept of compression on polarization modulation was successfully reduced to hardware implementation. The paper and pencil analyses of PCD were completed and successfully closed the gap between theory and experience, thus establishing a theoretical basis for future applications of IPAR.

1.2 THE IPAR CONCEPT

IPAR utilizes dual channel polarization diversity to code transmit pulses in polarization (currently left and right circular polarizations are utilized) on a subpulse basis and, to subsequently, compress the reflected pulses to the subpulse width. Since all the compression coding information is contained in the relative phase between the received horizontal and vertical polarization channels, the compression process is independent of absolute carrier phase and thus is totally immune to the losses and velocity-distance ambiguity inherent in the classical pulse compression processes. IPAR thus provides an all-velocity pulse compression scheme that does not require system coherency or the banks of Doppler filters usually required for such a process.

Since the IPAR process is independent of absolute carrier phase, it can be implemented with various RF sources. In particular, the IPAR process works just as well with a wideband noise source or a frequency agile source as it does with a narrow band carrier. This latitude in the choice of carrier has potential applications in the areas of target/clutter discrimination (clutter decorrelation via frequency agility and polarization processing), generation of lower probability of intercept (LPI) waveforms (reduced power spectral densities per Hertz and polarization-diverse transmissions), and electronic counter-countermeasure (ECCM) techniques (jam resistance due to polarization coding and the use of spread spectrum waveforms).

In addition to the theoretical innovation embodied by the IPAR concept and the wealth of potential signal processing applications its simultaneous polarization and

frequency agile capabilities generate, IPAR represents the state-of-the-art in processor design. In particular, as presently configured, IPAR is capable of a 100 MHz real time operational rate so that resolutions on the order of 10 meters and pulse compression ratios up to 32:1 can be achieved.

The following subsections give a brief review of what are, for our purposes here, the most salient features of: (1) pulse compression coding, (2) polarization phenomena, and (3) the synergism that results from the merging of the two technologies. These subsections thus form the conceptual/theoretical footing for the IPAR process.

1.2.1 PULSE COMPRESSION CODING

A radar pulse may be coded in any one of a number of ways so that both the effective resolution and power of the transmitted pulse are greatly enhanced. Such coding is termed pulse compression coding.

The concept of pulse compression is best illustrated by an example. Referring to Figure 1.1(a), the given transmitted pulse of duration T has been coded with a sequence of thirteen carrier phase reversal intervals (where "+" denotes no phase reversal and "-" denotes a reversal of 180°), each of which is said to have duration τ ($\tau = \frac{T}{13}$). The ideal echo receiver filter (in terms of optimal signal-to-noise ratio is matched to the transmit waveform, as depicted in (b) of the figure. Assuming a completely undistorted (in phase) echo return, the output from the matched filter is given in (c) of Figure 1.1. The most salient features of this signal are its effective resolution of $\tau/2$ seconds and its effective voltage level of 13 units. Note that the uncoded pulse would have achieved a resolution of T/2 seconds and a relative voltage level of 1.

The coding used for the above example is called binary phase coding of the carrier. Binary phase coding has been employed using various coding schemes (Barker, pseudorandom, combined Barker, etc.), and it, together with various frequency coding schemes (linear frequency modulation and frequency hopping, for examples), make up the bulk of pulse compression schemes put into use over the last thirty years. The practice of pulse compression utilizing frequency and phase coding is well understood and routinely used in modern-day radar systems.

The widespread application of pulse compression results from the following list of well-established operational advantages of such a system over a simple pulse system:

- Extremely high range resolution and range accuracy as well as resolution flexibility.

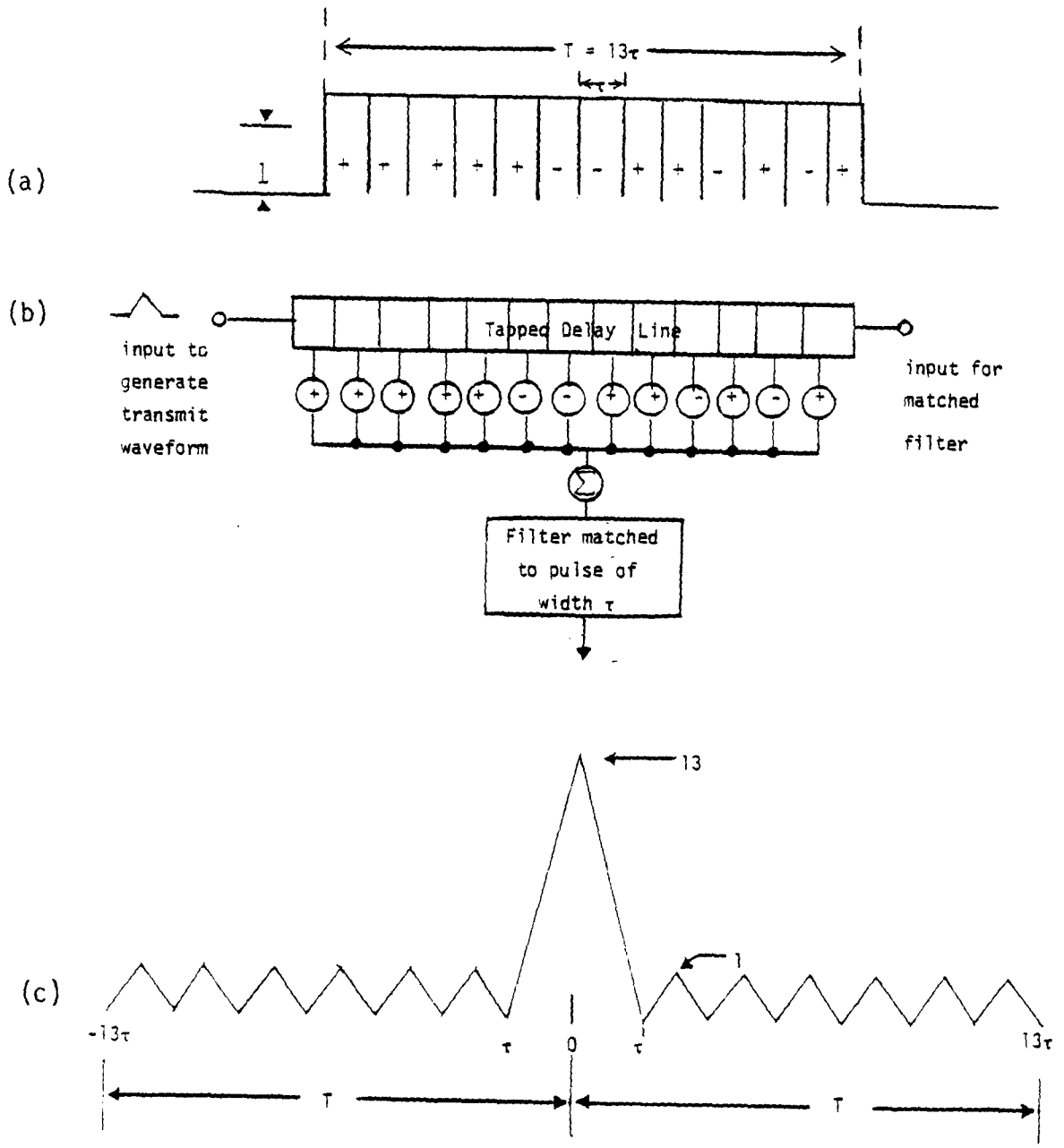

Figure 1.1 Binary-coded pulse compression.

- Improved signal-to-noise ratio (SNR) for a transmitter with a given peak power.
- Clutter reduction in target cell.
- Multipath reduction.
- Lower probability of intercept (LPI) potential.
- Electronic counter-countermeasures (ECCM) potential.

The nucleus of the IPAR concept is that pulse compression can be achieved utilizing coding of the polarization of the transmitted electromagnetic wave as opposed to the classical methods of coding the phase or frequency of the carrier. The resulting waveforms have potential for power and resolution enhancement similar to that of the classical waveforms, but the IPAR waveform is sensitive to different waveform perturbations and behaves substantially differently when reflected by complex targets.

The next subsection briefly describes the basic properties of polarization that are essential to understanding the IPAR pulse compression process.

1.2.2 POLARIZATION

Radar signals may be polarized in the sense that the E-field voltage modulation can be constrained to a particular plane in 3-dimensional space or the plane of modulation can be varied in a particular manner. Figure 1.2 depicts two orthogonal linear polarizations: a vertically (V) polarized electromagnetic wave in (a) and a horizontally (H) polarized wave in (b). The planes of polarization can be defined as the plane perpendicular to which no E-field modulation can be detected. Electromagnetic waves with <u>elliptical polarizations</u> are generated by transmitting sinusoidal H and V polarized waves simultaneously, but out of phase. If the amplitudes of the H and V sinusoids are equal, the polarization is said to be <u>circular</u>. Figure 1.3 depicts two orthogonal circular polarizations. In 1.3(a), the H component lags the V component by 90°. The resultant wave's plane of polarization varies according to the right hand rule in the direction of propagation. Such a wave is said to have <u>right circular</u> (RC) polarization. Figure 1.3(b) depicts a similar situation where the H component, however, leads the V component by 90°. As can be seen by the depiction of the resultant field vector, the wave is now left circularly (LC) polarized.

The circular polarization of a reflected wave is affected by the nature of the reflecting surface. In particular, the circular polarization of a wave reflected from an

(a)

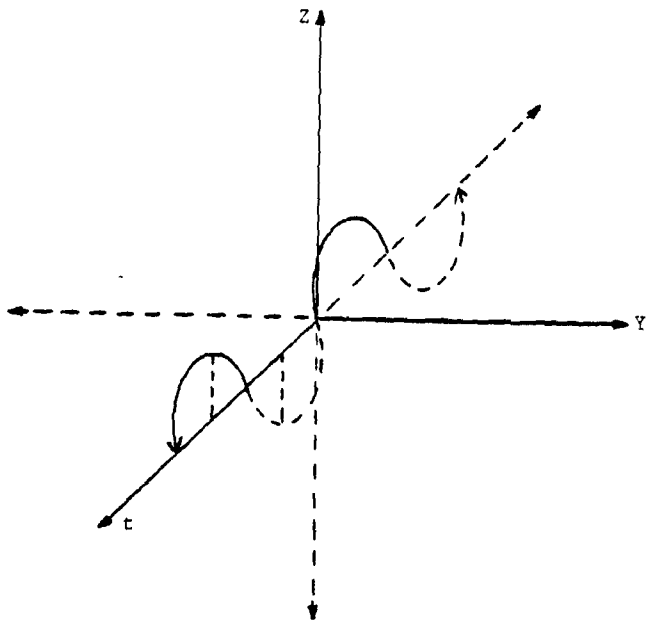

VERTICAL POLARIZATION

HORIZONTAL POLARIZATION

(b)

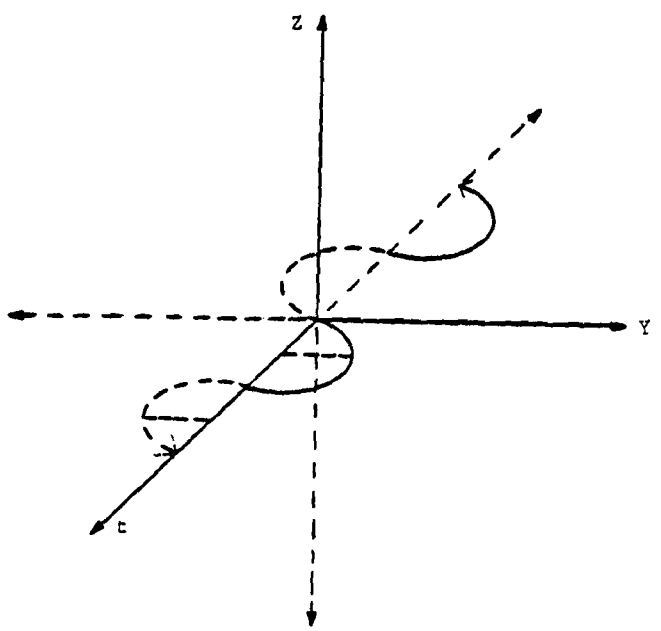

Figure 1.2 Orthogonal linear polarizations.

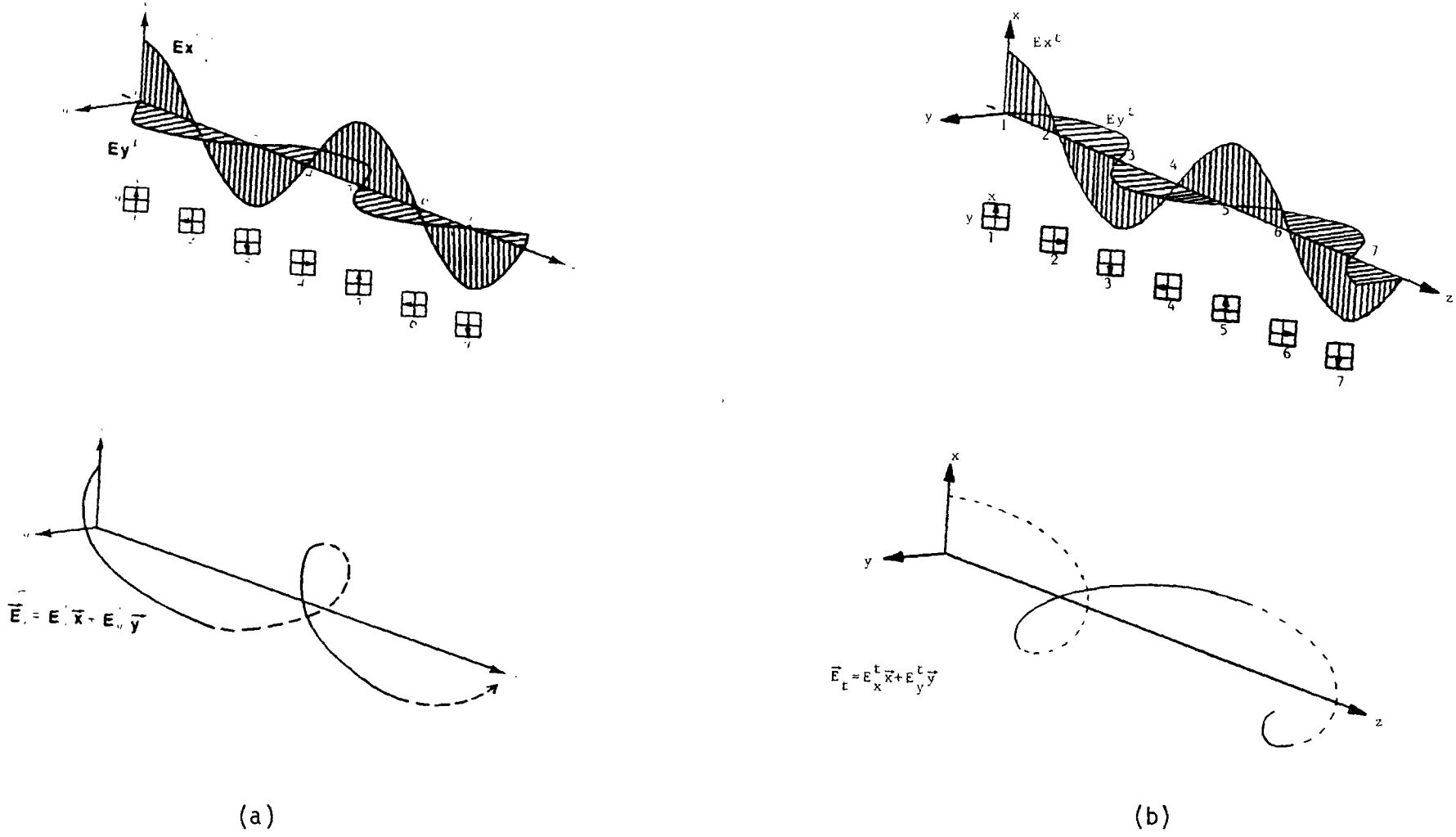

Figure 1.3 Right and left circularly polarized waves.

odd-bounce scatterer is opposite in sense from the polarization of the incident wave (e.g., RC incident yields LC reflected and vice versa). As can be deduced from the odd-bounce case, even-bounce reflectors leave circular polarizations unchanged (e.g., RC incident results in RC reflected). Figure 1.4 depicts the single-bounce case.

The phenomenon underlying these effects is merely that on a single bounce the relative phase ϕ_{HV} between the H and V components of the wave remains unchanged (since both are flipped by 180° in phase) while the direction of the propagation is reversed. The net result is a change in handedness of the electromagnetic wave, just as one would observe a change in handedness of the rotation of a transparent clock when it is viewed from front and back.

The phenomena just described have been used to achieve rain and snow clutter reduction.[6] The most straightforward application has been to utilize a circularly polarized antenna, say RC, to detect aircraft in rain. Since raindrops are essentially spherical, they act as odd bounce reflectors and thus return LC polarized waves. An aircraft, on the other hand, is a complex scatterer that will return some energy in each of the circular polarizations. A right circularly polarized antenna will reject all the LC polarized rain return and accept only the RC polarized rain returns. The percentage of even-bounce reflectance that the aircraft exhibits thus determines the achievable target to clutter enhancement.

1.2.3 PULSE COMPRESSION ON POLARIZATION MODULATION

The prototype IPAR radar processor is capable of switching between right and left circular polarization on an intrapulse basis at rates of up to 100 MHz. Utilizing separate H and V ports on receive, IPAR downconverts the two channels separately, and accurately measures the phase between them. As before, let ϕ_{HV} represent the phase difference between the H and V channels (that is, $\phi_{HV} = (\phi_H - \phi_V)$, and recall that a signal is RC polarized if $\phi_{HV} = +90^{o}$ and LC polarized if $\phi_{HV} = -90^{o}$. For convenience, let $S = \sin\phi$. Then $S\phi_{HV} = 1$ for RC signals and $S\phi_{HV} = -1$ for LC signals, thus giving a natural correspondence between binary codes and intrapulse polarization modulation. IPAR utilizes this correspondence to construct well-behaved polarization codes from the class of well-known, well-behaved binary codes.

Figure 1.5(a) depicts a natural choice for an IPAR transmit waveform. According to the correspondence described above, the chosen code represents a 13-bit Barker code, and it makes possible a pulse compression ratio of 13 to 1. Figures 1.5(b)-(e) represent

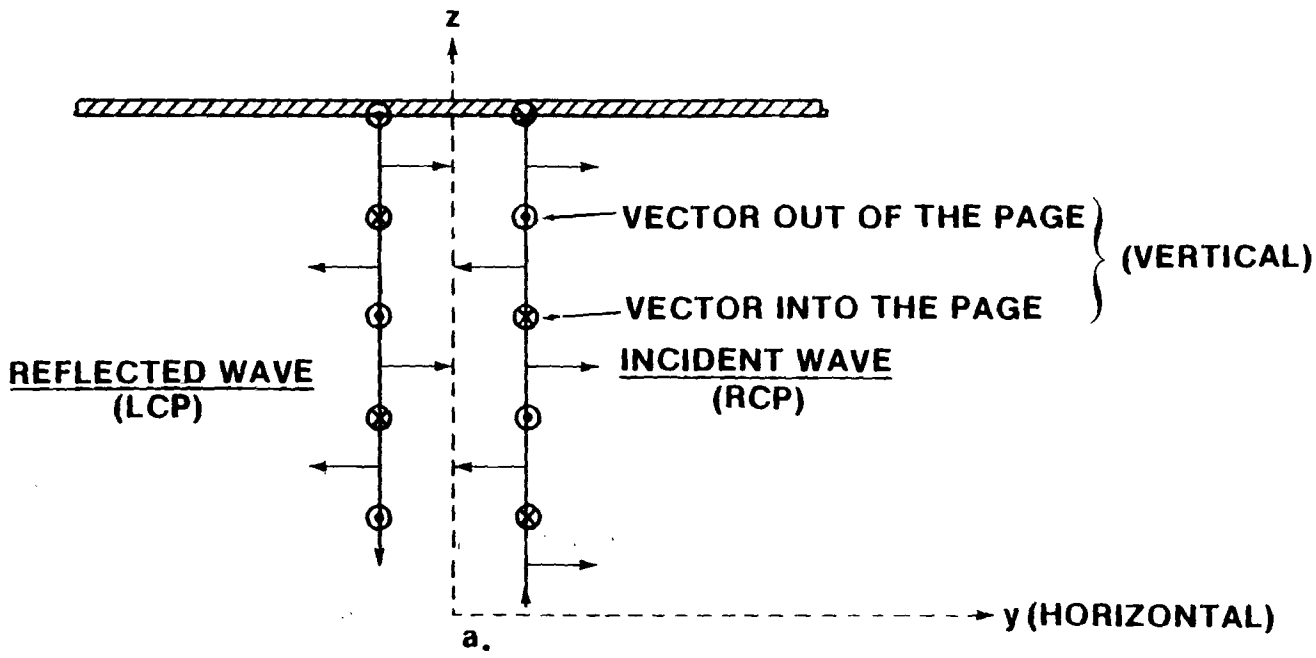

Figure 1.4 **RCP incident on flat plate.**

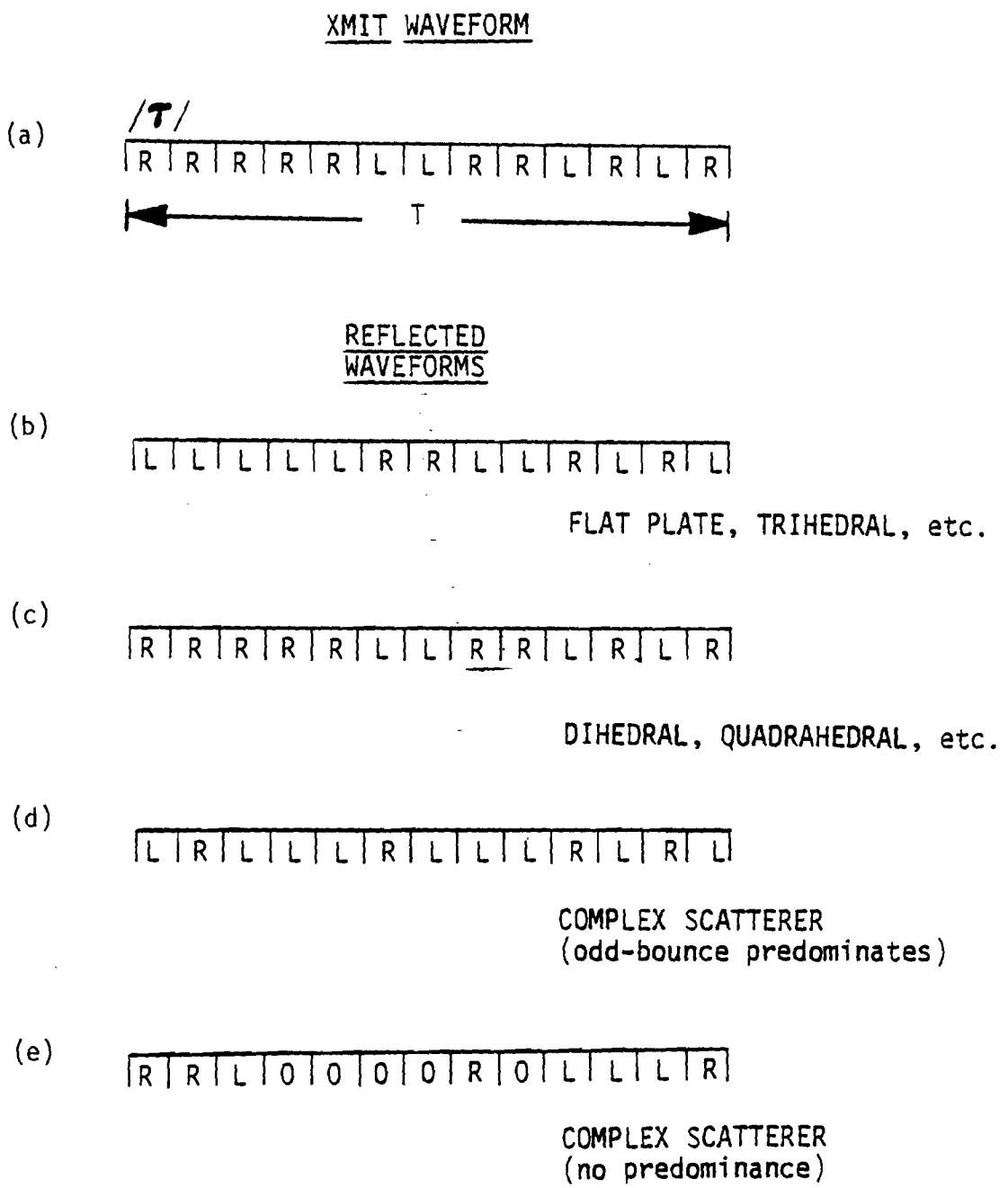

Figure 1.5 Simulated IPAR transmit and receive waveforms.

four of the possible reflected waveforms. Figure (b) represents the echo from a flat plate or any other odd-bounce scatter. As explained in Section 1.2.2, the polarization of the echo in this case is always opposite in sense from the polarization of the transmitted wave. Figure (c) represents the return from an idealized even-bounce scatterer; thus the polarizations are unchanged. Figures (d) and (e) represent likely returns from complex scatterers where each was generated assuming a simple probabilistic model. In (d), it was assumed that the echo source was predominantly odd-bounce so that 75 percent of the time the polarization sense was changed, 12.5 percent of the time the polarization remained the same, and 12.5 percent of the time the sense was sufficiently mixed so as not to exceed a threshold either way. In (e), it was assumed that the scatterer had an equal mix of odd-bounce and even-bounce scatterers so that neither type predominated over a period of time. Thus, the model assumed 33.3 percent polarization change, 33.3 percent retention of polarization sense, and 33.3 percent lack of sufficient bias to exceed a threshold either way (denoted by "0").

When receiving any of these four "possible" returns, the IPAR processor computes $S\phi_{HV}$ on a subpulse basis and passes the results through a matched filter essentially identical to that depicted in Figure 1.1. The resulting returns are catalogued in Figure 1.6. Figure 1.6(a) depicts the transmit waveform's autocorrelation, which is precisely the output of the processor in response to an even-bounce return (Figure 1.5(c)). Note that the resolution is $\tau/2$ rather than T/2 (a 13 to 1 improvement), and that the peak signal voltage is $\frac{T}{\tau}$ (13) times the nominal uncompressed level. Figure (b) represents the output in response to an odd-bounce scatterer. It's power characteristics are precisely the same as those of (a) although there is a change of sign in voltage. As the reflecting scatterer gets more complex, the degree to which the transmitted code is retained in the reflected waveform decreases. Figure (c) still shows a recognizable peak in response to the "predominantly odd-bounce" reflection, whereas Figure 1.6(d) depicts the noise-like return expected from a scatterer that shows no predominance.

1.2.4 POTENTIAL APPLICATIONS

The basic operating principles of IPAR have been observed in field tests of the demonstration IPAR system and can be used to briefly explain some of the most outstanding properties and potential applications of IPAR.

Since IPAR's pulse compression coding information is carried in the <u>relative phase</u> between the two simultaneously transmitted channels, this form of pulse compression is

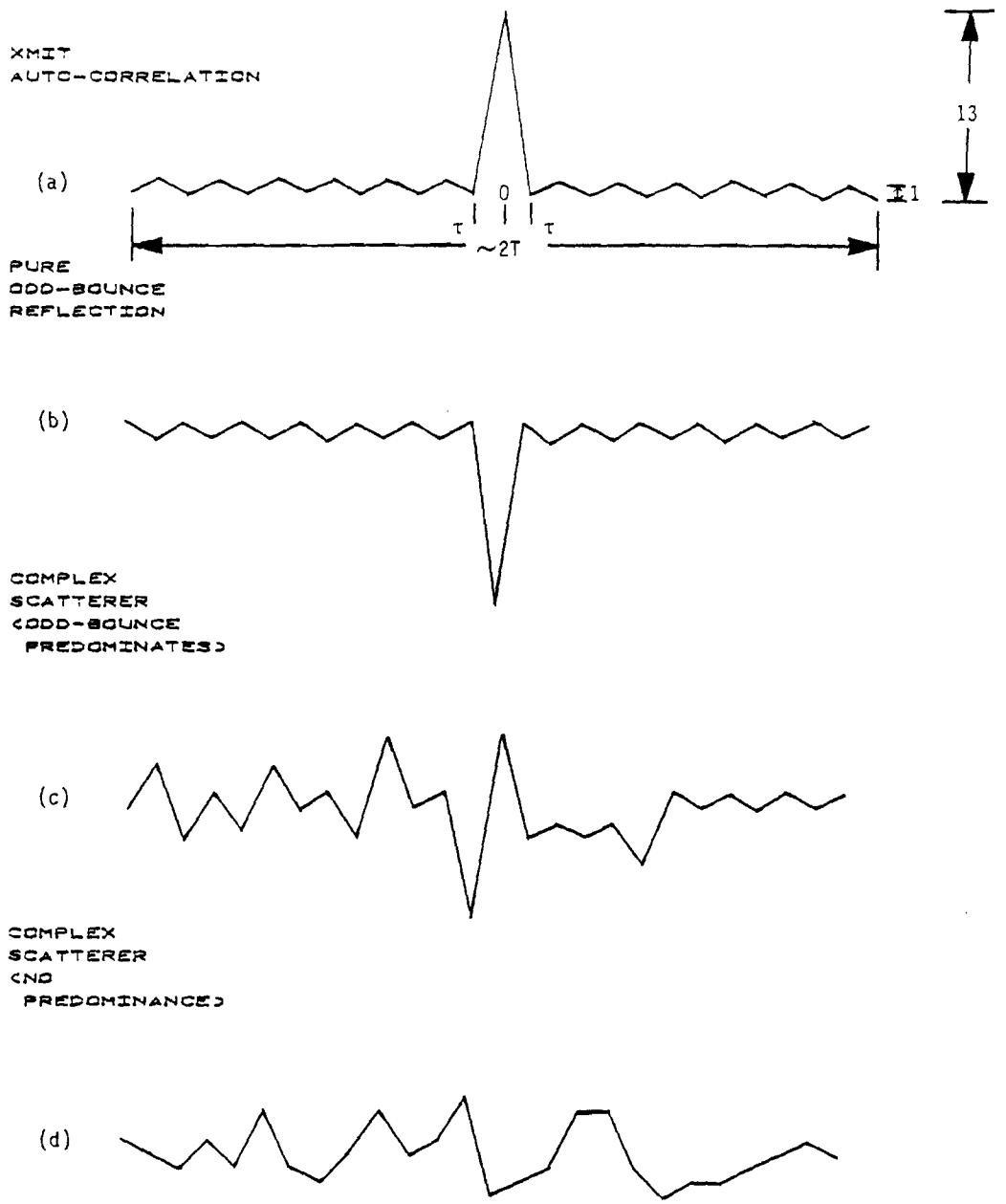

Figure 1.6 Compressed outputs.

practically invariant under Doppler shift (since both channels will be shifted by the same $\frac{2V}{\lambda}$ Hertz for any target travelling with radial velocity V). Although phase and frequency coding are practically invariant with respect to target reflection characteristics, the IPAR waveform will be quite sensitive to these characteristics. It seems that the analog of the ambiguity diagram (distance-velocity-amplitude), which is indispensable to the study of phase/frequency coded waveforms, for IPAR waveforms is a polarization ambiguity diagram (distance-target composition-amplitude).

Since absolute carrier phase is of no importance in an IPAR system, various carriers can be used. In particular, the RF may just as well be wideband noise or a frequency hopped carrier instead of a single narrow band frequency. These possibilities seem to hold a great deal of promise for lower probability of intercept (LPI) operation, electronic counter countermeasure (ECCM) techniques, and the selective decorrelation of clutter.

While the sensitivity of polarization coding to target composition necessitates detailed analyses of the waveform for various scenarios, this sensitivity also introduces many potentially useful characteristics. For example, if subpulse length can be reduced to enable range resolution on the order of one foot or so, it seems likely that many man made objects would appear to be made up of individual, simple scatterers--in which case, compression would be almost totally effective. On the other hand, many types of clutter such as leaves, windblown rain and snow, and field clutter would still appear to be made up of many independent scatterers--thus giving more noise-like returns. This difference in composition should allow for substantial target to clutter enhancement.

Similarly, in addition to the usual gains one achieves against multipath by employing pulse compression (by "gating out" double bounce returns on a range resolution basis), an IPAR type process would take advantage of the depolarizing effect of the second bounce to further reduce multipath interference, especially when the "ground" is the surface of a somewhat turbulent sea.

1.3 PROGRAM OBJECTIVES

The major objectives of the current program were to: (1) demonstrate proof-of concept for some of the theoretically predicted properties of IPAR-type waveforms, and (2) to perform the hardware modifications and enhancements, and preliminary planning necessary to prepare the IPAR processor/radar for a successful data collection mission in Panama City, Florida, which is scheduled for the next phase of the program.

1.4 PROGRAM SUMMARY

The IPAR radar/processor was tested both at the Georgia Institute of Technology Research Facility at Cobb County and at Lake Sidney Lanier. As a result of these tests, the equipment was found to be fully operational, enhancements necessary for a formal data collection field operation were identified, and qualitative proof-of-concept was established for various IPAR properties. Among the IPAR properties whose efficacy were established were:

(1) Pulse compression on polarization modulation.

(2) Target/clutter discrimination.

(3) Clutter suppression via frequency diversity.

(4) Real-time pulse compression at 100 MHz.

In response to the knowledge gained during the field testing of the equipment, a phase of hardware extensions was embarked on. These extensions included those that were both necessary and sufficient to ensure a fully capable and complete data collection radar system for the next phase of the IPAR program, i.e., the local and remote data collection field operations.

A dedicated digital-tape interface was built, tested, and interfaced to the IPAR processor. The interface allows for the recording of 32 range bins of IPAR data at up to a 2 KHz PRF. The interface was designed to link the IPAR processor to a Digi-Data 1700 series digital tape recorder that will be available in-house for the planned data collection programs.

A wideband noise source and swept frequency source were integrated with the RF section of IPAR to add noise and swept-frequency carrier capability to the existing narrow band 9.5 GHz carrier capability. The entire RF section was tuned so that the two independent channels were phase matched on both transmit and receive. In this way, any internal mismatches that would cause losses in a frequency diverse mode were eliminated.

SECTION 2
PROGRAM ACCOMPLISHMENTS

This section documents in detail the achievements of this phase of the IPAR program. Section 2.1 describes the digital and RF hardware modifications that have transformed the IPAR test system into a data collection system capable of operating in fixed frequency, frequency swept, or wideband noise modes. Section 2.2 documents the IPAR field testings that established proof-of-concept for some of its theoretically predicted properties and provided the data on which to base the necessary hardware modifications. Section 2.3 represents a preliminary test and data collection plan for the next phase of the IPAR program.

2.1 HARDWARE EXTENSIONS

A digital tape interface between the IPAR digital processor and a Digi-Data 1700 series digital tape recorder was built and integrated into the IPAR system. As a result, it is possible to record the quantized relative phase signals from each of the subpulse intervals in a given range gate of data.

A swept frequency source and noise source were incorporated to augment the system's 9.5 GHz narrow band carrier capability. The entire system was tuned so that the path length of signals through the two independent transmit and two independent receive channels were matched. As a result, the IPAR system can be operated in either of the two frequency diverse modes without the introduction of internal losses due to phase mismatch.

These hardware modifications are fully described and documented in the following subsections.

2.1.1 DIGITAL EXTENSIONS

It is highly desirable to record the quantized, relative phase signals from each of the subpulse intervals in a given range gate of the coded IPAR signal. Recording this data will enable the analysis of: (1) the effect of subpulse length on target signature, (2) the effect of multiple scatterers within the total pulse, but separated by more than the subpulse length, (3) the effect of different code lengths, (4) the "goodness" of different codes for various functions (detection, classification, etc.), and (5) the stability

(repeatability) of the received signal on a pulse-to-pulse basis (decorrelation time). Therefore, a digital tape recording capability was added to the IPAR digital processor.

The IPAR digital processor samples and stores the quantized received signal (32 subpulses) from the selected range gate. (By quantized is meant that the analog signal is digitized into two 32-bit words which together represent the three state (+1, 0, -1) phase quantization.) Front panel switches allow routing of these data to an external device under control of that device. Radar and Instrumentation Laboratory (RAIL) at Georgia Tech owns two digital tape drives which can be used to record this data. An interface box was built to interface the digital tape drives to the IPAR digital processor for recording the two 32-bit received data words onto digital tape at the PRF rate along with appropriate header data.

2.1.1.1 The IPAR Digital Tape Interface

This subsection documents the use of the IPAR digital tape interface and the format and contents of digital tapes written by this hardware. The interface communicates with a Digi-Data 1700 series digital tape recorder equipped with the dual buffered tape system and phase encoded formatter. Tapes are automatically written at 1600 BPI, phase encoded (PE) format.

The digital tape interface connects to IPAR via a 41 pin MS connector and to the tape equipment via a 100 pin edge connector. Both connectors with their cables are firmly attached to the interface unit. The interface derives its required power from the IPAR digital processor and is turned on and off by the IPAR power switch.

2.1.1.2 Use

Connect the interface unit to IPAR and the digital tape formatter via the supplied cables. Power up the tape transport, the formatter, and IPAR. Install a tape onto the transport and press the LOAD button on the transport. After the tape stops, press the ON LINE button on the transport. The tape unit is now ready to receive data from IPAR.

Adjust the switches on the IPAR digital panel to the desired parameters. All switches function normally and the full range of features provided by the IPAR processor are operational when connected to the digital tape interface unit. When used with the digital tape unit, the PRF switch must be in the 500, 1000, or 2000 Hz position. The MAN, 4000, and 8000 positions may not be used. The DATA display switch must be in the TO COMP position when data are being recorded; it may be moved to any other position

for manual examination of data, when desired, but it must be returned to the TO COMP position prior to recording data. Additionally, the RADAR CONTROL switch must be in the PANEL position for proper operation. After selecting the correct parameters, set the RADIATE switch to the red, radiate, mode. The digital tape interface uses the range gate signal following the transmit pulse for synchronization and will not operate unless IPAR is in the radiate mode. During recording of a file on digital tape, none of the IPAR switches should be operated, or unpredictable results will be obtained.

The interface unit panel is divided into four areas with the controls and indicators grouped according to function. The functions of the switches and indicators in the four sections are listed in the following paragraphs.

2.1.1.2.1 Control Section

START Switch: Causes a new file to be written to the digital tape starting with the header data. Operation of the START switch while writing a file has no effect.

STOP Switch: Ceases the writing of data to digital tape after completion of the present data record. No incomplete records will be written. An end of file (EOF) mark is automatically written after all the data are transferred.

EOF EN LED: The End Of File ENable LED indicates that the digital tape formatter will accept an EOF command. This LED should be off when data are being written.

Write EOF Switch: Causes an EOF mark to be written on the tape when the EOF EN LED is illuminated. If that LED is not illuminated, the switch has no effect.

2.1.1.2.2 Header Section

RUN NO Thumbwheel Switch: Any run number from 00 to 99 may be selected via this switch.

LOAD RUN NO Switch: Causes the number selected by the thumbwheel switch to be used for the next file on tape. The number will be indicated by the run number display.

HEADER RUN NO Display: Indicates the run number which was written into the header of the data file currently being written. The run number to be used for the next file to be written is determined in one of two ways: (1) if the LOAD RUN NO switch was operated after the last file was written, then the run number currently displayed will be written to tape; (2) if the LOAD RUN NO switch has not been operated since the last file

was written, then the displayed run number will be incremented by one and this new incremented run number will be used for the next header.

HEADER DATA Thumbwheel Switches: Determine the additional data, along with the run number, which will be placed on the header record of each file. If the switches are labeled in the order shown in Figure 2.1, then the data are written to the tape in three words in the order BA, DC, FE.

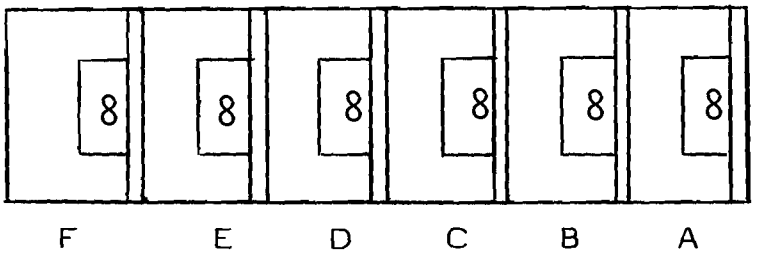

Figure 2.1 HEADER data switches.

2.1.1.2.3 Status Section

Interface LED: Indicates that the interface unit is ready to write a file to tape. The LED is not illuminated when a file is being written. The LED is turned back on when an end of file (EOF) mark has been written to the tape.

TAPE LED: Indicates that the digital tape recorder is under remote control, on line, and ready to receive data.

EOT LED: The end of tape (EOT) LED is illuminated when the EOT signal is received by the interface unit from the tape formatter. When this LED is illuminated, the operator must mount a new tape.

EOT RESET Switch: Turns off the EOT indicator until another EOT signal is received from the tape formatter.

2.1.1.2.4 Error Section

SYNC LED: Indicates that at least one record pulse was issued to the digital tape formatter when the FULL line from the formatter was active. This means that the A and B receive data are out of synchronization and there may be confusion when reading the tape. The SYNC indicator is turned off by the next START command. If the SYNC

indicator turns on while recording a file, that run should be discarded and the experiment should be repeated. The synchronization is self-correcting, however, and usable data might be able to be obtained if the experiment cannot be repeated.

BUSY LED: The BUSY LED is illuminated whenever one of the following occurs: (1) Power On. The BUSY LED remains on until the digital tape system is placed ON LINE at the load point. (2) While in the WRITE mode there are characters in both buffers and an INIT IRG command is received. The BUSY remains illuminated until one of the buffers is empty and INIT IRG and REC are both false. (3) The system is in the EOF mode. The BUSY LED remains lit until the completion of the EOF routine. Data transmitted while BUSY is true will be lost. (4) The system is OFF LINE. BUSY remains true while the tape drive is OFF LINE.

The BUSY LED should never become illuminated when a file is being written. That would indicate that data are being lost and the probable cause is that the IPAR PRF switch is in the 4000 or 8000 Hz position.

Parity Errors Display: Is an indication of the number of parity errors which occurred when the last data file was written. The parity errors are detected by the digital tape system by reading the data on the tape after it is written.

2.1.1.3 Digital Tape Data and Format

The format and contents of the IPAR digital data tape are indicated in Table 2.1. Refer to Figure 2.1 for the HEADER data switch nomenclature.

2.1.2 RF EXTENSIONS

During the field operation, the IPAR was reliable and observations indicated that the system performed well, except during swept frequency and noise source operation. After the field operation, these problems were investigated. Our findings and corrective hardware modifications are described below.

2.1.2.1 Phase Matching Within The System

It was observed in the field (see Section 2.2) that lower average correlations were achieved on simple targets when frequency diversity was introduced than when a narrow band carrier was utilized. The primary cause of these lower average correlations was traced to unequal path lengths in the two channels of the transmitter and the two channels in the receivers. The frequency versus phase sensitivity due to path length differences may be determined from the following set of equations:

TABLE 2.1 IPAR DIGITAL TAPE CONTENTS AND FORMAT

WORD NUMBER	DATA (BIT NUMBER)								COMMENTS
	7	6	5	4	3	2	1	0	Beginning of each file
1*	B8	B4	B2	B1	A8	A4	A2	A1	
2*	D8	D4	D2	D1	C8	C4	C2	C1	
3*	F8	F4	F2	F1	E8	E4	E2	E1	
4	R18	R14	R12	R11	R08	R04	R02	R01	Run No. (BCD)*
5	S7	S6	S5	S4	S3	S2	S1	S0	IPAR Status**
6	S15	S14	S13	S12	S11	S10	S9	S8	IPAR Status**
7	S23	S22	S21	S20	S19	S18	S17	S16	IPAR Status**
8	S31	S30	S29	S28	S27	S26	S25	S24	IPAR Status**
9	A7	A6	A5	A4	A3	A2	A1	A0	A Reference**
10	A15	A14	A13	A12	A11	A10	A9	A8	A Reference**
11	A23	A22	A21	A20	A19	A18	A17	A16	A Reference**
12	A31	A30	A29	A28	A27	A26	A25	A24	A Reference**
				INTER-RECORD GAP					
1	a7	a6	a5	a4	a3	a2	a1	a0	A Receive
2	a15	a14	a13	a12	a11	a10	a9	a8	A Receive
3	a23	a22	a21	a20	a19	a18	a17	a16	A Receive
4	a31	a30	a29	a28	a27	a26	a25	a24	A Receive
5	b7	b6	b5	b4	b3	b2	b1	b0	B Receive
6	b15	b14	b13	b12	b11	b10	b9	b8	B Recieve
7	b23	b22	b21	b20	b19	b18	b17	b16	B Receive
8	b31	b30	b29	b28	b27	b26	b25	b24	B Receive
9	a7	a6	a5	a4	a3	a2	a1	a0	A Receive
1024	b31	b30	b29	b28	b27	b26	b25	b24	
				INTER RECORD GAP					
1	a7	a6	a5	a4	a3	a2	a1	a0	A Receive
⋮									
1024	b31	b30	b29	b28	b27	b26	b25	b24	B Receive
				END OF FILE MARK					

The number of records per file is variable in comments' column.

*The numbers chosen by switches A through F are written in BCD format as is the run number. The most significant digit of the run number is in bit position 4-7.

**This data is inverted from that presented by the LED's on the IPAR front panel. The interpretation of the STATUS data is found in Table 2.2.

TABLE 2.2 STATUS WORD INTERPRETATION

IPAR STATUS WORD BIT POSITION	INTERPRETATION
0 - 15	No meaning - ignore
16	IPAR Display Switch Position 1 = to digital tape 0 = to panel If this bit is a 0 the data is bad. If it is a 1 it may be good.
17	IPAR Computer Flag Switch 0 = set 1 = clear Of no consequence if Radar Control Switch is in the Panel Position.
18	IPAR Run/Test 0 = run 1 = test In test mode, A Receive = all 0's and B Receive = all 1's.
19 - 21	Subpulse Length

Subpulse Length	Bit 21	20	19
10	1	1	1
20	0	1	1
40	1	0	1
80	0	0	1
100	1	1	0

22 - 25 PRF

PRF	Bit 25	24	23	22
man	0	1	0	1
500	0	1	1	1
1000	0	1	1	0
2000	0	1	0	0
4000	0	0	0	0
8000	1	0	0	0

26-31 Transmit Code Length

The code length is represented by a binary number from 0 - 32 with bit 31 the LSB and bit 26 the MSB. A "0" indicates a true level, thus the word 110011 has the decimal value of 12.

Let

$$\phi_{11} = \frac{2\pi L}{\lambda_1} ,$$

$$\phi_{12} = \frac{2\pi L}{\lambda_2} ,$$

$$\phi_{21} = \frac{2\pi(L+\Delta L)}{\lambda_1} , \text{ and}$$

$$\phi_{22} = \frac{2\pi(L+\Delta L)}{\lambda_2} ,$$

where ϕ is the absolute phase of the wave at distance L from the input port, ϕ_{ij} represents the phase of a signal at a particular point in the system where the subscript "i" refers to the frequency and the subscript "j" refers to the path traveled, and λ_i is the wavelength in the waveguide of the signal whose frequency is, say, f_i.

The phase error at the output is given by:

$$\Delta\phi = (\phi_{11} - \phi_{21}) - (\phi_{12} - \phi_{22})$$

or

$$\Delta\phi = 2\pi\Delta L \left(\frac{1}{\lambda_1} - \frac{1}{\lambda_2}\right)$$

Measurements performed on the IPAR system indicated that the total path difference in the two channels was approximately 1 meter. Approximately 30 cm of waveguide was required to balance the phase in the receiver channel, and approximately 60 cm of waveguide was added to one channel of the transmitter. Once a phase balance was achieved in both the transmitter and receiver paths, the residual phase error was on the order of $\pm$ 10 degrees over a frequency deviation of greater than 200 MHz. The residual phase shift is not a continuous function of frequency and appears to be the result of the VSWR of the various components used in the system.

2.1.2.2 Noise Source Spectrum

The noise source which was used to feed the transmitter showed slightly degraded correlation performance compared with the swept frequency source. The spectrum of the noise source was found to contain both upper and lower sidebands as well as many spurious frequencies spread over several hundred MHz. The problem was found to be

associated with spurious frequencies generated in the X-band Gunn oscillator and with a broken termination on the single sideband generator. The Gunn oscillator and termination were replaced and the spectrum was again checked. Figure 2.2 is a picture of the spectrum of the noise source after the problems were corrected. The total width of the spectrum is 140 MHz. Approximately 73% of the power is contained within the central 21 MHz portion. Table 2.3 shows the distribution of power in 7 MHz increments from 9.350 to 9.490 GHz. The lower sideband is suppressed approximately 25 dB and the carrier frequency is suppressed 23 dB. This source was installed and checked out in the radar; its performance was comparable to the swept frequency source.

2.2 FIELD VERIFICATION

The IPAR radar processor has been successfully demonstrated and field tested. Proof-of-concept for pulse compression on polarization modulation has thus been established. The following subsections describe in detail the results of the IPAR local field tests (Section 2.2.1) and Lake Lanier field operation (Section 2.2.2).

2.2.1 LOCAL FIELD TESTING

The initial testing and verification of the IPAR radar was accomplished at Georgia Tech's Cobb County Research Facility. The tests were conducted from the lobby of building 5, which overlooks a flat grassy area that offered a maximum range of approximately 500 feet. An 18 inch diameter antenna was used because of restricted space available in the lobby.

The radar RF system operation was verified by setting up targets of known radar cross-section and comparing the target video with a calibrated signal level injected into the receivers. From the radar range equation, the theoretical received power was calculated based on the target radar cross-section. The received power measured in this manner fell within ± 2 dB of the theoretical value predicted from the range equation. The power transmitted through each channel could be adjusted to 1.5 kW peak; however, for all system verification tests, a transmitted power of 1 kW through each channel was used. During system verification tests, a 25 cm trihedral was used.

After the RF system had been thoroughly checked for proper operation, the IPAR correlation processor was checked out using dihedral (even bounce) and trihedral (odd bounce) corner reflectors. During the system verification, the following tests were conducted to verify the theoretical predictions.

20 MHz/division
Horizontal axis.

10 db/division
Vertical axis.

9.39 GHz carrier
frequency.

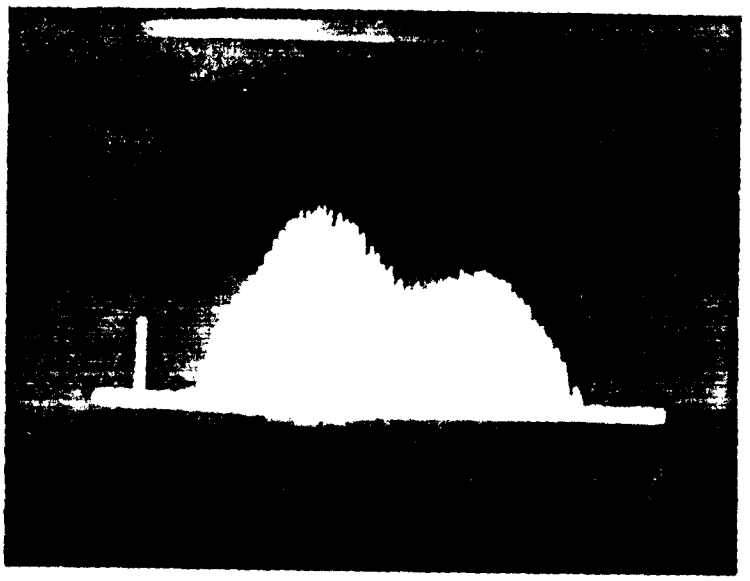

Figure 2.2 Noise specturm.

TABLE 2.3 DISTRIBUTION OF TOTAL POWER IN NOISE SPECTRUM

Frequency F (GHz)	Percent of Total Power Between F and F+7 MHz
9.410	0.03
9.417	0.23
9.424	0.90
9.431	2.52
9.438	10.70
9.445	20.69
9.452	25.78
9.459	17.69
9.466	8.33
9.473	2.86
9.480	1.15
9.487	1.02
9.494	1.23
9.501	1.73
9.508	2.09
9.515	1.79
9.522	0.82
9.529	0.31
9.536	0.11
9.543	0.02

(1) Odd bounce (trihedral) targets produced a positive correlation.

(2) Even bounce (dihedral) targets produced a negative or (anti) correlation.

(3) Tree clutter targets produced a correlation which changes from positive to negative in an unpredictable manner. The rate of change and duration of positive and negative correlations appeared to be on the order of the time required for clutter to decorrelate using standard fixed frequency radars.

(4) When using the swept frequency source, odd and even bounce targets produced results similar to that observed during fixed frequency operation.

(5) When using the noise source, odd and even bounce targets produced results similar to that observed using fixed frequency.

(6) When using either the swept frequency or noise source, tree clutter did not appear to correlate to a significant level and changed from positive to negative values very rapidly. No actual measurements of the decorrelation time of the tree clutter were made.

(7) The IPAR correlation function showed that the system did compress target signals to a single bit width.

(8) Multiple targets in the same resolution cell correlated separately and to a level inversely proportional to the separation distance. The dominant (largest) target correlated to the full 32 bit level and the smaller target correlated to a level determined by the number of bit separations.

After the initial testing, the radar system was disassembled and re-installed in a mobile radar van. The van is equipped with a self-contained 15 kW three phase gasoline powered motor generator set and a 4 foot dual polarized antenna. The antenna can be manually positioned in azimuth and elevation, and is mounted on top of the van. The antenna feed is positioned approximately 13 feet above ground level. This radar van provides an excellent facility for evaluating radar systems at remote locations.

The grounds of the research facility at Cobb County do not offer a range sufficient for measurement and testing of long pulse radars because of the surrounding tree line. For this reason, it was necessary to locate an area that provided a clutter free environment for making measurements on point targets and that also allowed measurements on larger, extended targets and clutter. It was also desirable to have access to an extended smooth surface for the evaluation of the radar operation in a multipath environment.

The pulse length of the IPAR radar's transmitted signal can be varied at the discretion of the operator from as short as 10 ns (20 ns minimum useable) to as long as 5.12 microseconds. The longest pulse length dictates that a minimum range of approximately 2,500 feet separate the radar from the target. The most likely candidate for a field site appeared to be a lake that offered a clear unobstructed view corresponding to twice this minimum range, and a variety of clutter areas and hard targets. In addition, it was necessary to have access to locations available to the setting up of point targets in clutter free areas.

A survey of Lake Sidney Lanier, located approximately 40 miles northeast from Atlanta, Georgia was made. Several camp sites and marinas, as well as the dam area were visited. The best available site which met the requirements for the intended test was atop the dam. The United States Corp of Engineers was contacted and permission was granted to use the parking area at the dam as a base of operations.

2.2.2 LAKE LANIER FIELD TESTING

The purposes of this field operation were to verify proper operation of the equipment, identify system deficiencies, develop procedural techniques which would be used for future detailed measurements and data collection, and observe the signals for unexpected occurrences. Within this scope of intended operations, the program goals were met. The field operation resulted in the identification of two significant problem areas. These problem areas are associated with unequal path lengths in the two transmitter and two receiver channels, and with the spectrum of the noise source. These are more fully described in subsection 2.1.2. The following effects were qualitatively observed, although the data were not recorded and no definitive results are available.

1. Effect of selected code and code length.
2. Effect of sinusoidal frequency sweep and of band limited noise transmissions.

In addition, experiments involving multipath reduction, Doppler-invariant pulse compression, and ECCM properties were attempted. The results of these experiments and observations are discussed in the following subsections.

2.2.2.1 Effects of Code Length

The length of the transmitted code determines the maximum amplitude to which a target will compress, while the code itself determines the sidelobe structure of the correlation function. The code length of the transmitted pulse can be varied between one and 32 bits; however, the correlator chips are not programmable in length and, therefore, perfect correlation is not possible for transmitted code lengths less than 32 bits. To minimize the effects of unused bits in the correlator, the unused positions are filled with alternate "1s" and "0s", we have termed this pseudo-correlation.

The total output of the correlation function including leading and trailing sidelobes is 64 bits long. An N bit transmitted code produces a true correlation for the first N bits of the 32 bit length. After the Nth bit, the correlation function is contaminated by the alternating "1s" and "0s" as well as by other targets and system noise. Figure 2.3(b) shows the correlation function recorded from an 8 inch sphere for a 13 bit Barker code. The peak of this function is 13 units high. A Barker code was chosen because it has the property of having unity sidelobes. As is shown in this figure, the sidelobes leading the peak of the correlation are ± 1. Following the peak, the sidelobes do not appear at a unity level because the length of the correlator is always 32 bits long. Another example of the effect of code length is shown in Figure 2.3(a). Here two consecutive 13 bit Barker codes were transmitted and the resultant correlation function shows the effect of the remaining alternating "1s" and "0s" on the tracking sidelobes. The first 13 bits of the total 26 bit long code produced a correlation 13 units high. At the 26th bit position, a correlation 26 units high is shown.

2.2.2.2 Frequency Effects

The IPAR was originally developed as a fixed frequency radar. Since the phase detection process relies only on the relative phase between the H and V polarized components of the receiver signal, frequency stability is not a requirement for either the transmitter or the local oscillator. It was predicted that the IPAR would operate with either a frequency agile source or with a band limited noise source. A controlled frequency agile source was not available to test the system, but an HP624C test set was substituted for the fixed frequency Gunn oscillator. The resulting test set has a sinusoidally swept FM mode, whose sweep limits are restricted to approximately 30 to 40 MHz. In this mode of operation, correlations of fixed targets was observed, although the performance was degraded to some extent. The targets which were observed consisted

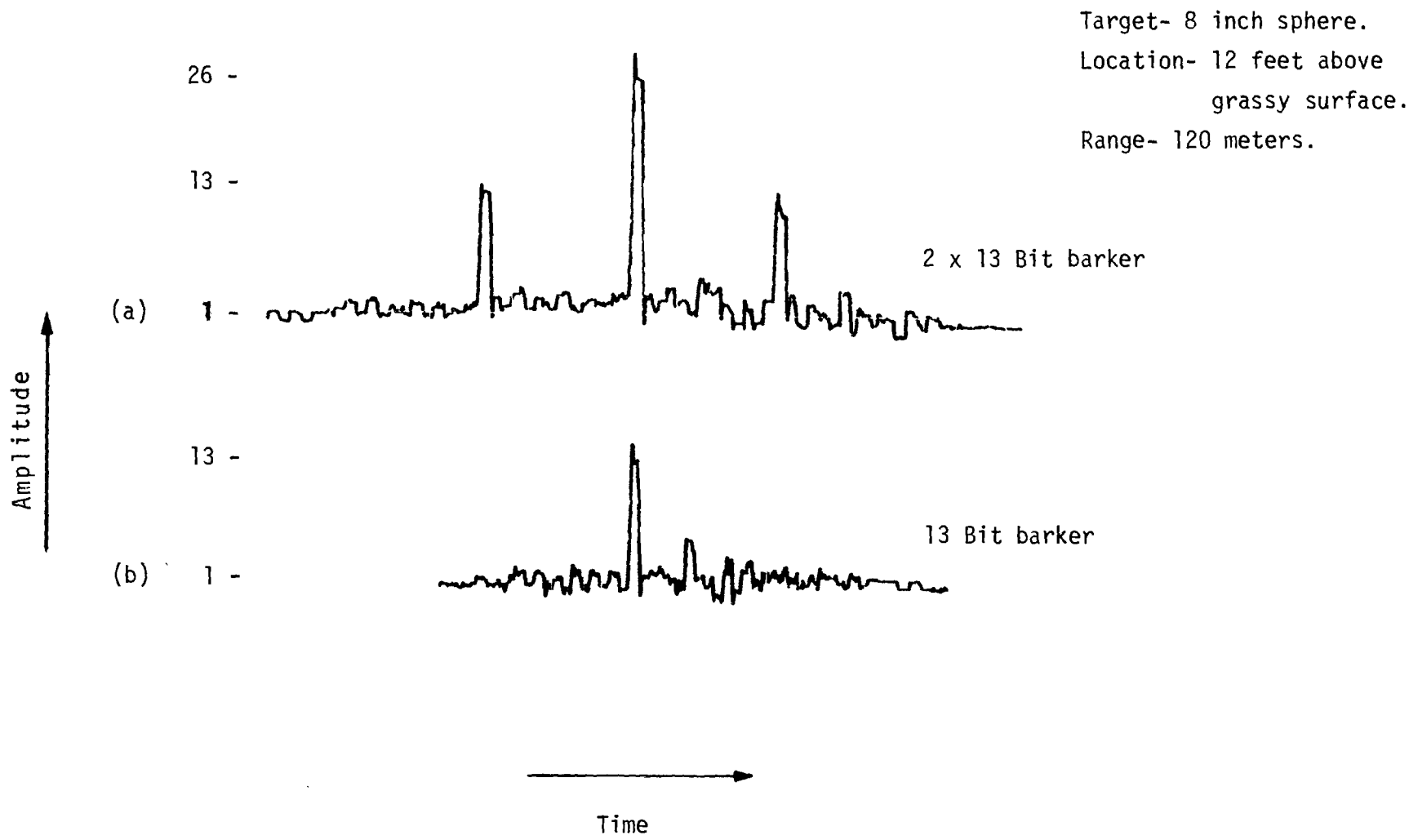

Figure 2.3 Compressed returns.

of two water tanks and a trihederal corner reflector. One of the water tanks was of a cone capped cylinderical shape and the other was shaped like an inverted teardrop supported by a central column. The corner reflector was a 14 inch trihedral supported by a 2 x 4 wooden post. The peak of the correlation function for all three targets exhibited some noise-like characteristics, although the correlations were of a generally strong nature; i.e., the average correlation was at least 75% of the expected maximum value. These targets were located at ranges of approximately 1 mile, 3 miles, and 3/4 mile, respectively.

As predicted by theory, it was possible to suppress clutter returns by utilizing frequency agility in conjunction with IPAR pulse compression. Figure 2.4 depicts compressed returns from tree clutter. The output shown in (a) of the figure resulted from illumination by a fixed frequency (X-band) IPAR waveform. The compressed output is suppressed relative to a simple scatterer of the same radar cross section, as predicted by the theory that was described in Section 1 of this report. Figure 2.4(b) illustrates further suppression of the clutter through frequency agility. The compressed return resulted from illumination by a frequency swept IPAR waveform. The frequency modulation apparently further decorrelated the major reflectors within each range bin so that the degree of decorrelation from subpulse to subpulse was accelerated.

A noise source was constructed by using a single sideband generator fed with an X-band source and a 60 MHz limited IF signal of 20 MHz bandwidth. This source also was used to drive the transmitter chain. The noise source produced results similar to those observed with the swept frequency signal generator. In both the swept frequency transmission and the noise transmission, correlation of targets was significant. When the noise source was used to drive the transmitter amplifier chains, correlation was only about 50 to 60% of the maximum. In both swept frequency and noise transmission, it was suspected that a hardware problem, rather than a problem in the theoretical concept, was the cause of the degraded performance. The cause of the degraded performance was not determined until after returning to the laboratory where a more detailed study of the problems were conducted. These problems and our subsequent solutions were discussed in detail in subsection 2.1.2 of this report.

2.2.2.3 Multipath

Multipath results when energy is returned to the radar by separate paths. There are four possible routes by which the energy can be returned to the radar antenna when targets are located over a smooth surface.

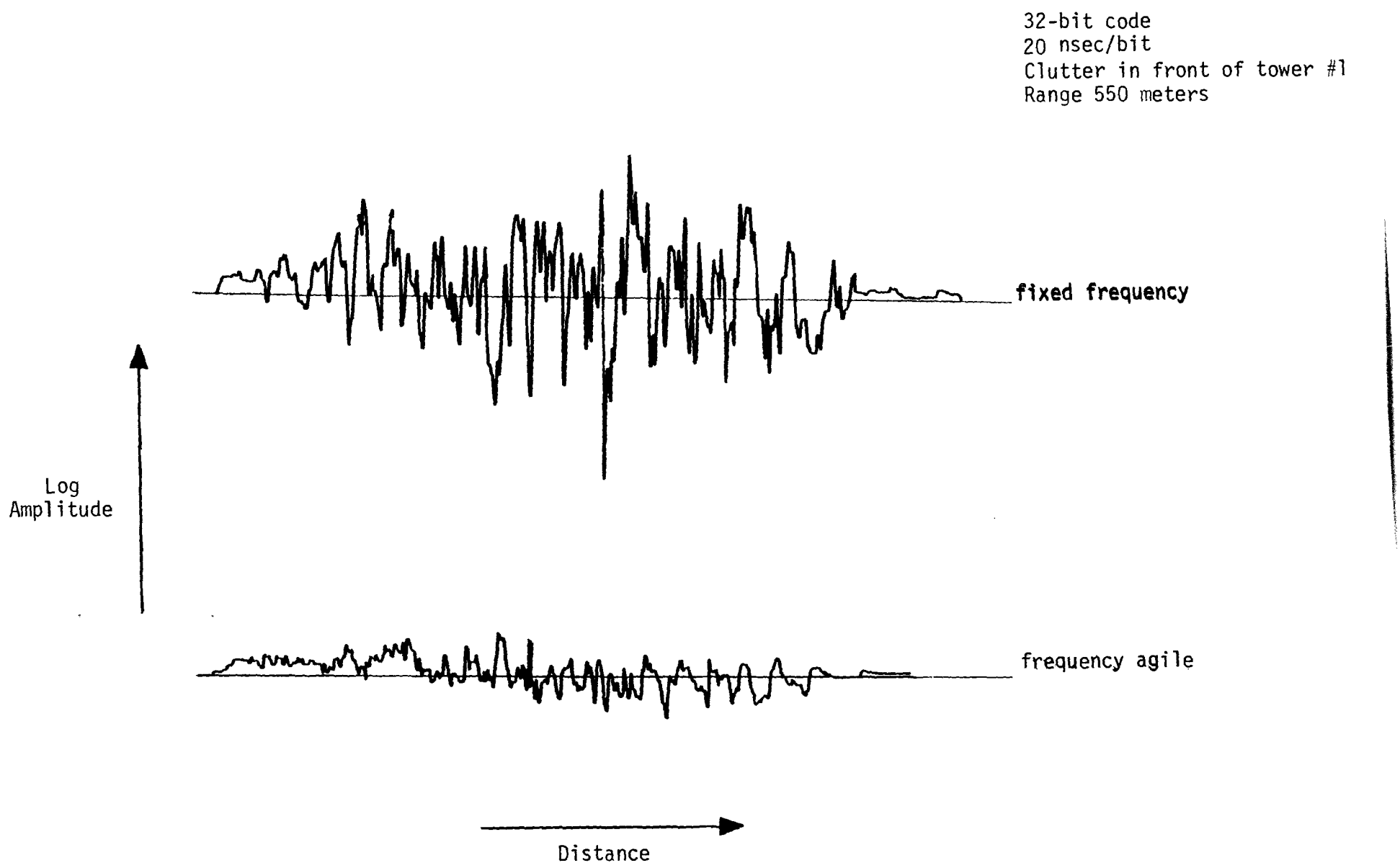

Figure 2.4 The effect of frequency modulation on a clutter return.

1. The direct ray from the transmitter striking the target and being returned over the same path.
2. The direct ray from the transmitter striking the target and being returned through an indirect path.
3. The ray striking an intervening surface and being reflected to the target and back along the same path to the radar.
4. The ray striking an intervening surface and being returned through a direct path to the radar.

The expected power return can vary widely depending on path lengths and surface reflectivities. There is a possibility that as much as 16 times the expected power will be detected in the radar receiver or that complete cancellation between the four different paths can occur. For small incident angles (less than two degrees) over smooth surfaces the equivalent field detected by the radar can be described by equation (1):
where

$$F = 16 \sin^4 \frac{2\pi h_1 h_2}{R\lambda} , \qquad (1)$$

where F is the propagation factor included in the radar range equation, h_1 and h_2 are the radar height and the target height, respectively, R is the range to the target, and λ is the transmitted wavelength. A surface roughness factor is not included because we are concerned, here, with the smooth surface of a lake; however, over an ocean surface the maximum and minimum values predicted by equation (1) would be modified by the above mentioned roughness factor.

An experiment was conducted to observe the multipath effect as a function of height of a target above the surface of the water. The experiment was conducted by mounting an 18 inch corner reflector, which could be manually raised and lowered, on a 14 foot high support. This support was set up in the water approximately 50 feet from the shore line of a small island in the lake. The bottom of the support was anchored approximately three feet below the water level. The vertical travel of the corner reflector was approximately 10.5 feet from the water surface to the maximum height. The rope and pulley system used to manually raise and lower the corner reflector resulted in a non-uniform rate of restricted travel. However, the results observed during

the experiment showed that a strong multipath effect was present in the amplitude of the radar return. Because of technical difficulties, unrelated to the radar, the experiment was not repeated using IPAR processing. Figure 2.5 is a plot of the amplitude signal which was recorded during the experiment. The height above the surface is only approximate since the rate of travel up the support was not uniform and height estimates were relayed by radio link from the shore of the island. Nonetheless, results within the expected variations due to the nature of the experiment are in good agreement with the results predicted by Equation (1).

2.2.2.4 Airborne ECCM Test

An experiment was conducted to qualitatively determine if the IPAR radar offered benefits in the area of ECCM. Having serendipitously discovered that classified electronic countermeasures (ECM) equipment was being tested near Lake Lanier by the United States Air Force, it was decided to test the IPAR waveform against the equipment. Two F-105's carrying the ECM equipment made four passes over the IPAR test site. In each case, the aircraft were detected by the IPAR system five to eight kilometers out (it was necessary to rely on visual acquisition because of the manual nature of the demonstration system) and were successfully tracked manually from detection all the way in to flyover. The aircraft was illuminated by either an unmodulated pulse or a polarization-modulated pulse on each of the passes. The pilot reported that he detected our beam most of the time, although it "seemed about 3 dB higher" when in the unmodulated mode.

The classified nature of the equipment, our lack of hard data, and the somewhat non-committal nature of the pilot's report led us to decide that the tests were inconclusive and to recommend further, better controlled, and better documented efforts in this area of inquiry.

2.2.2.5 Doppler-Invariance of IPAR Pulse Compression

The airborne ECCM test described above also presented an opportunity to observe the superiority of the IPAR pulse compression scheme over carrier phase and frequency pulse compression schemes (such as linear FM and binary phase coding) in the presence of Doppler. It is well known that phase and frequency codes show a marked sensitivity to signals which are Doppler shifted $\pi/2$ radians per pulse or greater (waveform degradation for phase codes and range slip for frequency codes).[5,7] The IPAR

Range = 1135.5m

$tC = 470 \times 10^{3} \times .68 \times 10^{-6}$

$h_1 = 15.8m$

32-Bit M code

h_2 = height of reflector above surface of water.

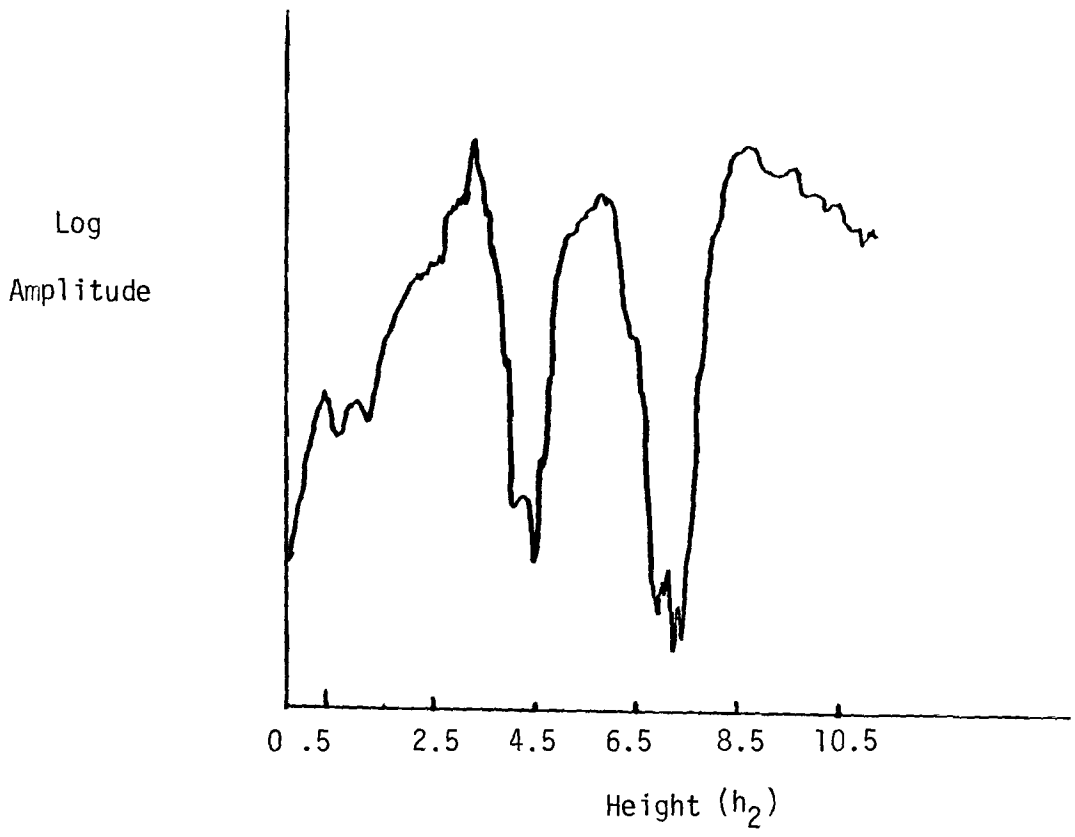

Figure 2.5 Multipath: amplitude vs. height.

waveform showed no degradation from the moment of target detection to the moment of flyover; however, the maximum radial velocity of the target generated a Doppler shift of only $\pi/20$ radians per pulse, which was not enough for the evidence to be considered conclusive.

2.3 PRELIMINARY TEST AND DATA COLLECTION PLANS

2.3.1 PURPOSE

The purpose of these measurements is to collect phase, amplitude, and compressed radar data which will provide a basis for analytical and statistical evaluation of some of the characteristics of the IPAR radar. These tests are intended primarily to address detection of targets in clutter and compression efficiency-resolution questions. The data collected in these tests may also be used to better understand the interaction between multiple scattering centers for application to the complex target identification problem. Some of these data will be used to predict relative performance parameters while others will be used to measure values of phase and amplitude. It is essential that the power measurements and calibration procedures be followed to assure validity and repeatability of the measurements.

2.3.2 EVALUATION METHOD

An evaluation of the IPAR technique should be accomplished, in part, by directly comparing the resultant data to data derived from a radar which employs standard well understood techniques. The IPAR radar is ideally suited for this purpose since the pulse length can be changed to the length of the compressed pulse, the power can be controlled, and coded or non coded pulses can be transmitted. These parameters will be adjusted if appropriate so that a comparison can be made directly without having to account for differences in radar characteristics and calibrations, as would occur if separate radars were used.

2.3.3 RADAR TARGETS

It is the intent of these measurements to establish a data base which can not only be used to evaluate the relative performance of IPAR, but also justified by analytical techniques, although the latter intent involves computer modeling and is not a part of the current program. These tests will be conducted by using simple odd or even bounce reflectors and clutter targets of a "homogeneous" nature. The reflectors will be trihederals, diplanes, and spheres or combinations of these targets as required to achieve the purpose of the measurement.

2.3.4 SYSTEM PREPARATION

The IPAR radar will be used to collect data which will be analyzed to determine system performance. Much of the performance evaluation will be based on relative measurements. However, it is essential for completeness that absolute radar cross section (RCS) data be collected. Absolute RCS can be determined by comparing the amplitude of the radar return to either a signal of known power or a signal derived from a standard RCS and correcting as necessary for differences in range between the target and the standard. Both methods require that the receiver transfer characteristic be known. In addition, the power comparison method requires that the transmitted power and the system losses be carefully determined. The primary method of determining RCS collected with the IPAR radar will be based on a received power calibration. The following procedures will assure that the system is adequately calibrated.

2.3.4.1 Power Measurements

A test port located in the ceiling of the van is provided to measure the transmitted power and to inject the receiver calibration signal. Connect a thermistor mount and power meter to the test port. The peak power may be calculated from the following equation:

$$P_p = \frac{\text{Power meter reading}}{\text{Coupling efficiency}} \times \frac{1}{(PRF)\ (N)\ (T_s)}$$

where coupling efficiency is -13 dB (0.05) for single channel measurements (10 dB coupler + 3 dB Magic Tee), PRF is the pulse repetition frequency, N is the number of subpulses selected, and T_s is the selected subpulse width. Ratings on the thermistor mount dictate that the factors $(N \times T_s) \leq 100 \times 10^{-9}$.

CAUTION

The thermistor mount will be damaged if its average power rating <u>or</u> its Watt-μs pulse rating is exceeded. These values are 15 mW and 5 Watt-μs, respectively.

Example of Power Measurement:

Select N = 10 (Code must be all 1's)

Select PRF = 1000

Select T_s = 10 ns

Select Top or bottom (not both) transmitter channel

Meter indication shows 5 mW

$$P_p \frac{5 \times 10^{-3}}{0.050} \times \frac{1}{(1000)\ (10)\ (10 \times 10^{-9})} = 1000 \text{ Watts}$$

This measurement should be made in each transmitter separately because the thermistor Watt-μs rating will be exceeded with both transmitters operating and because the summation of power in the magic tee is phase dependent and may give erroneous results.

The power output of each transmitter will be measured separately by the following step by step procedure.

1. Connect the thermistor to the test port.
2. Turn on the transmitter oscillator.
3. Turn on the 4 TWT amplifiers and allow them to warm up. Do not go to RADIATE SWITCH position.
4. Turn on the correlator-timing and control.
5. After allowing sufficient warm up time:
   a. Press the radiate switch on the correlator control panel.
   b. Select N = 5.
   c. Select T_s = 20.
   d. Set all code switches to up "1" position.
   e. Load code with momentary load switch.
   f. Reduce LOW POWER TWT gain to minimum (CCW position on both TWT amplifiers).
   g. Switch LOW POWER TWT No. 1 to radiate.
   h. Press Radiate Switch on Hi Power TWT No. 1.
   i. Increase Low Power TWT No. 1 gain pot until power meter reads desired level (2.5 mW).

      NOTE: Do not exceed ratings given in Example.
   j. Go to Stand-By on Both Low-Power and High-Power TWT amplifiers.
   k. Repeat Steps 5a through 5j for TWT amplifier Chain No. 2.
   l. Disconnect the thermistor mount from the waveguide.

2.3.4.2 Phase Adjustments

The ellipticity of the transmitted wave is affected by the power balance and by the phase between the two X-band signals arriving at the dual mode coupler. A rectangular waveguide horn is located on the antenna dish to provide a means of establishing the required circular polarization. This horn is adjustable in 45 degree increments with respect to the primary antenna feed. The horn must be positioned either at the $+45^{\circ}$ or -45° position before the final power and phase conditions can be established.

Several iterations of the following procedure may be required to establish a linear 45° polarization. Once the linear 45° polarization has been obtained, the calibrated phase shifter in the transmitter can be adjusted for a phase delay of 90° to achieve the condition necessary for circular polarization.

1. Connect a 50 ohm coax cable between the crystal detector located on the antenna and a 100 MHz bandwidth oscilloscope. Be sure that the coax line is terminated at both ends.
2. Position the test horn to 45° and lock the detent.
3. With the power balanced as indicated above (Be sure that the thermistor is disconnected at the roof test port), rotate the transmitter phase shifter to 0° and lock the calibration dial.
4. Set the code length to 32.
5. Set a 32-bit code of alternating 4-bits (111100001111 etc.) and load the code.
6. Turn on all 4 TWT amplifiers.
7. Observe the oscilloscope and adjust the phase shifter for a null in the one's position of the detected code.
8. The initial adjustment should achieve a null greater than 20 dB below the peak observed for the code zeros.
9. Increase the vertical sensitivity on the oscilloscope and adjust the gain pot on one, Not Both, of the low power TWT amplifiers to achieve a better null if required. The TWT current should not be changed from its power-balance condition by more than 2 to 3 percent.
10. An iteration between power adjustment and phase adjustment may be required to achieve the best null. Repeat steps 7 through 9 as required.
11. Once the "best" null is achieved, UNLOCK the phase shifter dial and set the phase to 90°.

12. Observe the oscilloscope to see that both the "1s" and "0s" of the code are the same amplitude.

The system is now adjusted so that the horizontally polarized and vertically polarized signals radiated from the primary feed are equal in power level and 90° out of phase. These are the conditions necessary to establish a circularily polarized radiated field.

2.3.4.3 Receiver Calibration

The radar receiver will be calibrated by injecting a signal of known frequency and power level into the same test port used to measure the transmitter power. The signal will be generated by an HP 624 test set. The signal levels from some targets will be reduced to low (near noise) values; therefore, it is necessary to define the small signal receiver transfer characteristics (lin/log transition region) in smaller increments than normally used. Calibrations for phase output voltage versus phase angle are also required.

Establish the test setup shown in Figure 2.6. The Georgia Tech analog tape interface contains five boxcar (sample-and-hold) circuits whose sampling time is determined by range gates potentiometers on its front panel. Note that this range gate and the IPAR digital processor range gate are completely separate units. The analog tape range gate may be electrically slewed via a front panel switch allowing the complete correlation function to be sampled. Note that in the following procedures both the analog and the digital data should be recorded. The digital tape recorder is controlled by the IPAR digital tape interface. The FM tape recorder is controlled directly.

Amplitude Calibration

The following procedure is to be used when calibrating the receiver video output vs. power input:

1. Turn on the HP 624 test set and allow 15 minutes warm up time.
2. Tune the test set to same frequency as the transmitter.
3. Perform an internal calibration on the test set.
4. Connect the test set to the power meter through the same coax cable that will be used to connect to the waveguide test port.

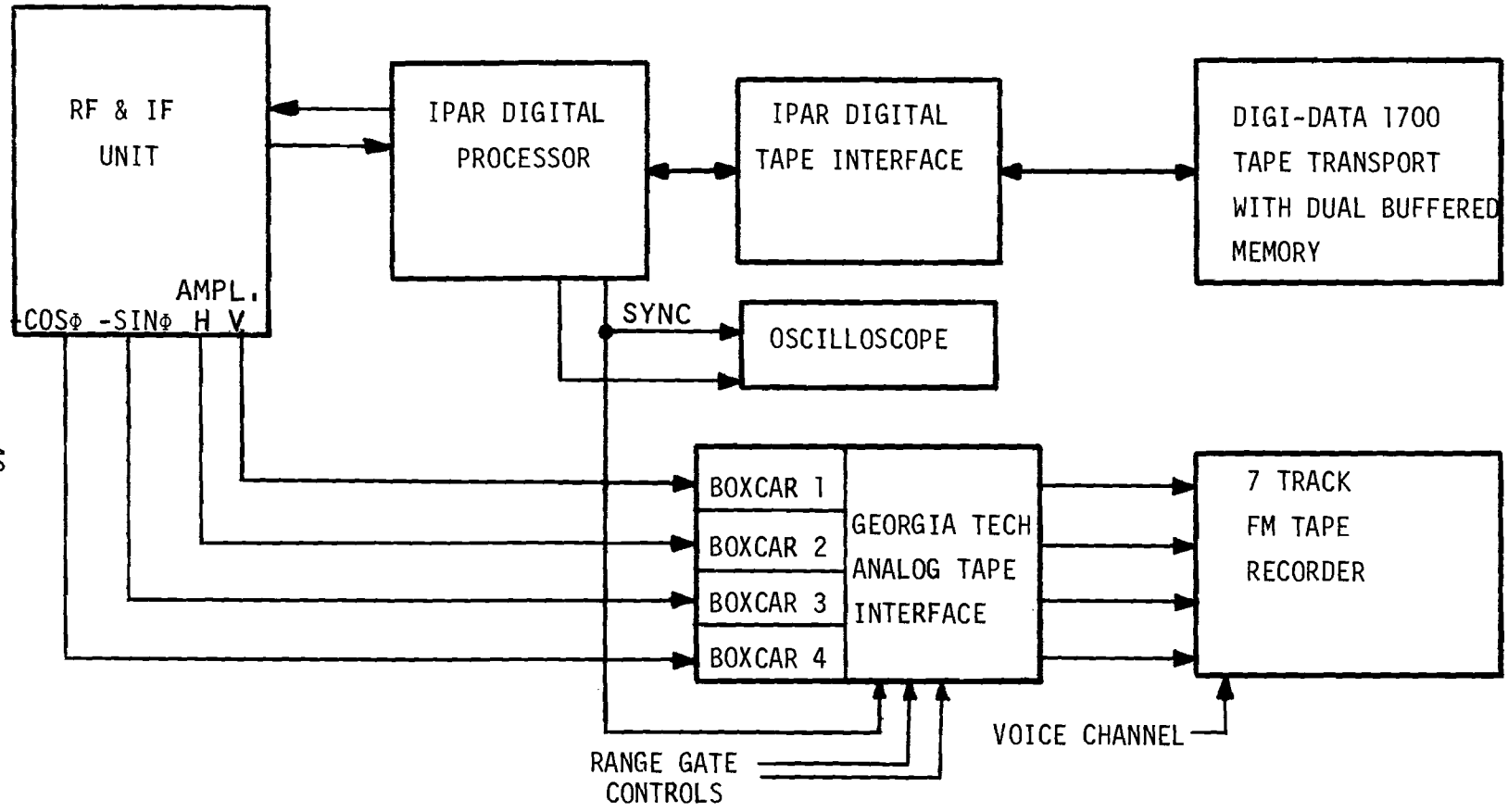

Figure 2.6 IPAR test setup.

5. Measure and record on the data sheet the power measured at the end of the cable.
6. Disconnect the cable from the power meter and re-connect to the waveguide test port.
7. Be sure that the receiver, transmitter and test set are tuned to the same frequency.
8. Start at zero dB on the test set on the receiver attenuators and record 10 second range gated samples for every 5 or 3 dB attenuation over the dynamic range of the receiver (digital and analog data). The last 15 dB of the dynamic range (small signal levels) should be calibrated in 3 dB increments.
9. Using the test set attenuator, record a series of maximum/minimum signal levels to aid in setting up scaling amplifiers use in the data reduction process.

Phase Verification

The phase angle between the horizontal and vertical components of the reflected signal can be determined from the I and Q outputs of the phase detector. The phase detectors consist of two identical DBM-200 double balanced mixers. The required 90 degree phase shift is achieved with a pair of coax cables which have been cut so that one cable is 1/4 wavelength longer than the other. It is essential that the sine/cosine relationship be verified before data collection is started. Follow the steps below to validate the phase detector connections.

1. See Figure 2.7 for phase detector schematic.
2. Attach a cable from boxcar circuit No. 4 to the Y axis of the oscilloscope and a cable from boxcar circuit No. 3 to the X axis input of the oscilloscope.
3. Apply a signal from the HP 624 test set to the waveguide test port.
4. Vary the phase shifter in the horizontal receiver and observe that the path of the "dot" on the oscilloscope traces out a circle - adjust the X and Y gain to equal maximum excursions.
5. If for the conditions set up in 4, the oscilloscope trace is not a circle, trim the cable length by using coax adapters until a circular Lissajous pattern is achieved.

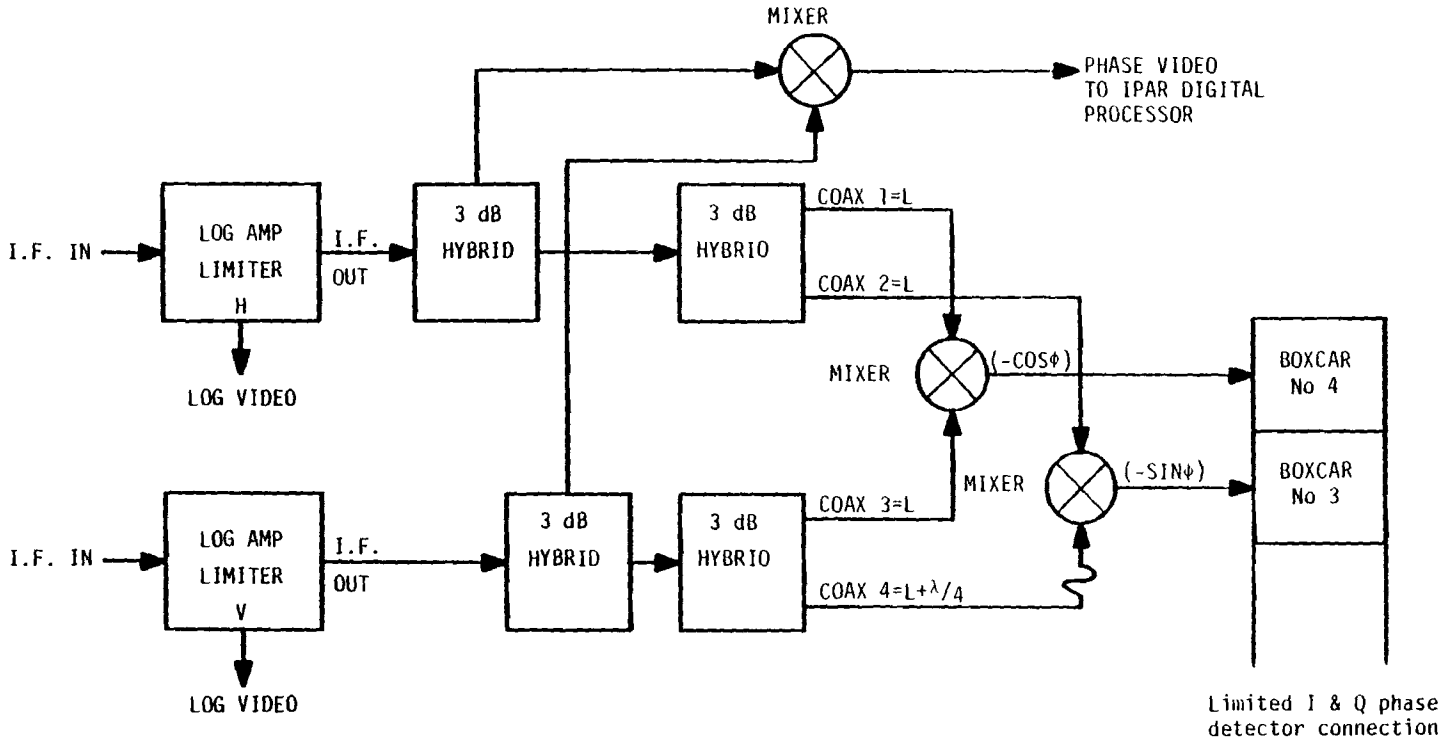

Figure 2.7 IPAR phase detector network.

Correlated Video Calibration

The correlator has ± 32 possible correlation levels. A test function is built in to the correlator which generates a 32 step output which is incremented in steps of 2 from -32 to +32. A calibration of the correlator can be generated by positioning range gate 2 to the most negative level and sweeping the range gate across the test function by pressing the range sweep switch. Record a single sweep of the test function on the digital and analog tape recorders.

Calibration Verification

The receiver calibration should be verified against the radar return from a standard corner reflector. The theoretical power return from the standard corner reflector can be calculated from the radar range equation. The level of the video return from the calibration target should be compared with the receiver calibration which was accomplished in paragraph 4.3. The calculated theoretical power should agree with the measured value within the limits of ± 2 dB. The received power can be calculated from:

$$P_r = \frac{P_t \, G^2 \, \lambda^2}{(4\pi)^3 \, R^4} \left(\frac{1}{L_1}\right) \left(\frac{1}{L_2}\right)$$

where:

P_t	=	measured value from paragraph 4.1
G^2	=	79.2 dB
λ^2	=	-29.9 dB
$(4\pi)^3$	=	33.0 dB
L_1	=	1.2 dB
L_2	=	3 dB (linear component of circular wave)
R^4	=	measured range to target (150 m/μs).

If the measured and calculated values do not agree within the acceptable limits, verify that the target is not subject to multipath effects.

2.3.5 MEASUREMENTS

The targets used in the measurements should be selected for appropriate size in relation to target supports and clutter background. Verify that the targets are located in a multipath free environment either by geometrical calculations or by direct measuement with a field probe. Make entry in data log to describe all applicable parameters. These entries should include the following:

1. Calibration target dimensions,
2. Data target type and size,
3. Transmission mode,
4. Transmitted code,
5. Subpulse width,
6. Radar PRF (1000 for all data),
7. Range to target,
8. Peak transmitted power,
9. Run number,
10. Date and time,
11. Other appropriate information.

Where appropriate, the data sheet information should be supplemented with photographs of the target and oscilloscope displays.

2.3.5.1 Isolated Simple Targets

These tests are intended to demonstrate the pulse compression and correlation efficiency of the IPAR radar for the three transmission characteristics: fixed frequency, swept frequency, and band limited noise. Two target types, odd bounce and even bounce, will be used to show the results for correlations and anti-correlations (in-phase and out of phase received codes). Signal to noise ratio and code length will be changed for each set of measurements. Follow the procedure given below for each data set.

Amplitude, Phase, and Correlation Function Measurements

1. Set up trihedral target.
2. Connect the phase detector network as shown in Figure 2.7
3. Transmit a fixed frequency.
4. Set and load code per Test Matrix I. (Table 2.4)
5. Set PRF to 1000 Hz.
6. Select a 20 ns subpulse width.
7. Select N = 10.
8. Position analog range gate 1 (top) and the IPAR digital processor range gate to the range of the target.

TABLE 2.4. TEST MATRICES

TEST MATRIX I

N	T_S	Code	Attn	REC-1	REC-2	REC-3	REC-4
10	20	All "1"	0			X	15 sec
"	"		20			X	"
"	"		T			X	"
"	"		N			X	"
10	20	ALL "0"	0			X	15 sec
"	"		20			X	"
"	"		T			X	"
"	"		N			X	"

TEST MATRIX II

N	T_s	Code	Attn	REC-1	REC-2	REC-3	REC-4
7	20	B-7	0,20,T,N	30 sec	X		
13		B-13	"	"	X		
16		PN-16	"	"	X		
31		PN-31	"	"	X		
7	40	B-7	"	30 sec	X		
13		B-13	"	"	X		
16		PN-16	"	"	X		
31		PN-31	"	"	X		

Code 8		
Code 7		
Code 6	0 1 0 0 1 0 0 0 0 1 0 1 0 1 1 1 0 1 1 0 0 0 1 1 1 1 1 1 0 0 1 1	31 BIT P/N
Code 5	1 1 0 0 1 1 0 0 1 0 1 0 0 0 0 1 1 1 1 1 1 0 1 0	23 BIT P/N
Code 4	0 0 0 1 0 1 0 1 1 1 1 0 0 1 1 0 1 1 0	19 BIT P/N
Code 3	1 1 1 1 1 0 0 1 1 0 1 0 1	13 BIT BARKER
Code 2	1 1 1 0 0 0 1 0 0 1 0	11 BIT BARKER
Code 1	1 1 1 0 0 1 0	7 BIT BARKER

Table 2.5 IPAR Code Listings

9. Adjust the receiver phase shifter for a 90° phase lag as indicated on the Lissajous display. Attenuators should be set to zero.
10. Select the fixed frequency source for the transmit oscillator and record the data specified in Test Matrix I.
11. Switch the transmitter frequency source to "INT FM" and adjust amplitude control to 20. Repeat Test Matrix I.
12. Change the transmitter frequency source to the noise generator. Repeat Test Matrix I.
13. Replace the trihedral target with a diplane (Seam Vertical) and repeat 10 through 12 above.
14. Set and load code 1 see Text Matrix II.
15. Select a 20/40 ns subpulse width per Test Matrix II.
16. Select N = Code length from Table 2.5.
17. Adjust receiver phase shifter for maximum phase voltage.
18. Using the fixed frequency source for the transmitter oscillator, record the data specified in Test Matrix II.
19. Switch the transmitter frequency source to INT FM and adjust the FM amplitude control to 20. Repeat the measurements in Test Matrix II.
20. Change the transmitter frequency source to the noise generator. Repeat the measurements in Test Matrix II.
21. Replace the trihedral target with a diplane (Seam Vertical) and repeat 10 through 20 above.

2.3.5.2 Combinations of Simple Targets

These tests are intended to demonstrate the ability of IPAR to compress and resolve targets located within the resolution cell defined by the total pulse width. A second benefit will be derived from the collection of phase and amplitude data which may be useful in gaining a better understanding of the interaction between major scattering centers of complex targets. These data should be useful in addressing the target recognition problem.

Amplitude and Phase Measurement

1. Set up two trihedral targets of comparable size at a separation of 150 feet. Attach the modulation line to the rear corner reflector.

2. Set and load a PN-31 Code.
3. Connect the phase detector network as shown in Figure 2.7.
4. Select fixed frequency transmitter source.
5. Set PRF to 1000.
6. Select a 20 ns subpulse width.
7. Select N = 31.
8. Set the IPAR digital processor range gate to center target 1 in the replay interval.
9. Position range gate 1 in front of 1st target and record a range profile (REC-3).
10. Position range gate 1 to subpulse 5 position.
11. Using modulation line modulate the position of the near corner through several wavelengths and record data (REC-4).
12. Position range gate 1 to subpulse 20 position.
13. Repeat 10 above.
14. Position range gate 1 to subpulse 20 position as measured from corner No. 2.
15. Repeat 10 above.
16. Position the IPAR processor range gate 2 to range of Target 2 and record data (REC-1).
17. Starting with the digital range gate at (R_1-32) step the range gate in increments of 1 step for 45 steps. Record data for 5 seconds at each step (REC-1).
18. Transmit a 1-bit (20 ns) Code and record a range profile (REC-3).
19. Repeat steps 2 through 18 for a trihedral as target 1 and a dihedral as target 2.

2.3.5.3 Targets In Clutter

IPAR is expected to enhance the signal to clutter ratio for target to clutter ratios which are small. This area needs to be investigated for several S/N ratios for both in-cell and out of cell clutter ratios. The procedures to follow during investigation will be governed by the basic procedures already developed; however, careful observation during the test may lead to additional investigation and the development of new procedures. The following initial steps should be accomplished to establish the target to clutter ratios which will be used as a basis for evaluating the IPAR concept.

Amplitude, Phase, and Correlation Measurement

1. Place a target a minimum of 5 subpulse intervals in front of the selected clutter cell, (20 x 5 ns). Set the IPAR processor range gate to the target range.
2. Record a range profile (REC-3) of the complete cell (equivalent to 32 bits).
3. Set range gate 1 to peak of target and record data for a minimum of 15 seconds.
4. Transmit Code PN 31.
5. Record a range profile (REC-3) of the entire cell.
6. Step the digital range gate from (R-32) to (R-132) and record data for 5 seconds at each step.
7. Place the target in the clutter cell and repeat steps 1 through 6.
8. Replace the target with a diplane and repeat the procedure (Steps 1 through 7).
9. Select targets both larger and smaller than the one used above and repeat the procedure steps (1 through 8) for each target.

SECTION 3
SUMMARY AND RECOMMENDATIONS

3.1 STATE OF THE EQUIPMENT

The IPAR radar/processor is fully operational and ready to be implemented as a data collection system. The system is capable of generating pulse lengths up to 5.12 μs. at various PRF's and pulse compression ratios. A maximum pulse compression ratio of 32:1 can be achieved at rates up to 100 MHz, that is, resolutions as fine as 10 feet, with essentially perfect compression. The X-band, wideband noise and swept frequency sources allow for operation in any of the three modes, allowing for experiments that will begin to quantify the various effects of simultaneously employing polarization and frequency agility. It is possible to sample, store, and record the entire quantized return (up to 32 subpulses) from any single range bin.

3.2 CURRENT PROGAM PLANS AND RECOMMENDATIONS

The next phase of the program is scheduled to begin April 1, 1982 under the auspices of the Naval Sea Systems Command (NAVSEA), with Mr. Charles Jedrey, Technical Monitor. The purpose of this phase is to collect and analyze data that will: (1) firmly establish proof of concept for polarization-coded pulse compression, (2) establish quantitatively the target-to-clutter advantages of an IPAR process with respect to an unmodulated, simple pulse polarized radar, (3) provide data to quantify IPAR's multipath characteristics. In addition, the subpulse information will provide a data base for the study and quantification of the effects of frequency spreading on both targets and clutter.

Since the current IPAR was built primarily to show feasibility of design and proof-of-concept, it was built to minimum operational specifications. We have, therefore, submitted an unsolicited proposal to Mr. Max Yoder, Office of Naval Research (ONR), for the construction of an advanced IPAR (A-IPAR) radar/processor. The A-IPAR will incorporate state-of-the-art VHSIC technology to achieve 100 MHz real-time operation utilizing X-band, wideband noise, and frequency agile carrier, in conjunction with pulse compression (64:1 compression ratio) on polarization modulation. The ensuing system will be capable of recording 6-bit quantized IPAR data from 256 range bins. These capabilities will allow A-IPAR to be utilized for: (1) range profiling of complex targets,

(2) an in-depth analysis of target-to-clutter enhancements with and without frequency agility, (3) the study of various detection schemes utilizing amplitude-only, phase-only, and phase and amplitude characteristics, and (4) a verification of IPAR's Doppler-invariance.

Finally, the technical staff of the Radar Applications Division of the Radar and Instrumentation Laboratory of the Engineering Experiment Station of Georgia Institute of Technology continues to inform and educate department of defense agencies and contractors regarding the properties and potential applications of polarization processing in general and the IPAR process in particular.

REFERENCES

1. J. L. Eaves, et. al., "An Airborne Investigation of Polarization Diversity for Target Discriminating" Proceedings of the Nineteenth Annual Tri-Service Radar Symposium, July 1973.

2. J. L. Eaves, et. al., "Investigtion of Target Enhancement Techniques," Air Force Contract No. F33615-71-C-1612, GIT Final Report, October 1974.

3. J. L. Eaves, "Flight Evaluation of Stationary Target Indication Techniques," Proceedings of the 22nd Annual Tri-Service Radar Symposium, July 1976.

4. L. C. Bomar, et. al., "Evaluation of Selected Target Discrimination Techniques," Eighth ARPA/Tri-Service Millimeter Wave Conferenece, April 1979.

5. B. C. Appling, E. S. Sjoberg, E. E. Martin, "Intrapulse Polarization Agile Radar," SCEEE Contract No. N00024-78-C-5338, SCEEE-NAVSEA/79-2, GIT Final Report, July 1981.

6. M. Skolnick, Introduction To Radar Systems, McGraw-Hill, Inc., New York, New York, 1980.

7. M. N. Cohen, "Pulse Compression," Principles of Modern Radar, Georgia Institute of Technology, 1981.